

Autor: Conf.dr.ing. DUMITRAȘCU Dorin-Ion
Titlul: Biofuels and Road Safety: Challenges and Solutions in the Context of Sustainable Mobility
Domeniu: INGINERIA AUTOVEHICULELOR

LISTĂ PORTOFOLIU DE LUCRĂRI

1. Dumitrascu D.-I., Influence of Road Infrastructure Design over the Traffic Accidents: A Simulated Case Study. Infrastructures, 9(9), 2024, ISSN 2412-3811, Impact Factor: 2.7, SRI: 1.232, revistă în zona Q2, WOS:001323498200001, <https://doi.org/10.3390/infrastructures9090154>
2. Rusu A.-N., Dumitrascu D.-I.*, Dumitrascu A.-E., The Electromagnetic Noise Level Influence on the Laser Micro-Perforation Process specific to Automotive Components. Materials, 17(16), 2024, ISSN 1996-1944, Impact Factor: 3.1, SRI: 1.792, revistă în zona Q1, WOS:001304651200001, <https://doi.org/10.3390/ma17164131>
3. Rusu A.-N., Dumitrascu D.-I.*, Dumitrascu A.-E., Monitoring, Control and Optimization in Laser Micro-Perforation Process for Automotive Synthetic Leather Parts. Processes, 12(6), 2024, ISSN 2227-9717, Impact Factor: 2.8, SRI: 1.029, revistă în zona Q2, WOS: 001256521600001, <https://doi.org/10.3390/pr12061275>
4. Dumitrascu D.-I., Morariu C.O., Dumitrascu A.-E., Ciobanu D.V., Reliability estimation of towed grader attachment using finite element analysis and point estimation. Transactions of FAMENA, 42(1), 2018, p. 85-98, ISSN: 1333-1124, Impact Factor: 0.797, SRI: 0.187, revistă în zona Q4, WOS:000432786300008, <https://doi.org/10.21278/TOF.42108>
5. Dumitrașcu D.-I., The influence of the gasoline octane number on a turbocharged engine performance. International Journal of Computational and Applied Mathematics & Computer Science, ISSN 2769-2477, p, 30-33, Volume 1, 2021, [https://www.wseas.com/journals/camcs/2021/icamcs\(2021\)-005.pdf](https://www.wseas.com/journals/camcs/2021/icamcs(2021)-005.pdf)
<https://journals.indexcopernicus.com/search/details?id=69674>
6. Dumitrascu D.-I., Dumitrascu A.-E., Chiru A., A Case Study Regarding the Implementation of Six Sigma in an Assembly Process for the Automotive Parts. 12th International Congress of Automotive and Transport Engineering (CONAT 2016), p. 643-650, October 26-29, 2016, WOS: 000390821400071, https://doi.org/10.1007/978-3-319-45447-4_71
7. Dumitrascu D.-I., Benea B. – The Energetical and Ecological Performances of D.I. Diesel Engine Fueled with Biodiesel, ADVANCES in PRODUCTION,AUTOMATION and TRANSPORTATION SYSTEMS, pp. 389-394, ISSN: 2227-4588, ISBN: 978-1-61804-193-7, June 1-3, 2013, Brasov, Romania, <http://www.wseas.org/main/books/2013/Brasov/ICAPS.pdf>
8. Dumitrașcu D.-I., Trușcă D.D., Vehicle-Pedestrian Accident Reconstruction, COMAT 2012, 18-20 October 2012, Brasov, Romania, http://scholar.google.ro/scholar?q=Vehicle-Pedestrian+Accident+Reconstruction%2C+Dumitrascu&btnG=&hl=ro&as_sdt=0%2C5

9. Dumitrascu D., Nedelcu A., Single Cylinder Diesel Engine Performances Estimation Using AVL Boost software, 12th International Conference - Recent Researches In Neuralnetworks, Fuzzy Systems, Evolutionary Computing And Automation, Transilvania University of Brasov, Romania, 2011, <https://dl.acm.org/citation.cfm?id=1991248>
10. Dumitrașcu D.-I., Assessment of potential risks that influence the traffic accidents, COMEC 2019, 21-22 Noiembrie, Brasov, https://intranet.unitbv.ro/Portals/0/UserFiles/User591/_Comec2019_Dumitrascu.pdf

Data: 09.12.2024

Conf.dr.ing. DUMITRAȘCU Dorin-Ion



Article

Influence of Road Infrastructure Design over the Traffic Accidents: A Simulated Case Study

Dorin-Ion Dumitrascu

Department of Automotive and Transport Engineering, Transilvania University of Brasov, 1 Politehnicii, 500036 Brasov, Romania; d.dumitrascu@unitbv.ro

Abstract: The influence of road infrastructure over the severity of road accidents, in particular some specific features of it, represents the subject of this study. Generally, when an accident occurs, its causes are represented by a number of factors such as driver experience, fatigue, driving under the influence of alcohol and other psychoactive substances, road configuration, weather conditions, speeding, distracted driving, and unsafe road infrastructure. Road design is a key factor regarding the safety of all traffic participants. In this paper, the influence of unsafe roadside element designs on the incidence of traffic accidents, the degree of vehicle passenger injury, and the level of car damage were investigated. The present study was inspired by the high number of accidents produced on European route E68 (DN1) in Romania, a significant part of which was generated and accentuated by the effects of improper roadside design.

Keywords: road infrastructure; accident; forgiving or unforgiving roadside; safety; ditch; accident simulation



Citation: Dumitrascu, D.-I. Influence of Road Infrastructure Design over the Traffic Accidents: A Simulated Case Study. *Infrastructures* **2024**, *9*, 154. <https://doi.org/10.3390/infrastructures9090154>

Academic Editors: Alessia Ruggeri and Orazio Pellegrino

Received: 4 August 2024

Revised: 2 September 2024

Accepted: 3 September 2024

Published: 9 September 2024



Copyright: © 2024 by the author. Licensee MDPI, Basel, Switzerland. This article is an open access article distributed under the terms and conditions of the Creative Commons Attribution (CC BY) license (<https://creativecommons.org/licenses/by/4.0/>).

1. Introduction

Road accidents and their causes and effects represent a major problem for any country from a medical, social, and economic point of view. In this context, identifying and understanding the complex factors that affect road accidents represent an essential research field for road safety.

Therefore, the need to improve road safety must be a mandatory objective for transport authorities, which can be met through certain strategies, such as new or improved infrastructure, tougher legislation, traffic participant education, etc. The sooner strategies are used to intervene on the contributing factors of road accidents, the more visible the preventive effect will be.

All these aspects must be included in a safety system approach [1] based on suitable procedures, methods, and policies in order to develop and improve road safety. The interest for studying factors affecting road safety—the effects of road and traffic characteristics—represents a dynamic field in continuous evolution.

The European Road Safety Observatory (ERSO) provides reliable and comparable data about road accidents, detailed information and analysis about road safety trends, and procedures and policies in the European Union (EU). Considering the ERSO annual report, the 2023 report reveals stalling progress in reducing road fatalities in too many countries [2]. Despite this, reducing traffic accidents and their fatalities and improving road safety represent a continuous concern for the EU.

In this regard, the European Commission [3] set a target for 2030 to halve the number of serious injuries in the EU, considering 2020 as a landmark, and set an ambitious objective of minimizing towards zero fatalities in the long term for the year 2050, termed “Vision Zero”.

This goal aligns with the United Nations resolution [4], which declared the period 2021–2030 as the Decade of Action for Road Safety, with the target of preventing at least 50% of all road traffic injuries and fatalities by 2030.

Going back to the ERSO report, it also reveals that Romania is characterized by one of the highest incidence of road accidents in the EU. Ref. [5] reveals that among the most common causes are excessive or inappropriate speeds, especially in bad weather conditions. In Romania, most road accidents take place on national roads, but it is important to mention that the most frequent fatal accidents take place on highways. Over 30% of the serious accidents that have occurred have been on national roads. It must be admitted that it is not only an infrastructure problem but also includes the fact that the accidents were caused by people.

The year 2022 represents the starting point of the National Road Safety Strategy implementation for the period of 2022–2030. The main directions of action stipulated by it are a high-performance management of road safety, safer conditions for the use of roads, increased security conditions for the infrastructure, and prevention and monitoring, as well as optimal interventions in cases of emergency situations [5].

In order to achieve similar goals, [1] foresees the implementation of a Safe Systems procedure for road safety, based on the following main elements:

- Human behavior—considering that no matter how well people are trained for responsible road use, they can make mistakes, and road infrastructure must be developed while taking this aspect into account.
- Human frailty—consisting of the limited resistance of the human body to various types of collisions and mechanical stress, the assessment of the injury risk, and the severity of injuries. It represents another design criterion.
- Forgiving systems—meaning that any human error must not be potentiated by the road, correlating with vehicle type and interaction with other traffic participants.

The forgiving roads concept [6] assumes the minimization of driving error consequences, rather than preventing them, and this is mainly because of the human factor, which can be estimated.

Having this principle as a guideline, the entire road infrastructure must comply with the following:

- Minimize the risk of vehicles leaving the carriageway by using vehicle active systems (e.g., line assist), correlated with appropriate road delineation.
- Provide an adequate stopping distance or recovery area when a car runs off the road.

If a collision still occurs with any roadside obstacles, it is mandatory that impact forces transmitted to the vehicle occupants be kept at minor levels (i.e., no fatal or serious injury outcomes). According to [7,8], the main approaches for studying road safety are represented by infrastructure characteristics (e.g., road type and configuration and investment levels), the environment (e.g., road geometrical design and weather conditions), and traffic conditions (e.g., vehicle types and traffic volume). These elements are critically related because proper road infrastructure will have a beneficial impact on the number and severity of accidents. Any other contradictory assumptions can be considered subjective, being dependent on drivers' experience and education.

An important aspect in the context of infrastructure sustainable development is to identify the risk factors related to it and their impact on road safety. It becomes obvious that such an in-depth analysis is specific to every EU country, for all road types, considering aspects such as road infrastructure design, environmental factors, and traffic volume and control.

Contributing factors to road accidents can be grouped as follows [7]: human factors (e.g., experience, fatigue, distracted driving, speeding, risky overtaking, and the influence of alcohol and/or psychoactive substances), road infrastructure factors (e.g., road type, surface type, road segment configuration—alignment, curve, tunnels, and junctions—and road side configuration), traffic factors (e.g., vehicle mix and density—congestion), environment and weather (e.g., winding road, fog, rain, frost, and snow), and vehicle design and physical conditions (e.g., safety systems, suspension condition, and tire wear).

In the above classification of road accident favoring factors it is mandatory to include weather conditions too, because in many circumstances they represent an aggravating factor in the frequency of accident occurrence [9,10] (accident risks are significantly higher during bad weather conditions). The meteorological phenomena type (e.g., rainfall intensity, fog, snow, etc.) is another element that must be considered during the road infrastructure design process, as well from the perspective of the forgiving roads concept [1]. Adverse weather conditions influence a driver's visibility (driver's standard reaction time is extended), reduce the friction coefficient between tires and carriageway, extend the stopping distance, while in the worst-case scenario they will determine the skidding and aquaplaning of the vehicle.

From the above analyses regarding the factors favoring the occurrence of accidents, having in mind [6], it becomes obvious that in addition to the human factor, any road infrastructure improvement can either prevent or, in the most pessimistic scenario, reduce the effects of human errors. So, a proper road system design can prevent human errors and this will be materialized in less traffic accidents. Ref. [6] considers three principles in order to prevent human errors during driving: keeping away from an unintended road use; avoiding considerable differences in direction, mass, and speed; preventing unpredictability amongst road users.

Passing from human error prevention to accident occurrence and injury severity, in [11] they are explained through the engineering system and human behavior as linked factors that represent two major elements of risk. An engineering solution can increase traffic safety, but at the same time it must not influence the driver's alertness. Road safety engineering and human behavioral adaptation represent key elements in reducing the number of accidents. In this regard [12] considers that road infrastructure design must be done in such a way as to ensure optimal driver behavior in terms of speed, anticipation, and attention. Situations as incorrect visibility of the carriageway, poor anticipation of road curves combined with inadequate speed, poor quality of tires or excessive wear of them, accentuated by unfavorable weather conditions (e.g., rainfall) can favor the occurrence of accidents.

The safe roads concept, in particular self-explaining roads [13], involves an understandable one from the driver's point of view, considering several important specific elements, such as: roadway quality in terms of adhesion and bump free asphalt surface, day and night visibility, predictable road regardless of weather conditions, road markings and traffic signs, road sector optimal geometric configuration, etc. On the other hand, a high density of road signs or markings in a complex traffic scenario, according to [14], may lead to an overload of information and an increased risk of driving errors. An optimal practical combination of those elements is able to level up driver confidence, anticipation, and attention, influencing his reaction time, both for safe driving and to avoid certain dangerous situations within reasonable limits.

Considering all the above presented aspects, by evaluating the dependence between infrastructure features and drivers' behavior, including limit situations, it is possible to decrease or suppress traffic accidents, especially those generated by the faulty design of road infrastructure.

Therefore it is mandatory to analyze accident causes and develop efficient countermeasures to eliminate these causes, by carrying out professional road safety analyses with appropriate implemented measures.

One of these measures refers to the introduction of consistency rules [6,15] in road design process. Design consistency refers to road geometry conformity with driver expectancy, generating predictability. Theoretically, drivers make fewer errors at geometric features that correspond to their expectations. An inconsistency in road design represents a geometric feature or a feature mix with unusual characteristics that drivers may approach in an unsafe manner. Such situations could lead to speed errors, inappropriate driving maneuvers, and finally to accidents. Their effects can be aggravated by inadequate roadside design, a fact which will be detailed in the following section.

2. The Study Scope

The paper's goal was to investigate the effect of the unforgiving roadsides on European route E68 (DN1) in Romania, over the degree of vehicle passenger injury, respectively, the level of car damage, and having as a base point specific accidents produced on the road sector between the cities of Braşov and Făgăraş, in Braşov county.

Also, the work aimed to reconstruct through software simulation the probable mechanism of the occurrence of such accidents.

The E68 (DN1) is one of the longest and most used roads in Romania, permanently recording high traffic values. The analyzed sector is a difficult one because of its configuration, and in addition the road sector is characterized by a high rate of accidents.

In the current study continuous hazards are addressed, and the ditches in particular, which generally are parallel to the roadway. The analyzed accidents were caused by vehicle run-off into ditches as can be seen in Figure 1.

Some relevant crashes are illustrated which occurred on the E68 (DN1) in Romania on the specified road sector. As can be seen in the photos, in most of the cases the impact between vehicle and ditch causes the car to overturn or roll over. In this scenario, apart from the material damage, it is also very important to evaluate the accident effect on the vehicle occupants.

The photos reveal that in most of the cases the vehicle–ditch accidents occurred in adverse weather conditions (wet road surface), a fact that indicates prior vehicle skidding, most likely induced by speeding or by a sudden steering maneuver due to poor understanding of that road section. Also, some photos show that the intervention of medical and extrication crews at the scene of the accidents was necessary, this fact representing an indicator of the crash severity.



(a)

Figure 1. Cont.



(b)



(c)

Figure 1. Cont.



(d)



(e)

Figure 1. Examples of accidents with hazardous roadside ditches—(a–e) vehicles overturning, rollover [16]. In the presented context two factors accumulate: first a human error, then accentuated by an unforgiving roadside, a ditch. Thus, the study becomes relevant by establishing the probable collision dynamics, respectively, through analyzing its effect on the vehicle’s occupants. More than this, some forgiving measures are necessary to be implemented in order to compensate such human errors, by reducing or eliminating its effects.

3. The Study Background

Generally, as it was mentioned before, there are a multitude of factors that can generate road accidents, related to the following: traffic volume, road type and its configuration, weather conditions, environment, and all categories of road users. In this regard, traffic characteristics (such as speed, density), insufficient driving skills, and road elements (such as geometry, quality and condition of the asphalt surface, roadsides design) can favor the occurrence of road accidents.

National roads in Romania, due to their multiple characteristics, constantly represent the category where a large number of serious road accidents occur, characterized by high values of injury and fatalities, speed being an important generating factor. Statistics show that 20% of serious traffic accidents in Romania are caused by speeding.

Several studies [17–21] analyzed the dependence between speed and accident frequency (accident rate), considering that increased speed causes more accidents. Certain drivers that are speeding, in limit situations, do not know how to manage them, or the reaction time combined with an avoidance maneuver does not allow them to avoid the accidents. In particular, a higher speed will also increase the total stopping distance of the vehicle while the probability of accident occurrence is also higher, especially in wet conditions (slippery road, poor visibility, different friction coefficients on tires, etc.). Thus, by reducing the speed, a decrease in accident rate can be obtained.

On the other hand, speed cannot be seen as a stand-alone factor of accident occurrence, and with the speeding theory it is necessary to include other mixed elements such as the following: variations, road-tire interaction, driver experience, weather conditions, visibility, sudden trajectory change, erroneous estimation of a curve radius, etc.

Another major element in the safety field is the road itself. Its main design characteristics (e.g., geometry, alignment, curves, junctions, and all other infrastructure elements, including roadsides) could play an important role in improving traffic safety. For example, an increased number of curves on a certain road sector can increase the possibility of accident occurrence. This fact can be accentuated by the adverse weather conditions and drivers’ lack of experience in managing the relevant road section. Depending on the particularities of the road sector, the type of accident, and the traffic conditions, only material damages can result, but in certain situations the occupant injuries can also occur. Herein, the improper design of road infrastructure can affect in a negative manner the road safety.

According to [14] a significant percentage of fatal road accidents in the EU are single-vehicle type accidents, classified as run-off-road accidents (vehicle leaves the carriageway and crashes to the roadside).

Roadside hazards can be grouped as follows [1,14]:

- Single fixed obstacles (e.g., trees, vegetation, utility poles, road signs, safety barrier terminations, rocks, drainage features, etc.);
- Continuous hazards (e.g., ditches, slopes, road restraint systems, curbs, etc.);
- Dynamic roadside hazards (e.g., pedestrian and bicycle facilities, parking).

In Romania, the special characteristics of the road (e.g., curve, tunnel, bridge, intersections, railway crossing, etc.) can be the generating factors for the occurrence of road accidents. Similarly, in this study for the analyzed years (2020, 2021, and 2022), the curve and the intersection represent the infrastructure elements with a high potential risk of accidents (Table 1, number of accidents per year). Ref. [22] represents the source of statistical data that are analyzed in the present section of the study.

Table 1. The situation of road accidents according to the characteristics of the road.

Year	Road without Specific Elements	Road Element	
		Curve	Intersection
2020	4092	1037	1061
2021	3332	744	790
2022	3138	739	795

The global analysis of the fatality index for the time period of 2020 to 2022 shows comparable values for the accidents in the case of the curve as the main characteristic of the road and for the case of the road without any specific characteristics (e.g., without curve or/and intersection—Figure 2). Although serious road accidents occur more frequently in intersections than in curves, the comparative statistical analysis indicates that the number of fatalities is lower in the intersection events (Table 2). It can also be mentioned

that the highest rate was recorded for serious accidents in the case of the two analyzed characteristics, curve and intersection (Figure 3, Table 3).

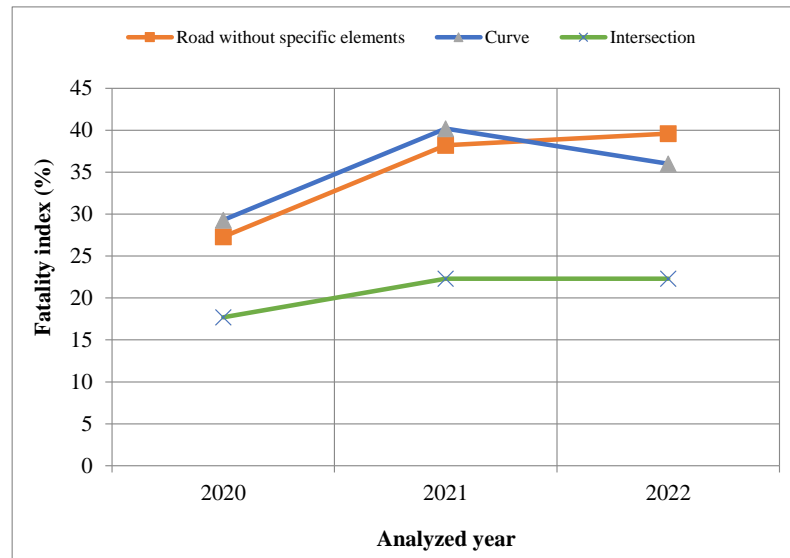


Figure 2. Comparative analysis of fatality index.

Table 2. Serious road accidents depending on road characteristics.

Year	Curve			Intersection		
	Fatalities	Serious Injuries	Serious Accidents	Fatalities	Serious Injuries	Serious Accidents
2020	304	975	1037	188	996	1061
2021	299	619	744	176	678	790
2022	293	601	739	177	686	795

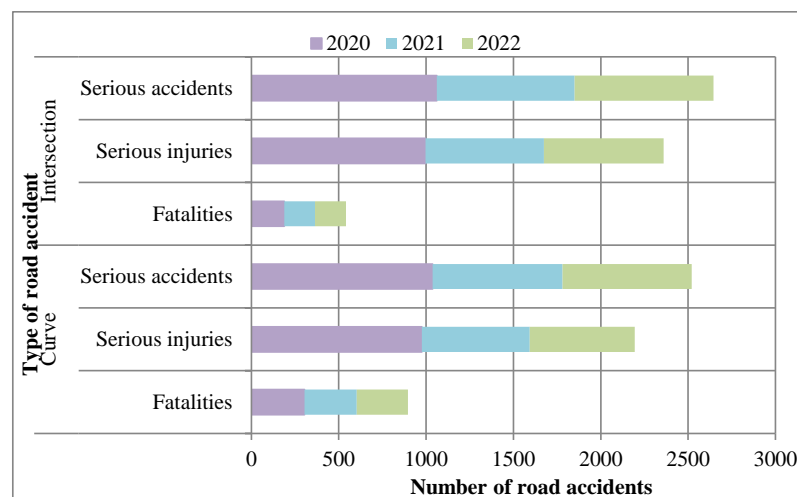


Figure 3. Accident analyses for the period 2020–2022.

Table 3. Fatality index.

Year	Road without Specific Elements	Road Element	
		Curve	Intersection
2020	27.3	29.3	17.7
2021	38.2	40.2	22.3
2022	39.6	36	22.3

4. Methodology

The literature regarding the vehicle ditch accident type is relatively limited [17], an experimental study being complex, expensive, and involving a considerable volume of work. A viable alternative solution is the software simulation of such a situation, considering as input data all the involved elements (e.g., vehicle rest position, deformations, road sector geometrical parameters, ditch main dimensions, weather condition, etc.). Through simulation, realistic results can be obtained and valuable information regarding the dynamics of this impact type (vehicle and occupants).

In the case of vehicle overturning or rollover, the strength of the vehicle body is an essential fact from the point of view of deformation amplitude, correspondence with occupant injury being a major factor regarding passive safety improvements.

Generally, overturning accidents have as the main cause cornering at high speeds, when the centrifugal force of the vehicle's mass is high enough to generate the overturning moment. A particular situation is represented by the impact of the wheels from one side of the vehicle with an obstacle on the roadside (ditch, curb), with overturning either or not preceded by skidding.

During the movement of the vehicle, sudden variations in the transversal inclination of the vehicle body appear as a result of the vehicle wheels from one lateral side passing over the ditch. The imbalances of the vertical reactions on the wheels generate a moment that produces overturning and eventually subsequent rolling.

4.1. Preliminary Data

As mentioned and illustrated previously, the present paper was inspired by specific traffic accidents (vehicles that run off into ditches) produced on the E68 (DN1) in Romania on the Braşov–Făgăraş sector; one important aggravating factor is the unforgiving roadsides, and bad weather conditions are also another element to be considered.

To carry out the study a relevant curved road sector with an unforgiving continuous element was chosen (Figure 4), where the main geometrical parameters of the ditch were measured. Other relevant geometrical elements (e.g., curve radius) of the considered road sector were imported from Google Maps application in the simulation software, including the map zone.



Figure 4. E68 (DN1)—curved road sector used for the study.

The aspects from photos regarding the vehicle positions, materialized damages, road conditions and roadsides represented the starting point in the development of the simulation, which allows the analysis of the dynamics of the accident.

4.2. Accident Simulation Scenario

For the simulation of vehicle–ditch collision, the specialized software PC-Crash 13.0 was used, that enables the reconstruction and analysis of various traffic accidents. The simulation goal was to investigate the cumulated effect of certain factors—curved road, weather conditions, unforgiving roadsides—over vehicle dynamics and occupant injury in the case of a vehicle that skids and runs off into the ditch, shown in Figure 4. The simulation scenario is a complex one and needs to consider and model a lot of parameters regarding road configuration, vehicle and occupant dynamics, including weather conditions that favor the occurrence of the event.

In order to generate the accident scene, the specific zone from Google Maps was imported in the PC-Crash 13.0 software, then a 3D road object tool was used to generate the specific road configuration, including the main ditch geometrical parameters (Figure 5).

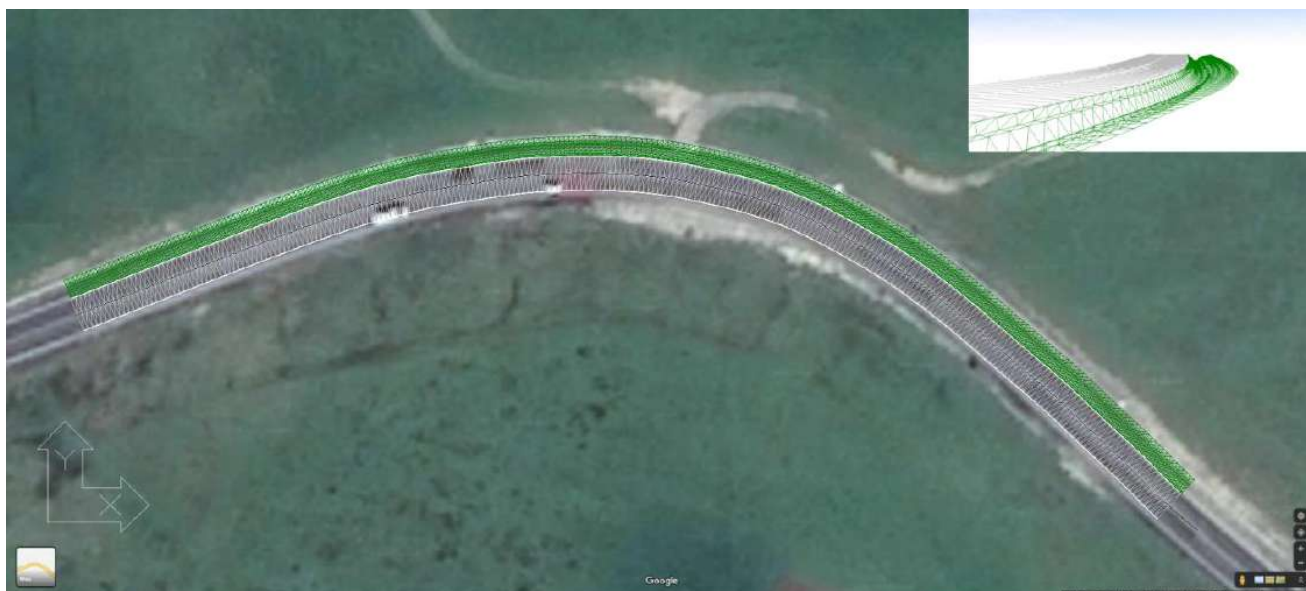


Figure 5. Simulation scene, ditch profile—E68 (DN1).

The simulation was conducted for rainy weather conditions, a preponderant scenario for such accident occurrence, and the coefficient of friction between wheels and carriageway was adopted accordingly (wet conditions).

As the vehicle for the simulation, an SUV type was used as this kind of vehicle is very popular in EU (in Romania, too). The vehicle dynamic parameter setup (e.g., speed, acceleration, braking, etc.) was made according to the geometrical road configuration and in such a manner as to accurately simulate a real-life vehicle skidding in the initial phase of the vehicle's movement into the curve, and after that the vehicle runoff into the ditch. In order to obtain a realistic accident mechanism and dynamics, the simulation parameters were continuously modified and optimized through iterations (e.g., speed, acceleration, braking, reaction time, etc.), until boundary conditions—vehicle rest position—were obtained.

For the calculation of movements and loads for vehicle occupants with PC-Crash software, the multibody model was used (Figure 6). Interaction of the occupants with the vehicle interior was also considered. Two restrained occupants were placed in the vehicle, on front seats in order to examine the motion during the impact. The individual bodies of the multibody system are interconnected by joints and for restrained occupants, seat belts are modeled using spring damper elements. In the multibody model, for each body

different properties can be specified, like: geometry (a body being defined as an ellipsoid), mass, moments of inertia, contact stiffness, and coefficients of friction [23].

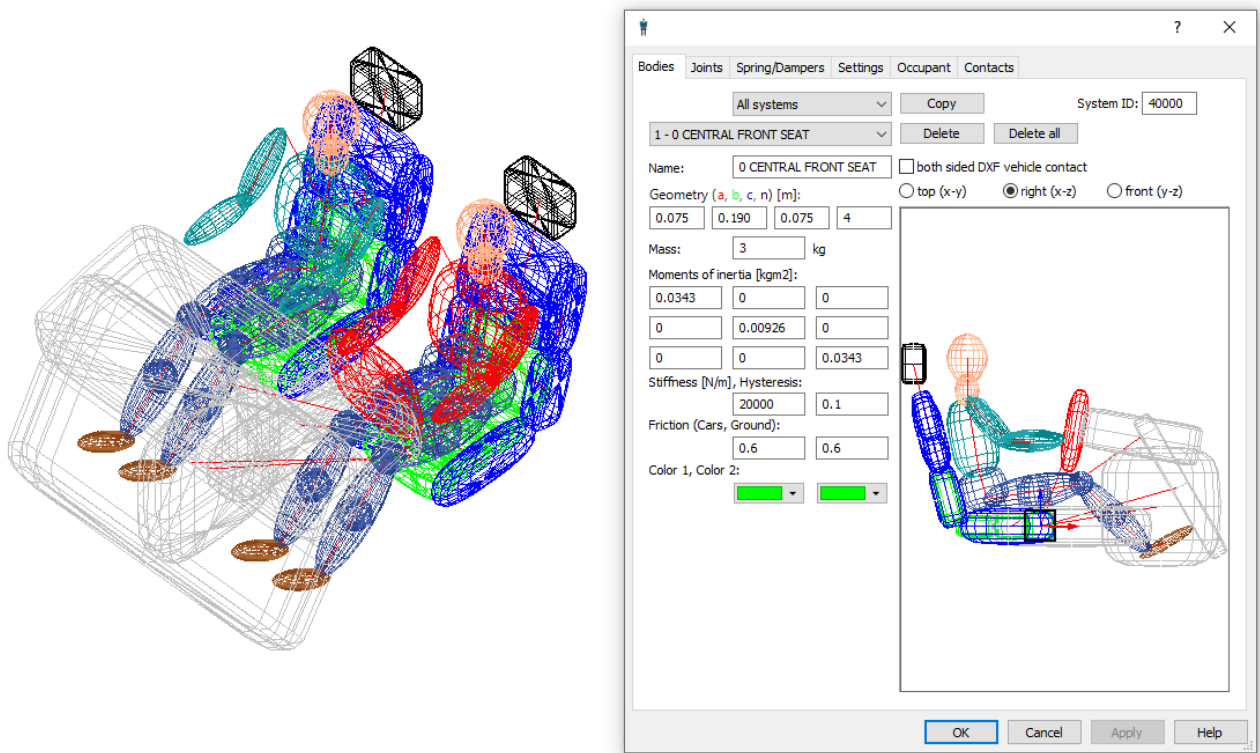


Figure 6. Multibody model used in simulation.

In Romania the speed limit on European national roads is 100 km/h. On the considered road sector, the input data for the simulation are detailed in Table 4.

Table 4. Simulation input data.

Vehicle Type	SUV, 4WD
Vehicle speed before entering the curve	90 km/h, case (a) and (b)
Friction coefficient, wet conditions	0.5
Maximum deceleration, wet conditions	4.91 m/s ²
Multibody model	2 front belted occupants: 80 kg, 1.8 m height each

4.3. Simulation Results

The performed simulation considered two possible scenarios inspired by accidents presented in Figure 1 and are presented as follows:

- (a) The vehicle entering into the curve is skidding, leaves the road, and enters into the ditch alongside with its direction of movement.
- (b) On entering the curve, the vehicle skids, enters on the opposite direction, and falls into the ditch on the left side of its travel direction. This scenario excluded the possibility of an impact with a vehicle coming from the opposite direction as this aspect is not the object of the present study.

For the proposed scenarios, the performed simulation revealed that the accident occurrence mechanism consists of two different phases: initially, the vehicle skidding appears to be due to the centrifugal force, and then the vehicle overturning and/or rollover is generated by the vehicle–ditch impact. In this case the vehicle overturning occurs independently of the road adhesion, being caused by the moment of the impact force.

These two phases are illustrated in Figures 7 and 8, that consist of successive frames of the accident dynamics at time intervals of 0.4 s for both analyzed cases. In Figures 9 and 10

the vehicle overturning and rollover for the same time intervals are detailed and for both cases.

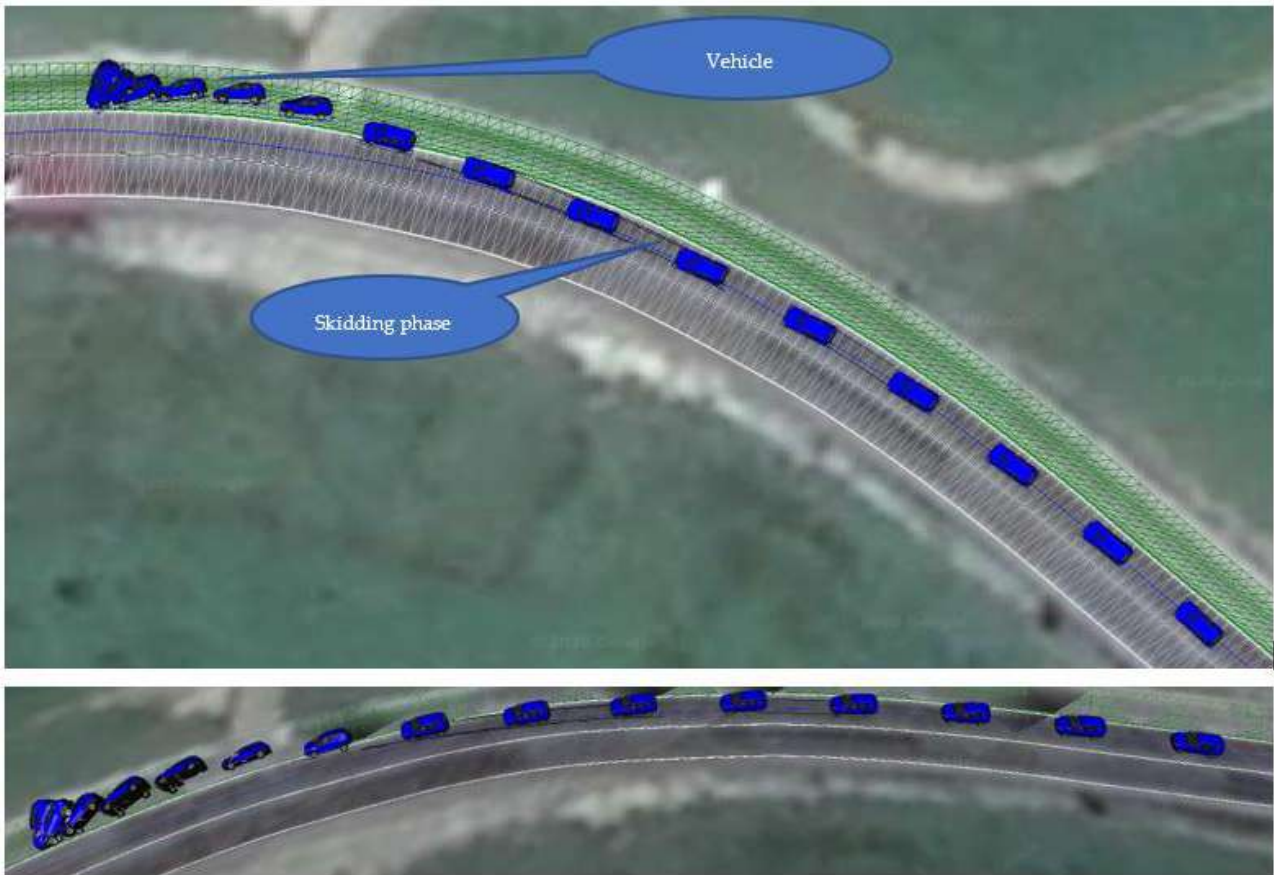


Figure 7. Consecutive simulation sequences at time intervals of 0.4 s—case (a).

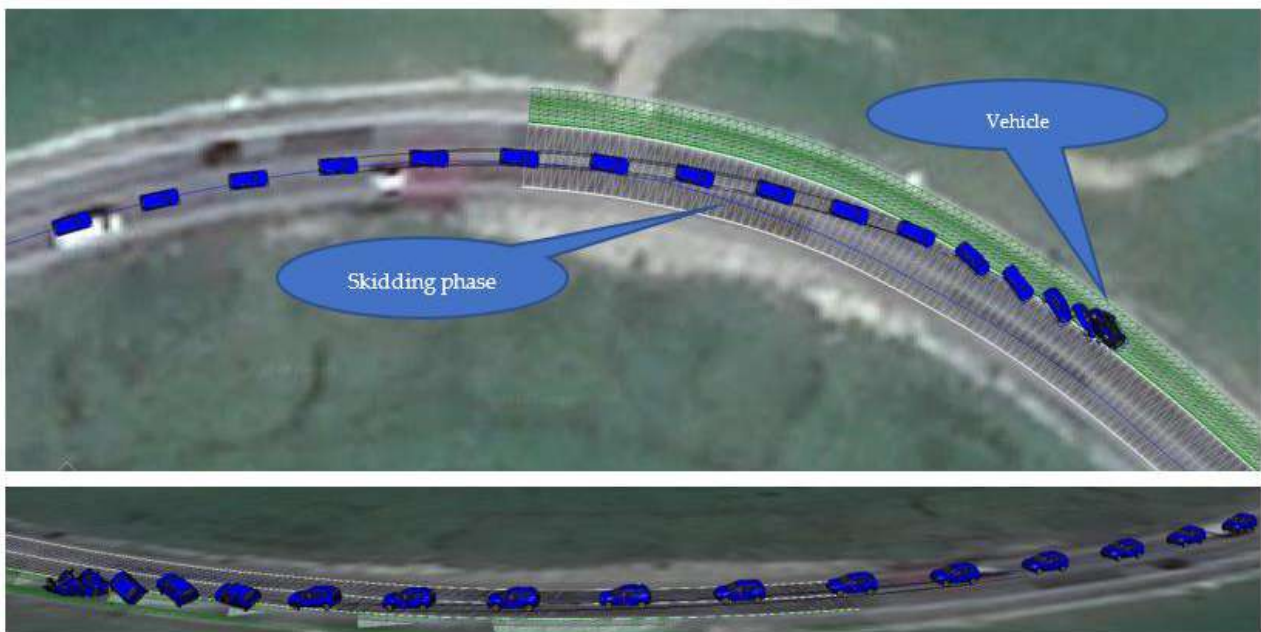


Figure 8. Consecutive simulation sequences at time intervals of 0.4 s—case (b).

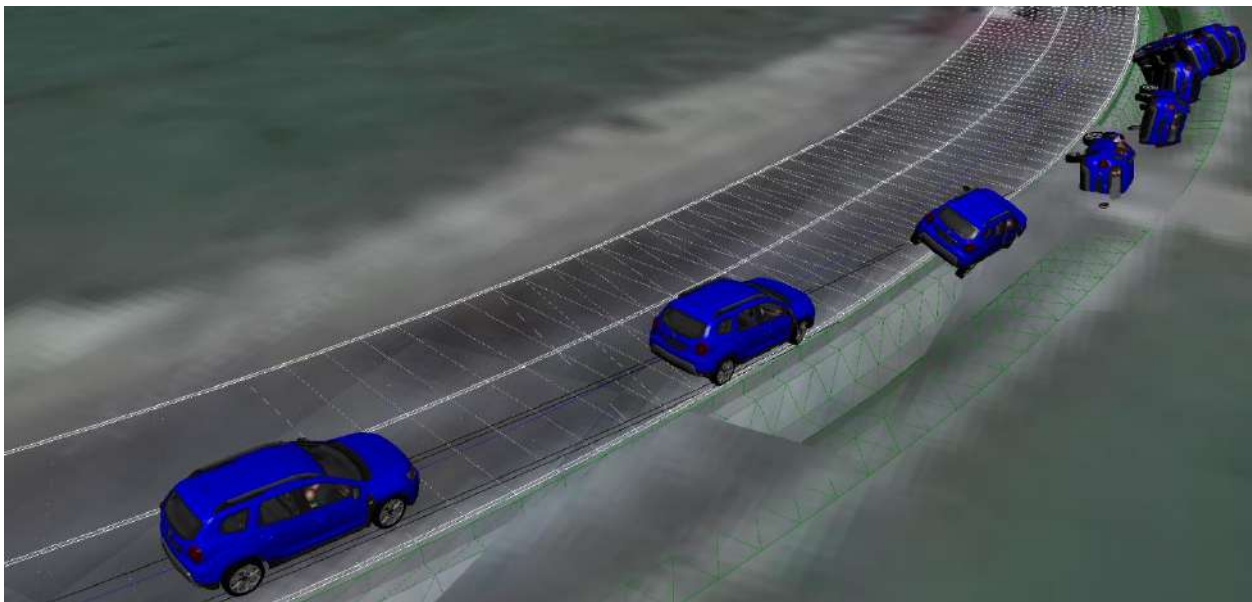


Figure 9. Vehicle overturning phase—case (a).

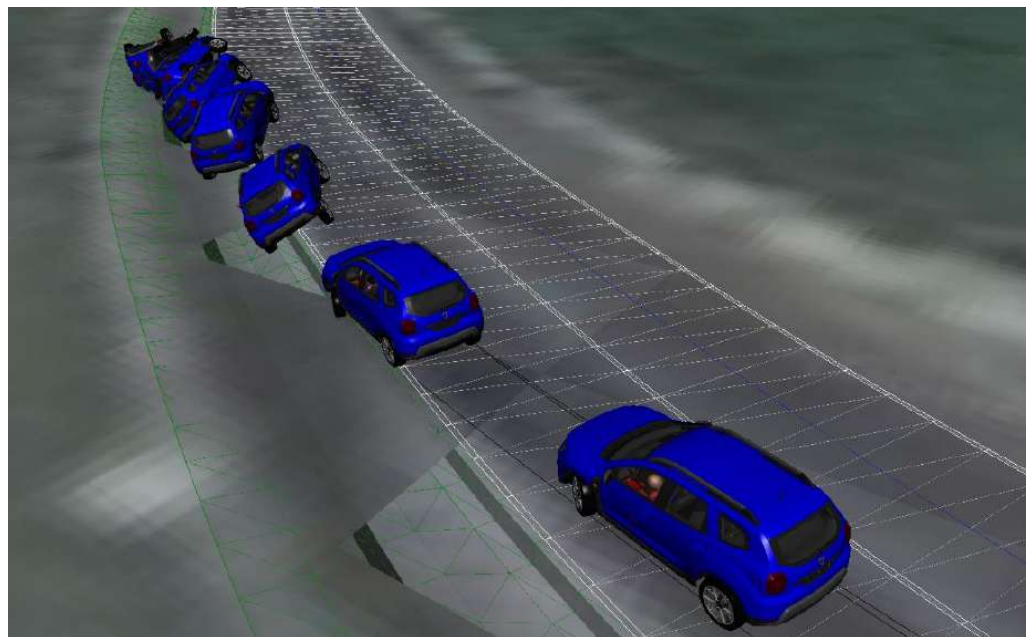


Figure 10. Vehicle overturning phase—case (b).

In both cases, the skidding phase begins with an instability of the movement, due to the inappropriate behavior of the driver, who did not adapt the speed properly to the road conditions (one of the significant factors that generates accidents in Romania).

The skidding phase that appears is characterized by additional energy consumption due to vehicle lateral deviation and rotation tendency, the friction with the road surface being more intense. The energy consumption is equivalent to the increase in rolling resistance. This phase is considered to be ended when the vehicle leaves the carriageway and starts to fall into the ditch.

Figures 11 and 12 show the vehicle speed variation in time. In case (b) compared to (a), the vehicle speed at the time when it starts to enter into the ditch is lower, 65 km/h versus 79 km/h, the initial speed being the same in both cases. In case (b) the higher initial speed decrease is determined by cumulated factors, such as: driver reaction and braking attempt, the vehicle that is skidding and enters in the opposite direction (the space traveled on the

carriageway is superior). Those elements generated a supplementary time that allowed, through controlled and uncontrolled actions, a lower impact speed of the vehicle with the ditch, theoretically with a direct effect on the occupant level of injury (but this is relative, depending also on the impact incidence angle of the vehicle).

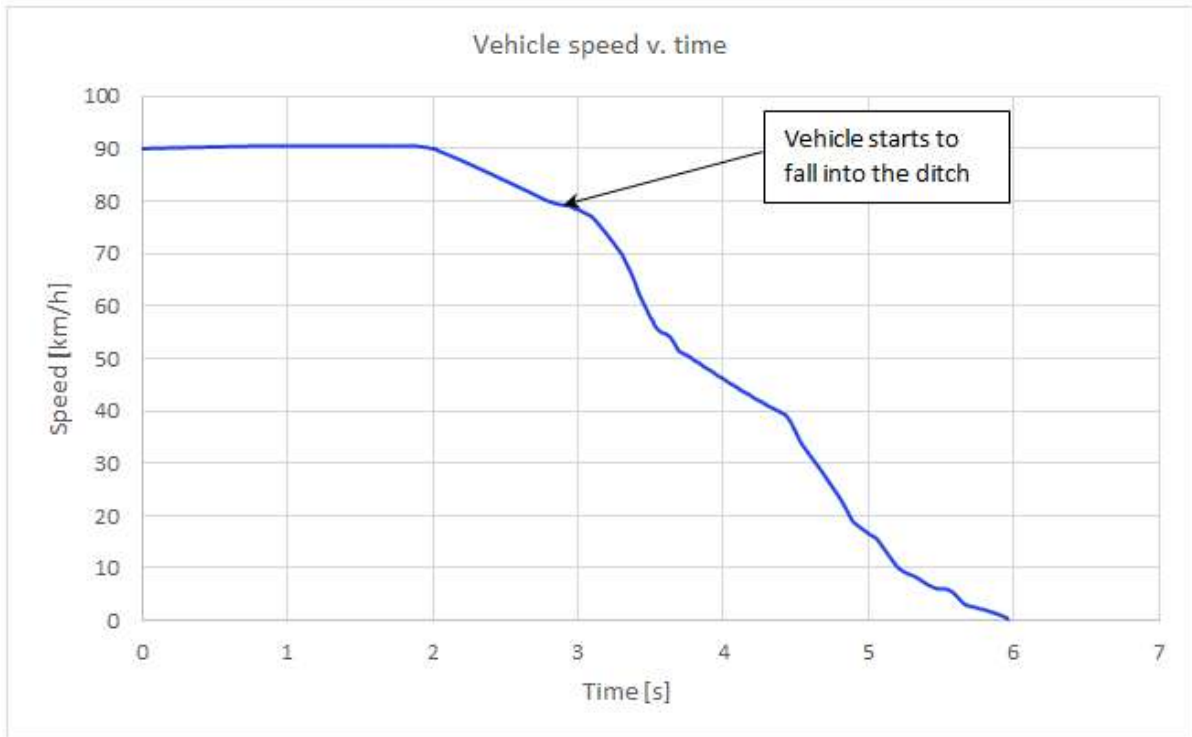


Figure 11. Vehicle speed—case (a).

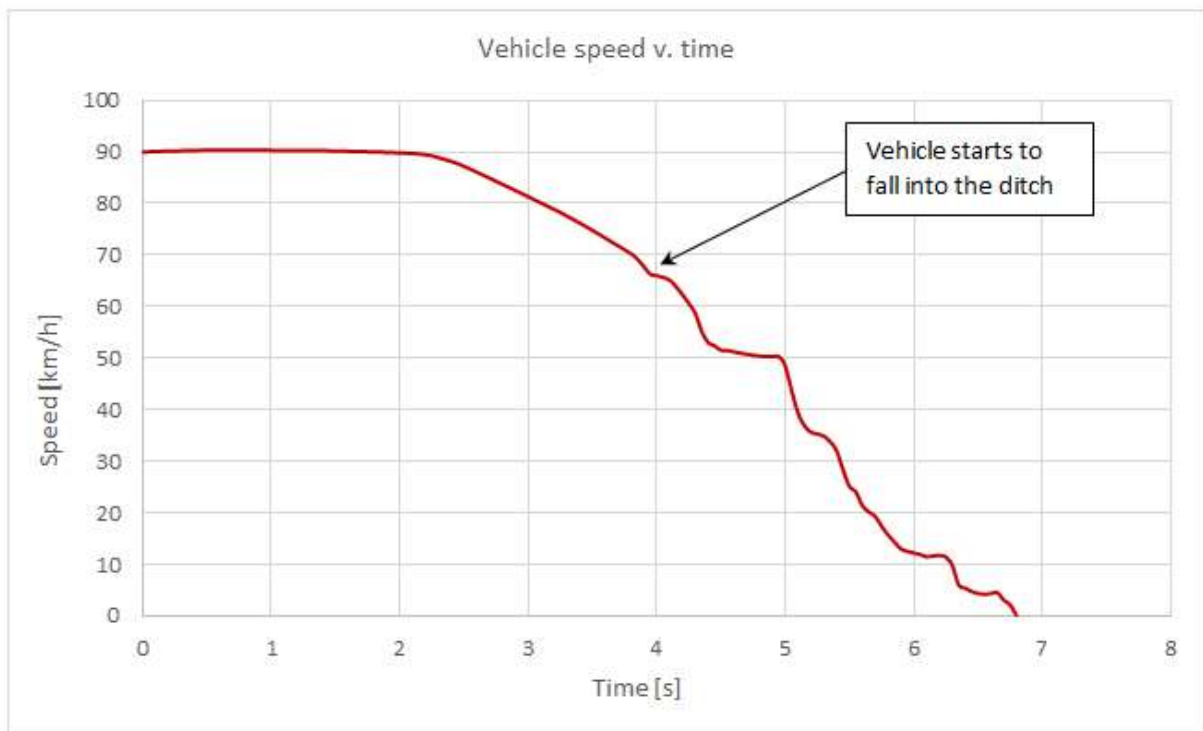


Figure 12. Vehicle speed—case (b).

The danger of injury to the occupants occurs mainly during the overturning phase, any intervention of the driver being excluded. The occupant level of injury depends in this phase on the vehicle kinetic energy and the obstacle (ditch) profile.

Practically, the overturning phase into the ditch is the one that generates vehicle damage and the injury level of the occupants, depending on the vehicle speed at the beginning of overturning or rollover and speed and acceleration variation during this phase (the initial impact incidence angle has to be taken into account too).

From Figures 11 and 12, it can be seen that the speed drop (kinetic energy, too) during the vehicle–ditch impact is determined by the following mechanism: vehicle body friction with the ditch surface and vehicle body deformation.

The impact between vehicle body parts and the ditch surface is highlighted by the acceleration graphs (longitudinal—long, lateral—lat, and vertical—vert), Figures 13 and 14. A Channel Frequency Classes (CFC) 60 filter was used for processing the impact signals, to eliminate the high-frequency noise and reduce the signal peaks. By comparing the graphs for (a) and (b) cases, it can be seen that the vehicle acceleration dispersion, as impact effect, is higher in case (a), but amplitudes are comparable. Thus, in case (a) predominant are the longitudinal accelerations with a maximal magnitude about 50 m/s^2 and lateral accelerations are about 30 m/s^2 , as a result of the vehicle sliding into the ditch. In (b) case a high amplitude of accelerations is obtained during the rollover of the car, but compared to (a), the time intervals where these peaks are obtained are narrow, about 0.5 s (interval 1, value 40 m/s^2) and 0.4 s (interval 2, value 85 m/s^2).

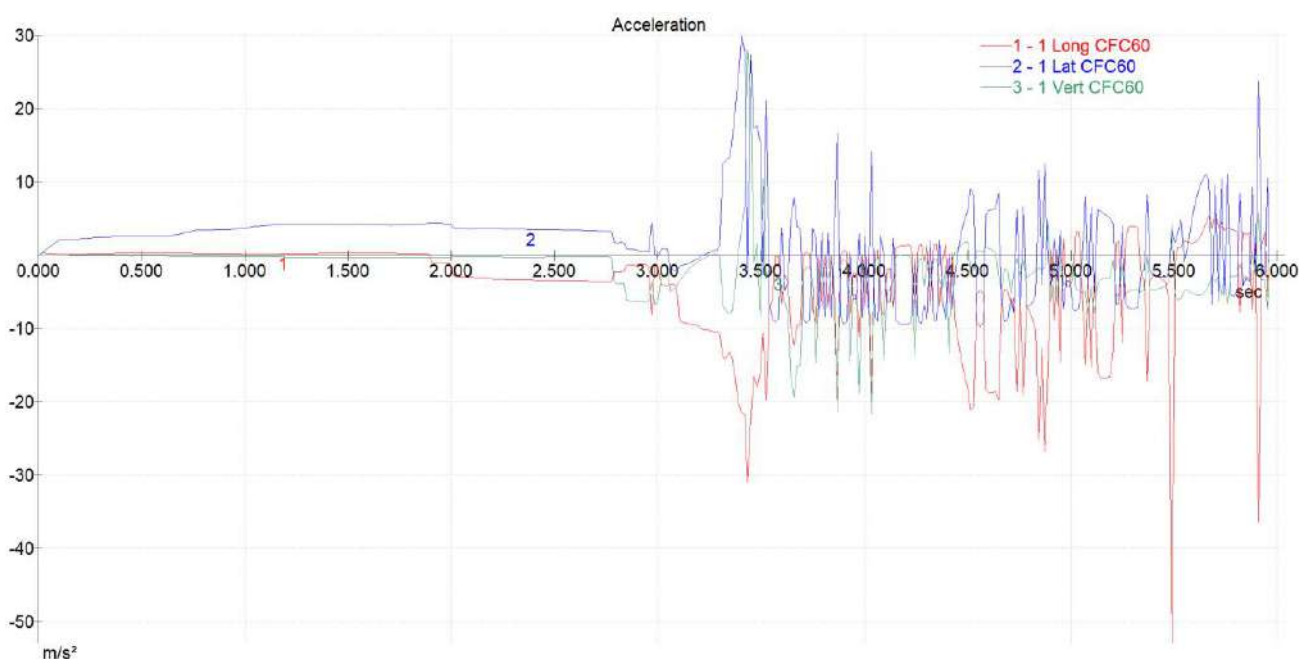


Figure 13. Vehicle acceleration—case (a).

The simulation frames and acceleration magnitude indicate an increased level of vehicle body damages induced exclusively by contact with the ditch surface. In case (a) the front and right side of the car are damaged. In (b) case, due to the vehicle overturn/partial rollover the entire vehicle body is affected (after a specialized damage evaluation it could be considered total damage).

As mentioned before, for the occupants’ kinematics the multibody module was used. For them, important speed differences occur in the case of collisions with other vehicles or obstacles. High accelerations appear when the vehicle, for example rotates around its longitudinal axis (overturning or rollover).

After the multibody system simulation is performed, the most important data are those related to accelerations, because the severity of the occupants’ injuries depends on

them. In the case of the current research, the most susceptible human body parts that can be seriously injured are head and neck. This is because of the possibility of the head hitting the car roof or practically with any hard parts inside the passenger compartment. In this type of accident other elements that can influence the injury severity are: the vehicle size, vehicle body deformation level, rollover number, obstacle size, obstacle that penetrates passenger compartment, etc.

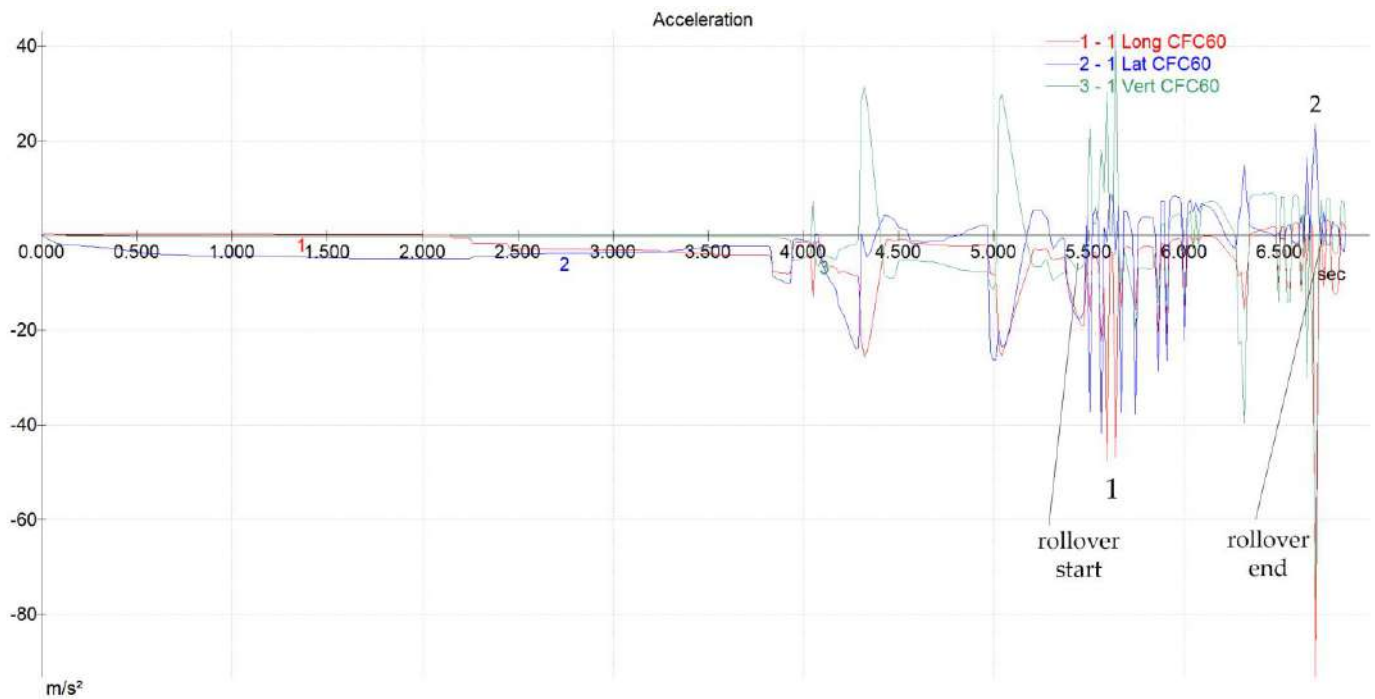


Figure 14. Vehicle acceleration—case (b).

In order to avoid head injury, in theory the acceleration magnitude should not exceed a certain level, as studied through the head injury criterion (HIC) that considers the duration and severity of the impact. According to [24] HIC is the most important parameter regarding human survival. It characterizes the brain injuries due to the impact of the head in vehicle accidents. An alternative evaluation method refers to average acceleration that is greater than 80 g for no longer than 3 milliseconds (ms).

In [25], it is mentioned that the human body supportability limit is about 10–35 g, at gradients of 500–1000 g/s with a maximum duration of 0.15–0.4 s. According to [26] the human body exposure to acceleration higher than 30 g lasting longer than 0.2 s may cause fluid displacement or tissue deformation. The symptoms appear as a blood pressure drop, pulse rate rise, weakness, and skin pallor. These aspects refer to a forward seated position. In the backward-seated position, acceleration up to 35 g can be tolerated without significant difficulties [26].

In the current study, in case (a) (Figures 15 and 16) the maximum obtained value of head acceleration (right-side occupant) was about 240 m/s², 24 g, that correspond to HIC15 < 130 (equivalent acceleration < 55, for 3 ms) inducing no concussion to the occupant, possibly headache or dizziness, with effects for less than an hour according to [27].

In case (a) the vehicle entered tangentially into the ditch and an important amount of the kinetic energy of the vehicle was dissipated through the friction between the lateral side and the ditch wall, an effect that contributes to non-injury of the occupants (but this is a particular aspect induced by particular dynamics) and only some temporary, minor effects. For the right-side occupant, the acceleration is higher due the fact that the vehicle hits the ditch first with its right lateral side.

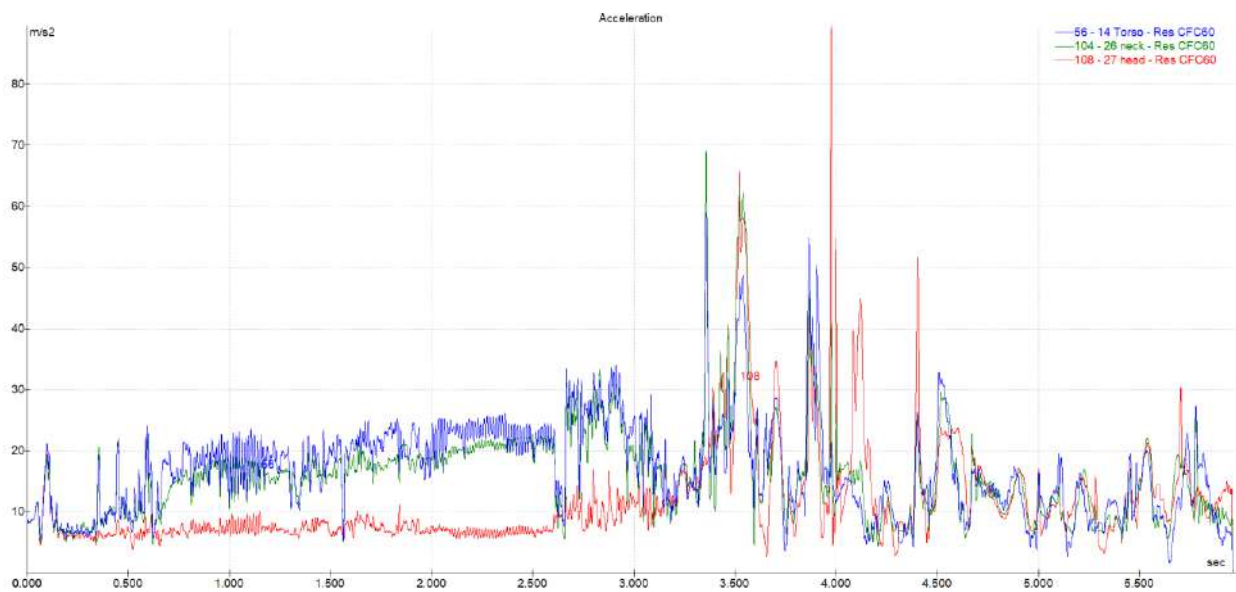


Figure 15. Driver acceleration—case (a).

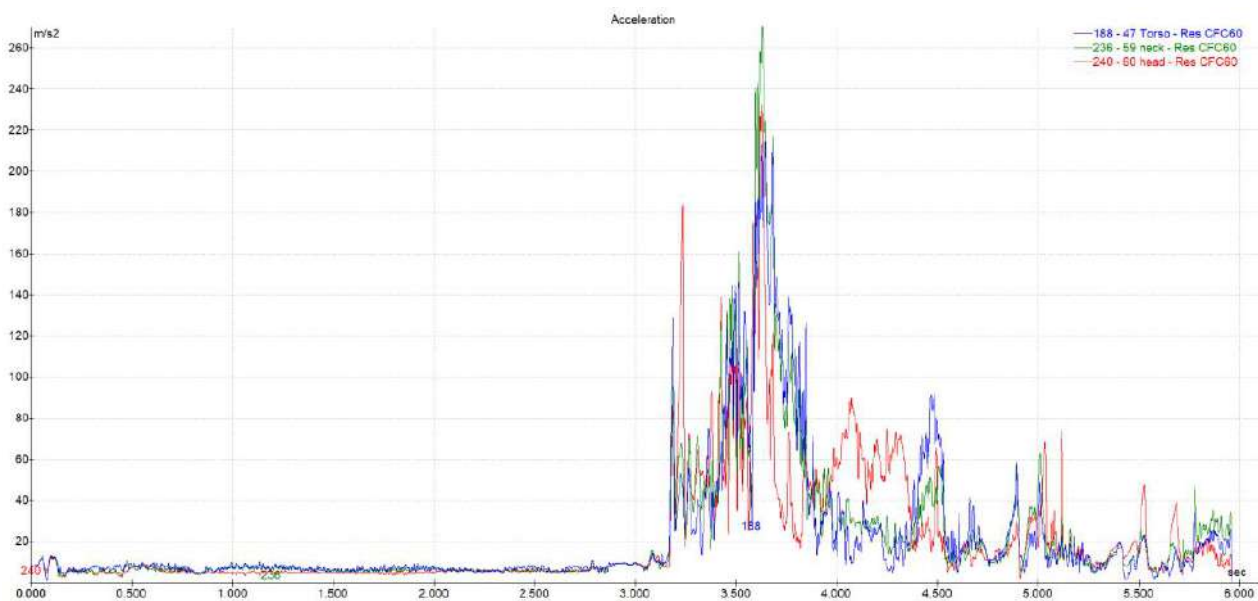


Figure 16. Front right-side occupant acceleration—case (a).

In case (b) (Figures 17 and 18) the maximum value obtained for the acceleration for the driver’s head was about 210 m/s², that correspond to HIC15 < 130 (equivalent acceleration < 55, for 3 ms) inducing no concussion to the driver, possibly headache or dizziness, with effects for less than an hour according to [27]. The maximum value for acceleration for the right-side occupant was about 412 m/s², 41 g, a value that corresponds to HIC15 180, the occupant suffering mild concussion according to [27].

In the analyzed (b) scenario, the vehicle overturn (partial rollover) induced higher accelerations for both occupants, which indicates a different mechanism of kinetic energy dissipation for that impact type.

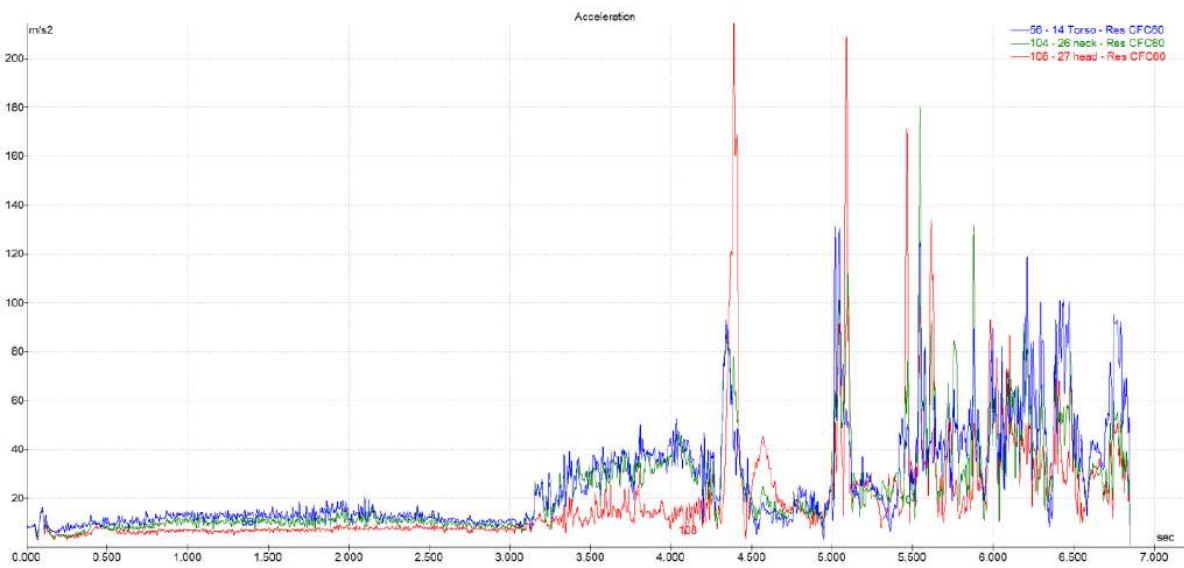


Figure 17. Driver acceleration—case (b).

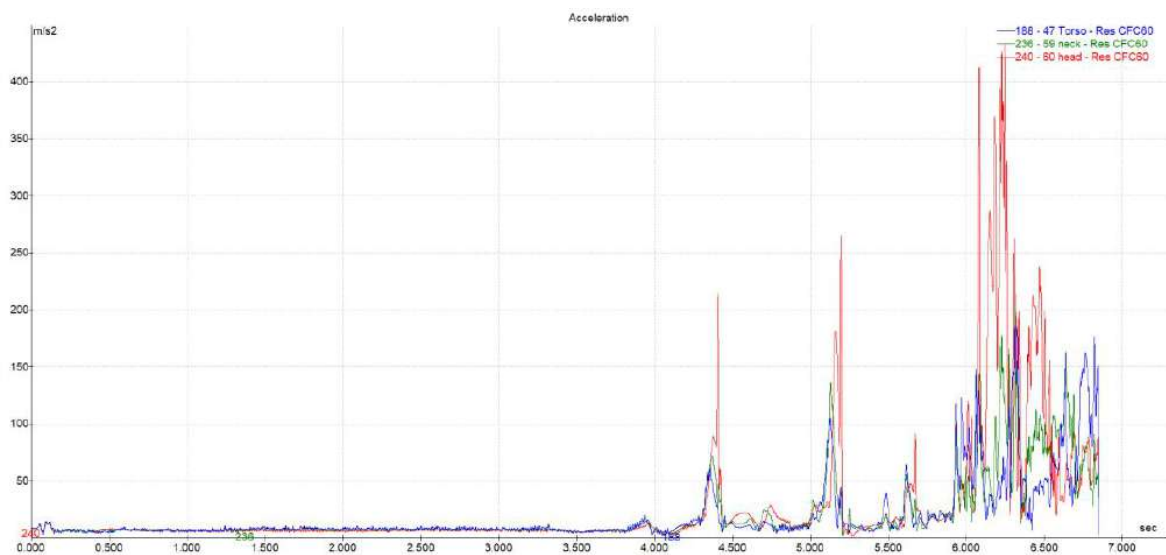


Figure 18. Front right-side occupant acceleration—case (b).

5. Discussions and Recommendations

The majority of the accidents involving vehicle overturning or rollover occur outside the carriageway (the vehicle leaves the road and enters the roadside), this type of accident being considered as a run-off-road accident [14]. Every such accident is unique due to its particularities: vehicle type and load, terrain characteristics, obstacles, road design, driver experience and perception, the incidence angle of the impact, obstacle dimensions, etc. If the vehicle during the rollover does not hit any obstacles this kind of accident is less dangerous due the fact that vehicle kinetic energy is dissipated over a longer time compared to a crash between two vehicles.

The objective of the present study was to particularize and analyze the situation when the vehicle’s overturn or rollover was induced by an unforgiving roadside, as the effect of a run-off-road phenomenon. Simulation results show major damage of the vehicle body induced exclusively by the impact with the ditch and obviously a considerable repair cost. In the situation of vehicle rollover, the necessity to replace the car with a new one may have to be considered.

From the performed analysis results that the ditch represents an unforgiving roadside, because due to human error, it caused the actual accident, as it was in contradiction with the concept of a forgiving roadside [1,14]. Through this idea, in the case of a run-off vehicle, the roadside through its design, must either avoid the accident or minimize its consequences.

In this context the most important factor is the health and safety of the occupants and as could be observed this type of accident can affect this in a certain manner. A more dangerous scenario, compared to the analyzed one, could appear anytime in the case of some other types of vehicles, if the driver/occupants are not seat-belted, with different vehicle dynamic parameters, especially including a different vehicle incidence angle with the obstacle (ditch). Different dynamic conditions than those analyzed in the present paper could generate serious injury and vehicle damage.

For both studied cases, the vehicle damages took precedence compared to the level of occupant injury, this being a positive aspect of the research. The injury level was a little bit more serious in case (b). Both scenarios had as starting point the inappropriate road configuration estimation by the driver, materialized by over speeding in wet conditions (a frequent real scenario). Even if the injury level obtained through PC-Crash software simulation was not a significant one for the front occupants, the potential psychological trauma cannot be ignored.

From the presented aspects, the study highlights the influence of an improper roadside design over traffic safety in the case of human error occurrence. Another relevant element that results from the research is the importance of auditing problematic road sectors in order to implement on existing roads the forgiving roadside systems.

Following the elements detailed before in the paper, for the analyzed problem (ditch-vehicle impact) as recommendation, the next solutions can be implemented in order to transform an unforgiving roadside into a forgiving one:

- Cover the ditch and create a safety zone in the proximity of the carriageway, combined with the measure of eliminating extra potential obstacles in problematic areas with a high rate of roadsides accidents. In this manner the vehicle that is out of control will pass over the covered ditch and there will exist the possibility to regain its control or to stop on the field without major or zero damages. It is necessary that the adherence of the covering material be close to that of the asphalt one. This fact is illustrated in Figure 19, where by such a measure, the covered ditch with an appropriate carriageway shoulder represents a recovery area, which will allow the driver in limit situations to perform recovery maneuvers. The effect will be injury free occupants and a vehicle free of damages.
- Modify ditch slope ratio; the slopes should be kept as shallow as possible. A shallow slope will allow the driver to regain control over the vehicle (Figure 20) [14].
- Isolate the ditch by mounting appropriate roadside barriers (e.g., rolling barrier), that will minimize the effects of a vehicle out of control. This is recommended where a previous solution is not possible through environmental limitations (Figure 21).
- Enlarge and pave the road side shoulder (Figure 22), and by that measure, in reasonable limits, a recovery zone is created for the drivers (where it is possible on existing roads), in a similar way to the ditch covering solution presented previously. This is known as a safety zone, where a driver can regain the control over the vehicle.

In this study, a few possible solutions were indicated, through which implementation of real conditions a reduction in frequent roadsides accidents was created and an increase of traffic safety in any conditions obtained, both on the studied road sector and in general on Romanian national roads. The paper had in mind the evaluation of vehicle damage level and occupant injury severity for a simulated situation, inspired by real traffic accidents on the same European road sector. On the other hand, the paper can be seen as an input study for also implementing the concept of forgiving roads in Romania, with real life benefits in reduction of traffic accident and their injury severity.

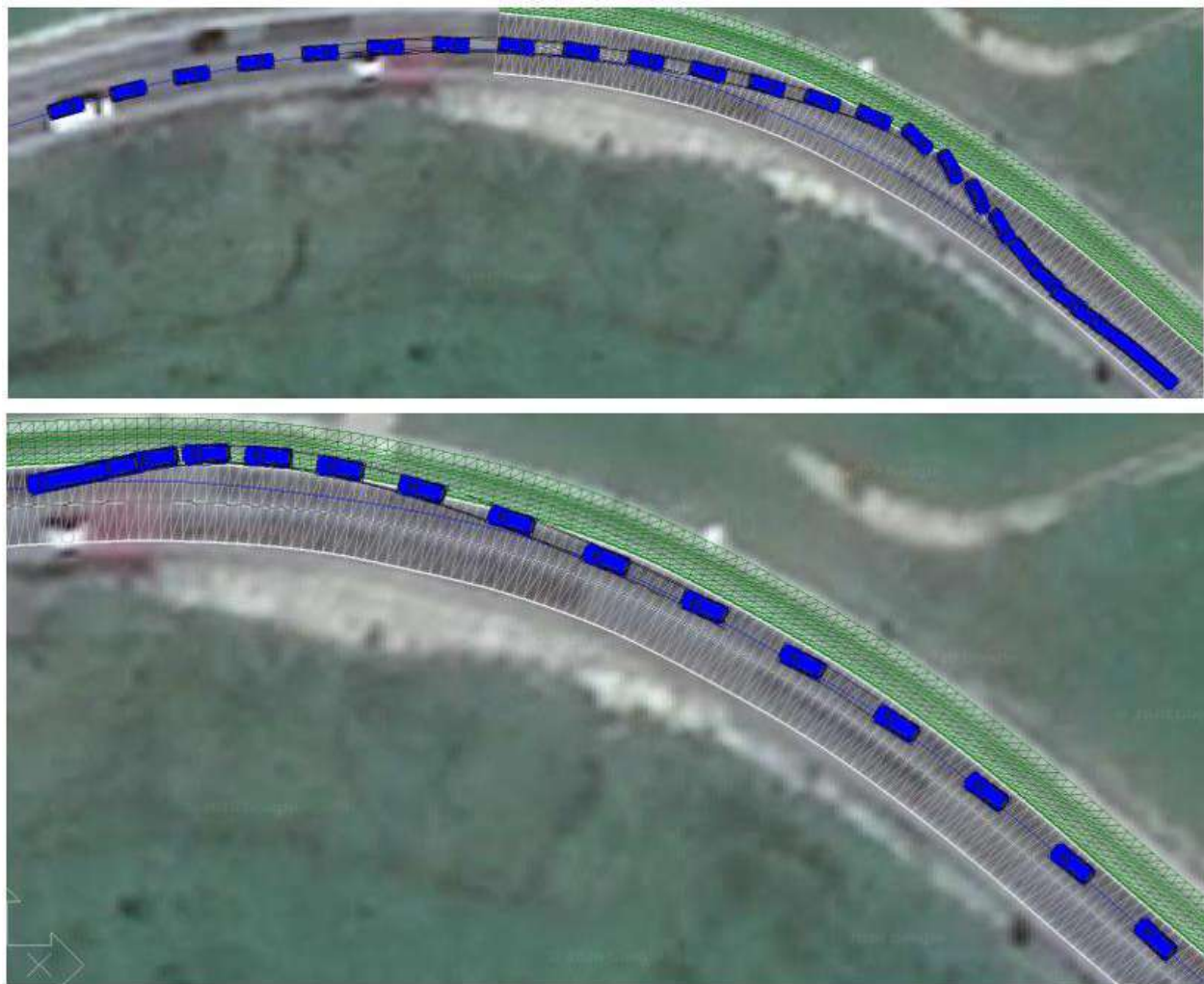


Figure 19. The effect of covered ditch solution.

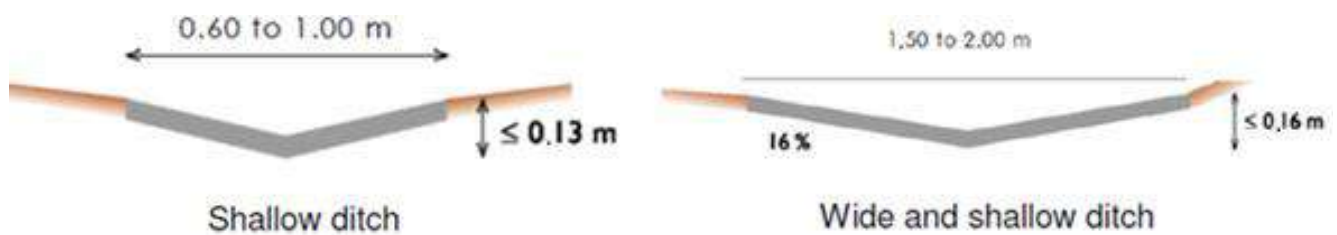


Figure 20. Examples of safe ditch [14].

The forgiving road concept, through its multiple possible technical solutions, will increase road safety and through it, the confidence of all traffic participants during usage of the Romanian national road network.

The study also reveals the practical utility of developing a road safety system, including adequate technical solutions to transform a road into a forgiving one with direct effect on traffic safety. From this point of view the relevant technical solutions and good practices experience can be the starting point for a standardization in the field of road safety.



Figure 21. Rolling barrier [28].



Figure 22. Enlarge and pave the road side shoulder—safety zone.

Funding: This research received no external funding.

Data Availability Statement: The data are contained within the article.

Acknowledgments: The author is grateful to the Transylvania University of Brasov for technical and financial support.

Conflicts of Interest: The authors declare no conflicts of interest.

References

1. A Guidance Document for the Implementation of CEDR Forgiving Roadsides Report. National Roads Authority (NRA). Available online: <https://www.tii.ie/media/3idngybj/forgiving-roadsides.pdf> (accessed on 10 May 2024).
2. European Road Safety Observatory (ERSO), European Commission, 2023. Available online: https://road-safety.transport.ec.europa.eu/european-road-safety-observatory_en (accessed on 12 July 2024).
3. European Commission, 2020. Next Steps towards 'Vision Zero': EU Road Safety Policy Framework 2021–2030. Directorate-General for Mobility and Transport, Publications Office, 2020. Available online: <https://data.europa.eu/doi/10.2832/391271> (accessed on 22 May 2024).
4. Improving Global Road Safety. Resolution A/RES/74/299, United Nations, 2020. Available online: <https://www.who.int/teams/social-determinants-of-health/safety-and-mobility/decade-of-action-for-road-safety-2021-2030> (accessed on 19 May 2024).
5. Buletinul Sigurantei Rutiere. Available online: <https://www.politiaromana.ro/ro/prevenire/buletinul-sigurantei-rutiere> (accessed on 12 May 2024).
6. Wegman, F. Influence of Infrastructure Design on Road Safety. In Proceedings of the International Symposium on Traffic Safety, A Global Issue, Kuwait, 15–17 January 1995.
7. Papadimitriou, E.; Filtness, A.; Theofilatos, A.; Ziakopoulos, A.; Quigley, C.; Yannis, G. Review and ranking of crash risk factors related to the road infrastructure. *Accid. Anal. Prev.* **2019**, *125*, 85–97. [CrossRef] [PubMed]

8. Albalate, D.; Fernández, L.; Yarygina, A. The road against fatalities: Infrastructure spending vs. regulation? *Accid. Anal. Prev.* **2013**, *59*, 227–239. [[CrossRef](#)] [[PubMed](#)]
9. Bergel-Hayat, R.; Debbarh, M.; Antoniou, C.; Yannis, G. Explaining the road accident risk: Weather effects. *Accid. Anal. Prev.* **2013**, *60*, 456–465. [[CrossRef](#)] [[PubMed](#)]
10. Malin, F.; Norros, I.; Innamaa, S. Accident risk of road and weather conditions on different road types. *Accid. Anal. Prev.* **2019**, *122*, 181–188. [[CrossRef](#)] [[PubMed](#)]
11. Wang, C.; Quddus, M.; Ison, S. The effect of traffic and road characteristics on road safety: A review and future research direction. *Saf. Sci.* **2013**, *57*, 264–275. [[CrossRef](#)]
12. Acerraa, E.M.; Lantieria, C.; Vignalia, V.; Pazzinia, M.; Andreaa, S. Safety roads: The analysis of driving behavior and the effects on the infrastructural design. *Transp. Res. Procedia* **2023**, *69*, 336–343. [[CrossRef](#)]
13. Matena, S.; Louwerse, W.; Schermers, G.; Vaneerderwegh, P.; Pokorný, P.; Gaitanidou, L. *Road Design and Environment—Best practice on Self-explaining and Forgiving Roads*; RIPCORD-ISEREST project deliverable D3, Bergisch Gladbach, Bast European Commission: Bergisch Gladbach, Germany, 2008.
14. La Torre, F. *Forgiving Roadsides Design Guide*; Conference Europeenne des Directeurs des Routes: Brussel, Belgium, 2013; ISBN 979-10-93321-02-8. Available online: https://www.cedr.eu/download/Publications/2013/T10_Forgiving_roadsides.pdf (accessed on 10 July 2024).
15. Fitzpatrick, K.; Anderson, I.; Bauer, K.; Collins, J.; Elefteriadou, L.; Harwood, D.; Irizarry, N.; Krammes, R.; McFadden, J.; Parma, K.; et al. *Evaluation of Design Consistency Methods for Two-Lane Rural Highways, Executive Summary*; Report No. FHWA-RD-99-173; US Development of Transportation, Office of Safety Research and Development: Washington, DC, USA, 2000. Available online: <https://highways.dot.gov/sites/fhwa.dot.gov/files/FHWA-RD-99-173.pdf> (accessed on 2 September 2024).
16. Accidents Photos Sources. Available online: <https://mytex.ro> (accessed on 10 January 2024).
17. Nilsson, G. *Traffic Safety Dimensions and the Power Model to Describe the Effect of Speed on Safety, Bulletin*, 221; Lund Institute of Technology, Department of Technology and Society, Traffic Engineering: Lund, Sweden, 2004.
18. Aarts, L.; van Schagen, I. Driving speed and the risk of road crashes: A review. *Accid. Anal. Prev.* **2006**, *38*, 215–224. [[CrossRef](#)] [[PubMed](#)]
19. Elvik, R.; Christensen, P.; Amundsen, A. *Speed and Road Accidents: An Evaluation of the Power Model*; TOI Report 740; The Institute of Transport Economics: Oslo, Norway, 2004.
20. Taylor, M.C.; Baruya, A.; Kennedy, J.V. *The Relationship between Speed and Accidents on Rural Single-Carriageway Roads*; TRL Report 511; Transport Research Laboratory: Berkshire, UK, 2002.
21. Taylor, M.C.; Lynam, D.A.; Baruya, A. *The Effects of Drivers' Speed on the Frequency of Road Accidents*; TRL Report 421; Transport Research Laboratory: Berkshire, UK, 2000.
22. Dinamica Accidentelor Rutiere Grave 2019–2023. Available online: <https://www.politiaromana.ro/ro/structura-politiei-romane/unitati-centrale/directia-rutiera/statistici> (accessed on 22 June 2024).
23. PC-CRASH. *A Simulation Program for Vehicle Accidents, Operating and Technical Manual*; Version 12.1; Dr. Steffan Datentechnik: Linz, Austria, 2020.
24. Virzi Mariotti, G.; Golfo, S.; Nigrelli, V.; Carollo, F. Head Injury Criterion: Mini Review. *Am. J. Biomed. Sci. Res.* **2019**, *5*, 406–407. [[CrossRef](#)]
25. Gaiginschi, R. Road Accident Reconstruction and Expertise. In *Reconstrucția și Expertiza Accidentelor Rutiere*; Publishing House Tehnica: Bucuresti, Romania, 2009. (In Romanian)
26. Deceleration Injury. Available online: <https://www.britannica.com/science/deceleration-injury> (accessed on 17 July 2024).
27. Head Injury Criteria Tolerance Levels. Available online: <http://www.eurailsafe.net/subsites/operas/HTML/Section3/Page3.3.1.htm> (accessed on 26 July 2024).
28. Google Maps. Available online: <https://www.google.com/maps> (accessed on 29 July 2024).

Disclaimer/Publisher's Note: The statements, opinions and data contained in all publications are solely those of the individual author(s) and contributor(s) and not of MDPI and/or the editor(s). MDPI and/or the editor(s) disclaim responsibility for any injury to people or property resulting from any ideas, methods, instructions or products referred to in the content.

Article

The Electromagnetic Noise Level Influence on the Laser Micro-Perforation Process Specific to Automotive Components

Alexandru-Nicolae Rusu ¹, Dorin-Ion Dumitrascu ^{2,*} and Adela-Eliza Dumitrascu ¹

¹ Department of Manufacturing Engineering, Transilvania University of Brasov, 5 Mihai Viteazul, 500036 Brasov, Romania; alexandru.rusu@unitbv.ro (A.-N.R.); dumitrascu_a@unitbv.ro (A.-E.D.)

² Department of Automotive and Transport Engineering, Transilvania University of Brasov, 1 Politehnicii, 500036 Brasov, Romania

* Correspondence: d.dumitrascu@unitbv.ro

Abstract: This article focuses on the influence of generated electromagnetic noise (energy) during the micro-perforation process. This study aims to investigate the critical parameters and effects of using laser technology in the processing of textile materials for airbags. Different levels of electromagnetic noise and material thicknesses were investigated to ensure the quality of manufactured parts and the best component performance. A factorial analysis (DOE) was developed to evaluate the influence of electromagnetic noise levels over pull test results and its effect on the micro-perforation process. The overall inferential analysis concludes a significant influence of the noise levels on micro-perforation processing. The detailed analysis suggests that 1.2 V is an optimal level of electromagnetic noise where the material maintains its mechanical properties in a more predictable and consistent manner. Additionally, the factorial design provides significant evidence for an interaction and main effects' influences of analyzed factors. The obtained results in this study have demonstrated that monitoring and controlling the noise level have beneficial effects over the laser processing. This ensures that the safety aspect of the produced parts is entirely upheld and protected. Also, this research contributes to improving the manufacturing process and ensures that high-quality products are obtained, being suitable for use in sensitive applications such as automotive airbags.

Keywords: laser micro-perforation process; synthetic leather; electromagnetic noise analysis; pull test force; design of experiments (DOE); airbag components



Citation: Rusu, A.-N.; Dumitrascu, D.-I.; Dumitrascu, A.-E. The Electromagnetic Noise Level Influence on the Laser Micro-Perforation Process Specific to Automotive Components. *Materials* **2024**, *17*, 4131. <https://doi.org/10.3390/ma17164131>

Academic Editors: Andrea Di Schino, Ming Li and Wenyong Zhang

Received: 4 July 2024

Revised: 3 August 2024

Accepted: 19 August 2024

Published: 21 August 2024



Copyright: © 2024 by the authors. Licensee MDPI, Basel, Switzerland. This article is an open access article distributed under the terms and conditions of the Creative Commons Attribution (CC BY) license (<https://creativecommons.org/licenses/by/4.0/>).

1. Introduction

Laser technology has transformed numerous industrial applications, notably in the material processing field, where its precision and efficiency are unmatched [1–4]. One critical application is in the manufacturing of textile components for airbags. The quality of these components is paramount, as they play a crucial role in ensuring the safety and performance of the final product. The micro-perforation process, specifically, must adhere to strict standards to prevent any compromise in the structural integrity of the airbag materials.

Previous research has focused on optimizing laser parameters for various applications without deeply exploring the effects of electromagnetic noise on the quality and uniformity of laser-perforated holes, especially in critical safety components like airbags. Noise in the context of laser processing refers to unwanted energy variations that can affect the stability and precision of the laser beam. Such variations can lead to inconsistencies in perforation size, shape, and edge quality, all of which are critical parameters for maintaining the functionality and safety of airbags.

Earlier studies have extensively explored the optimization of laser parameters to enhance processing efficiency and material quality for micro-hole perforation. For instance, Guo et al. [5,6] presented the fabrication of surface micro-nanostructures on metals using

femtosecond (fs) laser irradiation, leading to significant advancements in creating highly absorptive surfaces. While these studies have provided substantial insights into the structural transformations induced by laser processing, the specific impact of laser noise on the quality and uniformity of the resulting structures has not been thoroughly investigated.

Various researchers have since endeavored to enhance the antireflective characteristics of fs laser-formed surface micro-nanostructures to minimize metal surface reflectance [7,8]. For instance, Iyengar et al. [9] applied fs lasers to produce conical microstructures on titanium surfaces, achieving low surface reflectance values of approximately 3% over a broad spectral range (0.4–1.6 μm) and angular range (0–60°), with the lowest reflectance recorded at about 1.8% for specific wavelengths.

The fabrication speeds of conventional fs lasers make the process time-intensive for producing black metals by focusing fs laser beams directly on sample surfaces. To enhance processing efficiency, Paivasaari et al. [10] proposed a four-beam interferometric fs laser ablation technique, which facilitated the creation of hole-array structures on stainless steel and copper surfaces. Although nearly total absorption was achieved for stainless steel across the 200–2300 nm spectrum, copper samples exhibited a gradual increase in reflectance to approximately 50% at 800 nm. Additionally, nanosecond lasers have been utilized to blacken copper, achieving consistent absorption rates above 97% in the 250–750 nm range through the formation of highly organized periodic microstructures. However, a linear rise in reflectance up to 30% was noted between 750 nm and 2500 nm.

Research efforts have also investigated the antireflective properties of nanoscale structures formed by an fs laser on metal surfaces. Due to their dimensions being comparable to visible light wavelengths, nanoscale structures often exhibit selective optical responses. Dusser et al. [11] created oriented nanostructures on metal surfaces, which induce colorful surface effects and have been leveraged for generating specific color patterns.

Challenges persist in achieving effective light harvesting and minimizing surface reflection across a broad spectrum without wavelength dependence, critical for various applications. This necessitates continuous advancements in antireflection strategies, including conventional quarter-wavelength films, multilayered film stacks for destructive interference [12], direct moth-eye mimics, nanowire/porous-based dielectric structures for the gradient refractive index [13,14], single-scale metallic micro- or nano-features, multiscale hierarchical structures for light trapping [15], meticulously designed and fabricated metamaterials, and their patterned and dimension-varied counterparts for inducing resonance in ϵ and μ individually [16]. Ongoing research is also exploring novel light-harvesting approaches [17–22].

A significant breakthrough in antireflection research has been the development of coatings comprising vertically aligned carbon nanotubes, achieving ultra-low reflectance (<1%) across an ultra-broadband spectrum (from UV to far-infrared) [23,24]. Furthermore, advancements in ultra-broadband light harvesting from UV to THz ranges have been achieved by fabricating nanotip arrays on silicon surfaces, highlighting the potential for enhancing antireflection properties on metal surfaces.

From the perspective of micro-nanostructure fabrication, considerable challenges remain in achieving the designable, predictable, controllable, and scalable fabrication of surface micro-nanostructures across various materials. Addressing these challenges remains a continuous pursuit among researchers aiming to develop general strategies and techniques for fabricating such structures.

2. Objectives and Scope of This Study

This study focuses on the influence of generated noise (energy) during the laser micro-perforation process of synthetic leather airbag components. Noise in the context of laser processing refers to the unwanted energy variations that can affect the stability and precision of the laser beam. Such variations can lead to inconsistencies in perforation size, shape, and edge quality, all of which are critical parameters for maintaining the functionality and safety of airbags. By closely monitoring and controlling noise levels, the

aim is to optimize the production process, ensuring that the resulting airbag components meet stringent quality and safety standards. This approach not only enhances the overall efficiency of the manufacturing process but also contributes to the development of high-quality products suitable for critical applications in the automotive industry.

In this context, this paper details the experimental analysis, including the equipment and methodologies used, and presents a comprehensive assessment of the results. To assess the effects of electromagnetic noise levels on pull test force results, a factorial analysis was applied to underline the influences of the main effects and interactions of examined factors. The study findings will underscore the importance of controlling laser noise to maintain the integrity and performance of airbag components, ultimately contributing to advancements in the field of laser material processing.

The research from this paper presents a niche in the field of the impact of electromagnetic noise on the quality and consistency of laser micro-perforations in textile materials for airbags. Previous studies have largely concentrated on optimizing laser parameters without exploring deeply into how external factors like electromagnetic noise influence the process. By filling this gap, the research provides valuable insights into how controlling electromagnetic noise can improve the manufacturing process and enhance the safety and reliability of airbag components.

3. Materials and Methods

3.1. Materials and Equipment

The material subjected to testing is synthetic leather made from polyvinyl chloride (PVC) [25], with a nominal thickness of 0.8 mm. It is laminated with a spacer material having a nominal thickness of 2.99 mm and a specified tolerance of ± 0.3 mm. The combined material must meet strict strength and flexibility criteria to ensure airbag functionality.

The synthetic leather parts used in this study were selected to represent common materials utilized in the automotive component manufacturing industry for airbag production. The sample size consisted of 400 parts for each analyzed parameter: the laser noise, material thickness, and pull test results. For the factorial analysis, 1200 samples were considered.

The used equipment:

- ZwickRoell Z100 Testing Machine (Ulm, Germany) features a maximum force capacity of 100 kN. It provides a testing speed range from 0.0005 to 1000 mm/min with an accuracy of $\pm 0.1\%$ of the set value. It ensures force measurement accuracy within $\pm 0.5\%$ of the measured value, up to 1/1000 of the maximum load cell capacity. The machine has a test stroke of 1100 mm without accessories and operates on a power supply of 230 V, 50/60 Hz.
- The INSTRON 5967 Testing Machine (Norwood, MA, USA), with a maximum force capacity of 30 kN, offers a testing speed range from 0.001 to 3000 mm/min with an accuracy of $\pm 0.1\%$ of the set value. It ensures force measurement accuracy within $\pm 0.5\%$ of the measured value, up to 1/1000 of the maximum load cell capacity. The machine has a test stroke of 1130 mm without accessories; operates on a power supply of 100–240 V, 50/60 Hz; and utilizes Bluehill Universal software 4.5.

The ZwickRoell Z100 testing machine is used for evaluating the mechanical properties of laser-processed materials. Its features, such as high force capacity and measurement precision, make it ideal for testing textile materials, ensuring compliance with technical specifications.

The INSTRON 5967 testing machine is used for smaller-scale testing and applications requiring lower forces. With similar accuracy and flexible power supply, it complements the capabilities provided by the ZwickRoell Z100.

3.2. Evaluation Methodology of the Quality of Laser Micro-Perforations in Airbag Zones' Components

The quality of laser micro-perforations' process applied to materials used for airbags is evaluated based on several critical parameters. The size and uniformity of the perfora-

tions must be consistent across the entire material surface, as variations can compromise the functionality of the airbag. The ideal shape of the perforations is circular, and any deformation may indicate issues with laser parameter settings or beam quality.

The quality of the perforation edges is also essential; they should be smooth and well defined to prevent material degradation during airbag deployment. The depth of the perforations must be precisely controlled to ensure optimal performance, thereby avoiding any risk of structural failure.

The material surrounding the perforations must maintain its structural integrity without showing signs of thermal or mechanical degradation. It is important that the perforation process minimizes residue generation, as the presence of residues can affect both the aesthetics and functionality of the airbag.

The efficiency and speed of the micro-perforation process are important parameters for industrial production. An optimal balance between speed and quality is necessary to maintain efficient and economical production. To achieve high-quality perforations, it is crucial to optimize and precisely control laser parameters such as power, frequency, scanning speed, noise (energy in the electromagnetic field), and beam focus. The use of appropriate calibration equipment and regular maintenance significantly contributes to maintaining optimal performance.

For the analysis of the quality of laser micro-perforations in airbag zones, three test samples, each containing 400 pieces, were examined. These samples underwent a rigorous set of tests to evaluate the influence of the previously mentioned parameters: power and noise (energy in the electromagnetic field). The results of these tests provided essential data to ensure compliance with the safety and performance standards specific to the automotive industry.

3.3. Laser Processing

The laser used in this experiment has a total power of 2 kilowatts (kW), representing 100% of the device nominal power. The experimental settings include using 25% of the total power, while the two laser powers are set at 50% used from this percent. Additionally, within this 0.5 kW setting, the powers P1 and P2 are adjusted to 50% of 0.5 kW, equating to 0.25 kW each. The measurement of the laser power is conducted in discrete increments of 100 watts, up to the full 2 kW capacity, to ensure a comprehensive evaluation of the laser efficiency across its operational range. These settings are crucial for evaluating the performance and efficiency of the material perforation process (Figures 1 and 2). The pulse duration is 200 fs (femtosecond). This is unusual for CO₂ lasers, which traditionally have much longer pulse durations (in the order of nanoseconds). However, there are advanced technologies where different types of lasers are combined to achieve very short pulse durations, such as the Ti series pulsed CO₂ lasers.

With a production cycle of 15 s per part, it is crucial that the quality of the part in the visible area is ensured throughout the vehicles' lifespan. This means that micro-perforations resulting from the laser processing must not be visible and should not be influenced by factors that could compromise the integrity of the airbag or the esthetic appearance of the components.

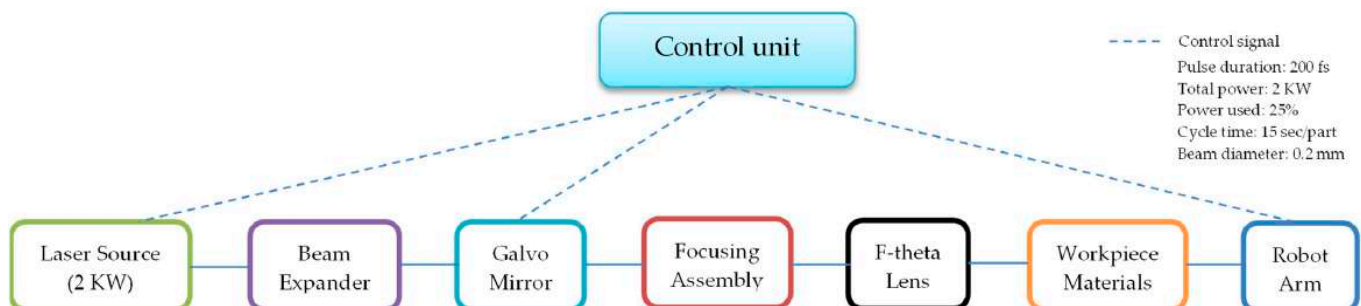


Figure 1. Schematic diagram of experimental setup with robot integration.

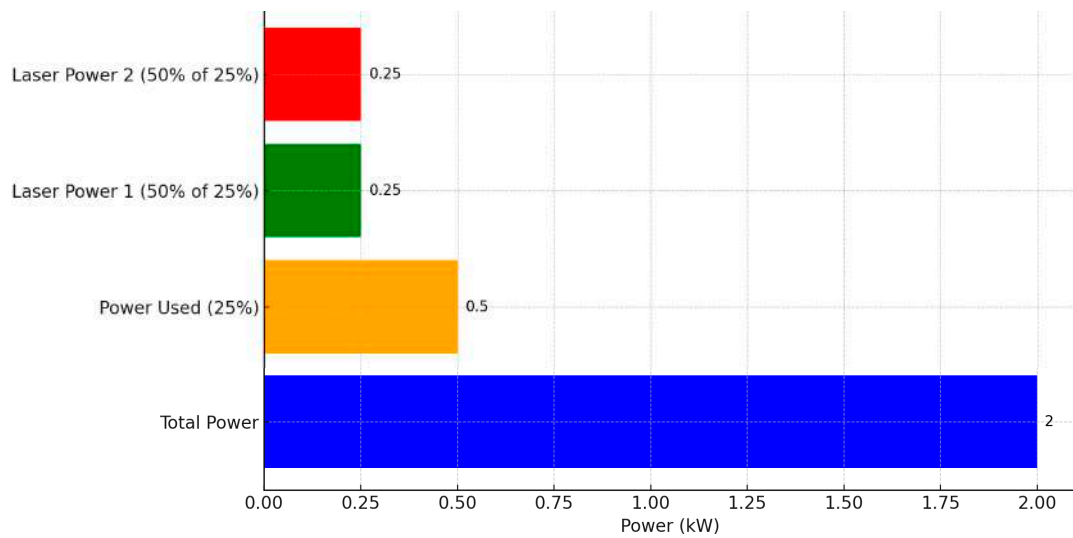


Figure 2. Laser power settings and distribution.

In conclusion, the Ti series pulsed CO₂ laser with a pulse duration of 200 fs (Figure 3) is a costly but efficient option for precision applications in airbag component production, ensuring high quality and long-term durability of the manufactured parts.

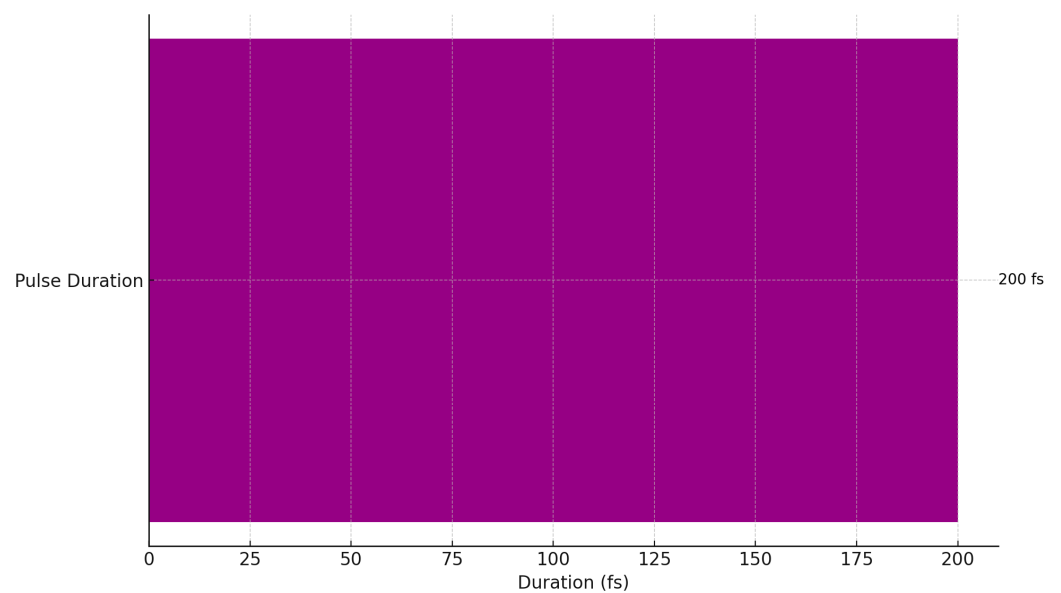


Figure 3. Laser pulse duration.

3.4. Optical Configuration

The laser optical system includes f-theta scanning lenses, beam expanders, focusing assemblies, and Galvo mirrors, all designed to operate at the wavelengths of CO₂ lasers. The beam diameter is 0.2 mm, ensuring precise focusing. The focal length of the optical system depends on the specific type of lenses and mirrors used. For f-theta scanning lenses and Galvo mirrors, the focal length can be adjusted according to application requirements. The beam size is controlled by the optical system and can be adjusted to obtain a small focal point, essential for precise processing of textile materials (Figure 4).

The material is placed precisely at the focal plane of the optical system. This ensures optimal focusing of the laser beam and precise processing of the material.

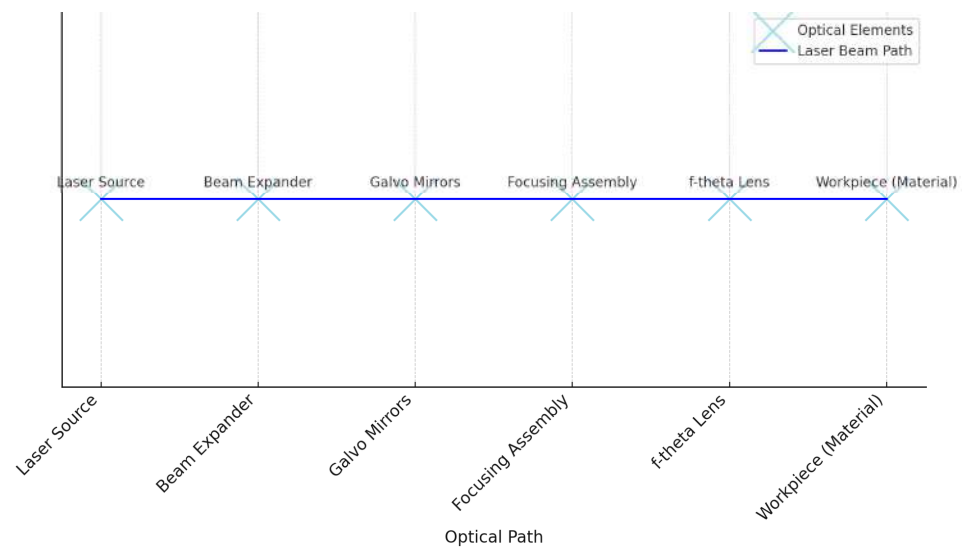


Figure 4. Optical configuration of laser system.

3.5. Collection and Statistical Analysis

The experiments were conducted with meticulous attention, taking into account the imposed conditions and using advanced instrumentation and equipment.

The statistical analyses of the experimental data were performed using the Minitab v17 software (Minitab LLC., State College, PA, USA). Considering a 95% confidence interval (CI) and a significance level of $\alpha = 0.05$, the normal distribution of the experimental data was qualitatively and quantitatively validated by using the normal Anderson–Darling test (AD) [26,27]. A factorial design (DOE) [28,29] was applied based on the process particularities by choosing the main control factors that affected the micro-perforation characteristics. To evaluate the influence of the electromagnetic noise levels, the interaction effects and main effects of factors were studied.

4. Influence of Electromagnetic Noise (EMI) on Laser Processing

During the experiment, electromagnetic noise (EMI) was monitored and controlled to understand its impact on the quality of laser perforations. Electromagnetic noise can be generated from various sources in the surrounding environment and can affect the stability and precision of the laser beam.

To evaluate the influence of EMI, pull tests were performed on the perforated materials under different electromagnetic noise conditions.

4.1. Statistical Analysis of Experimental Data

Considering the 95% confidence interval (CI), the electromagnetic noise levels and materials' thicknesses were statistically analyzed. In particular, the Anderson–Darling normality test was applied to validate the data distribution. Additionally, the homogeneity of the experimental data was tested by assessing the goodness of fit with probability plots (Figures 5–8), indicating the nominal electromagnetic noise level.

The goodness-of-fit normality test results are presented in Table 1. The comparative analysis of the probability plots shows that all points are within the lower and upper confidence boundaries, respectively, and the p -value is over the specific significance level of 0.05. Based on the estimated Anderson–Darling statistics (AD) and correlation coefficient, it can be mentioned that the analyzed experimental data are homogeneous and it follows the normal distribution.

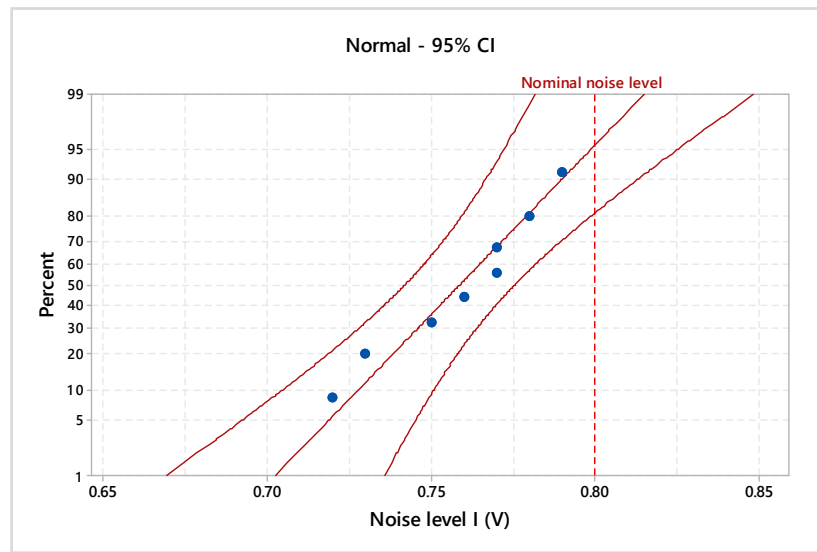


Figure 5. Probability plot of noise level I for 0.8 V.

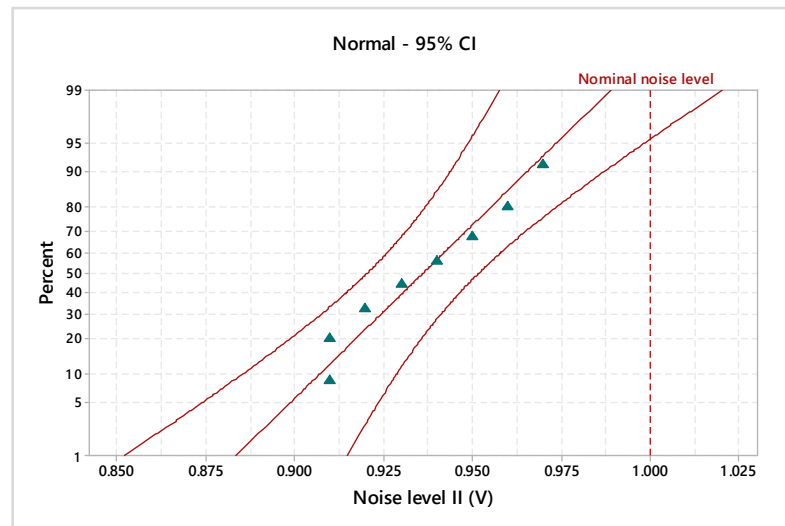


Figure 6. Probability plot of noise level II for 1 V.

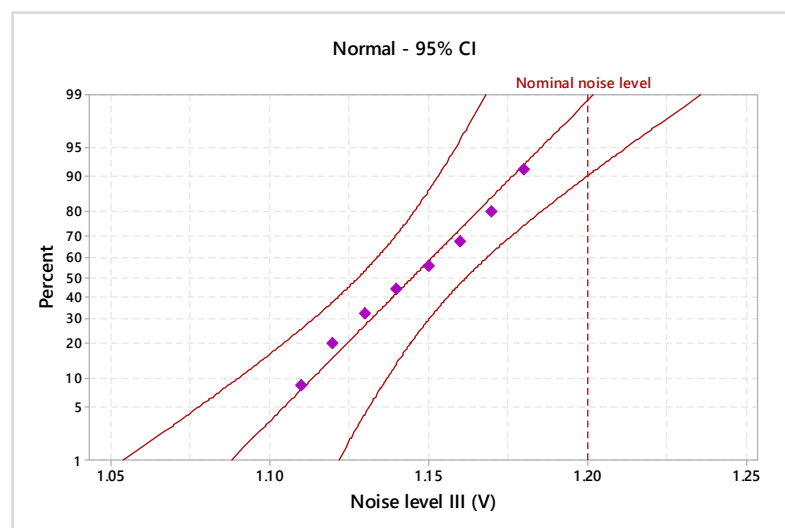


Figure 7. Probability plot of noise level III for 1.2 V.

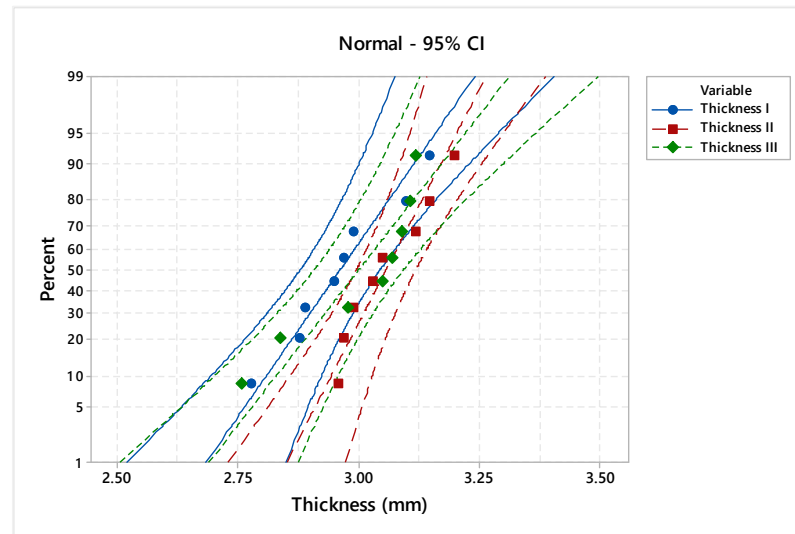


Figure 8. Probability plot of analyzed material thicknesses.

Table 1. Anderson–Darling normality test.

Characteristic	AD	Correlation Coefficient	p-Value
Noise level I (V)	0.247	0.979	0.649
Noise level II (V)	0.225	0.980	0.731
Noise level III (V)	0.134	0.996	0.961
Material thickness I (mm)	0.198	0.985	0.826
Material thickness II (mm)	0.287	0.972	0.524
Material thickness III (mm)	0.615	0.919	0.407

The descriptive statistics of analyzed electromagnetic noise levels and material thicknesses are synthetically presented in Tables 2 and 3.

Table 2. Descriptive statistics of analyzed noise level.

Statistical Parameter	Noise Level I (V)	Noise Level II (V)	Noise Level III (V)
Mean	0.759	0.936	1.145
Minimum	0.720	0.910	1.110
Maximum	0.790	0.970	1.180
Median	0.765	0.935	1.145
StDev	0.024	0.023	0.024
Q1	0.735	0.913	1.123
Q3	0.778	0.958	1.168
Skewness	−0.54	0.23	0.010
Kurtosis	−0.744	−1.412	−1.200

Table 3. Descriptive statistics of analyzed material thicknesses.

Statistical Parameter	Material Thickness I (mm)	Material Thickness II (mm)	Material Thickness III (mm)
Mean	2.964	3.059	3.003
Minimum	2.780	2.960	2.760
Maximum	3.150	3.200	3.120
Median	2.960	3.040	3.060
StDev	0.120	0.089	0.134
Q1	2.883	2.975	2.875
Q3	3.073	3.143	3.105
Skewness	0.201	0.487	−1.159
Kurtosis	−0.287	−1.264	−0.035

The estimated mean of electromagnetic noise level I is 0.759 V (95% confidence intervals of 0.738 V and 0.778 V), the standard deviation is 0.024 V (95% confidence intervals of 0.015 V and 0.049 V), and the median is 0.765 V (95% confidence intervals of 0.729 V and 0.780 V). With a significance level of $\alpha = 0.05$, the estimated parameters do not exceed the imposed nominal level of 0.8 V. Based on descriptive statistics results for electromagnetic noise levels II and III, it indicates falling within the specified limits for 1 V and 1.2 V.

In the case of the material thicknesses, the means are between 2.964 mm and 3.059 mm, and the standard deviations are between 0.089 mm and 0.134 mm with medians around 3 mm. Although the differences between the main estimated statistical parameters are not significant, each piece is analyzed individually, and the material thickness influences the regime of the laser process.

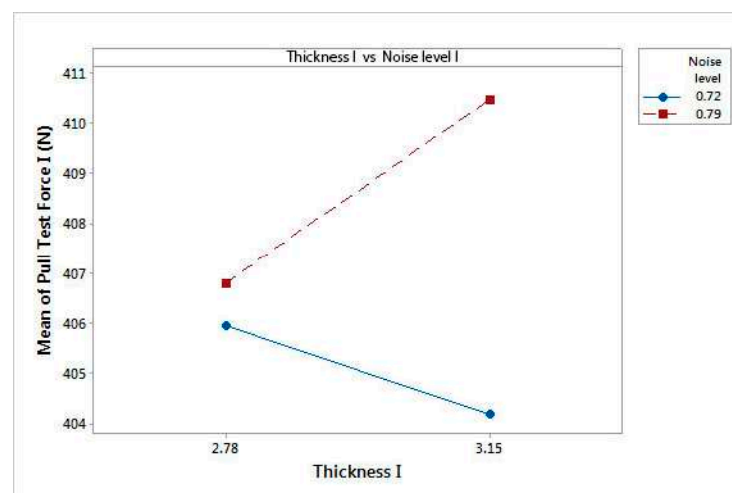
4.2. Analysis of the Main Factors in the Laser Micro-Perforation Process

The influence of electromagnetic noise levels and material thicknesses over pull test results is based on the factorial design of experiments (DOE). The goal of this study is to examine these factors to determine which ones have the greatest influence. Because it was assumed that three-way and four-way interactions are negligible, a resolution IV factorial design was adopted. We decided to generate a 16-run fractional factorial design. The interaction effects and main effects for factorial design results are presented in Figures 9 and 10.

The interaction plots show that there is a high degree of interaction for pull test force I and pull test force III. The electromagnetic noise level with the highest values has significant influence on pull test force results (Figure 9a,c). Specific to pull test force II depicted in Figure 9b, the plot indicates no interaction.

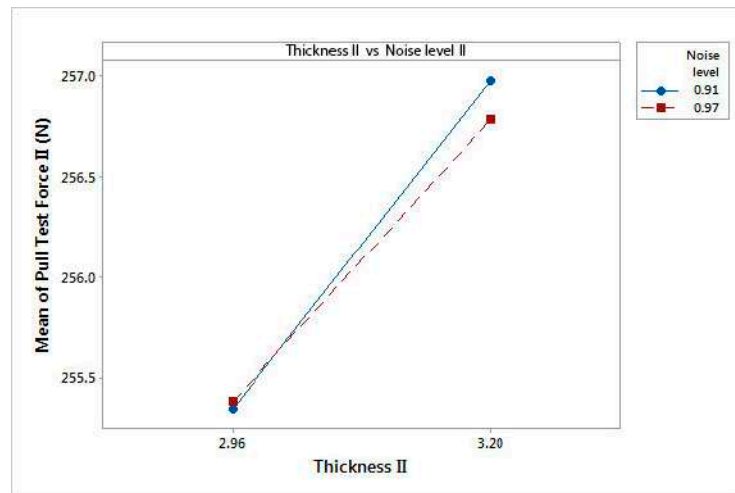
The pull tests' forces are adjusted according to the thickness of the material and its texture, the target value of the pull test being 303 N. From Figure 9a, it follows that for a value of noise level I of 0.79 V, the force for the pull test is 410 N, this value not falling within the agreed tolerance. From Figure 9b, it can be seen that for 0.97 V, the maximum value recorded in the pull test is 257 N. This result does not reflect the fulfillment of the imposed requirements. Analyzing Figure 9c, the pull test force value is 302 N at a noise level of 1.18 V, a result that indicates the supply of compliant products, but also the stability of the laser micro-perforation process.

The main effects' plots indicate that the electromagnetic noise levels and material thicknesses influence the results of pull tests (Figure 10). Specifically, the noise levels compare to a nominal noise level of 0.8 V that has a negative influence on the results of the pull test, while, for a nominal noise level of 1.2 V, it has a positive influence.

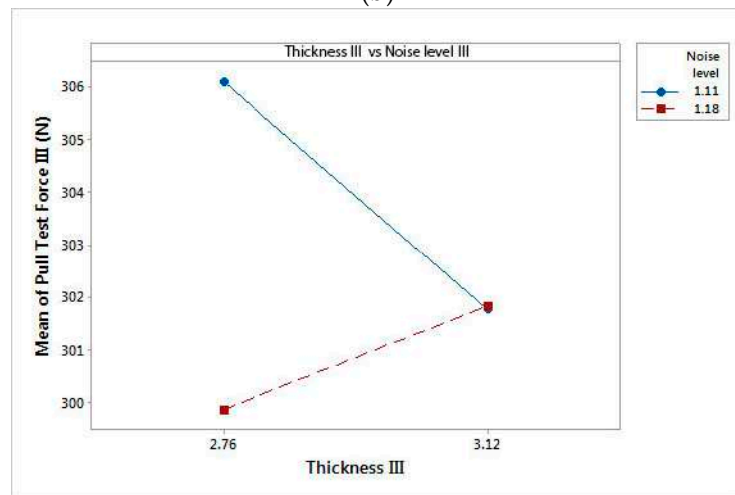


(a)

Figure 9. Cont.

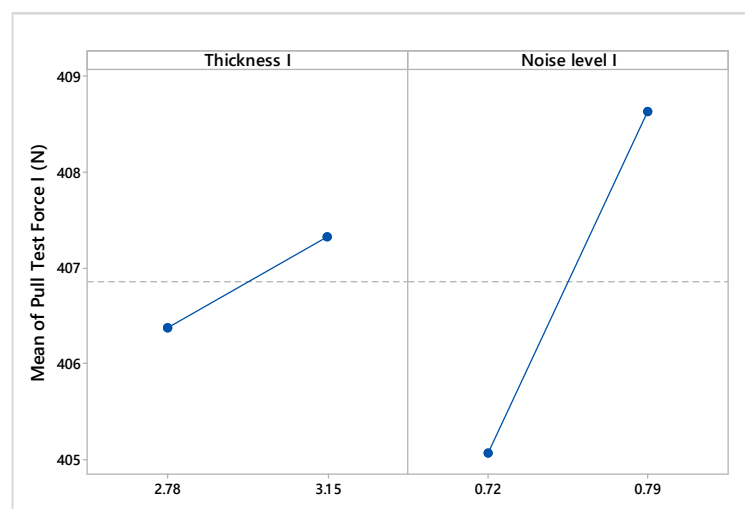


(b)



(c)

Figure 9. Interaction plot of analyzed factors: (a) interaction effects of pull test force I; (b) interaction effects of pull test force II; (c) interaction effects of pull test force III.



(a)

Figure 10. Cont.

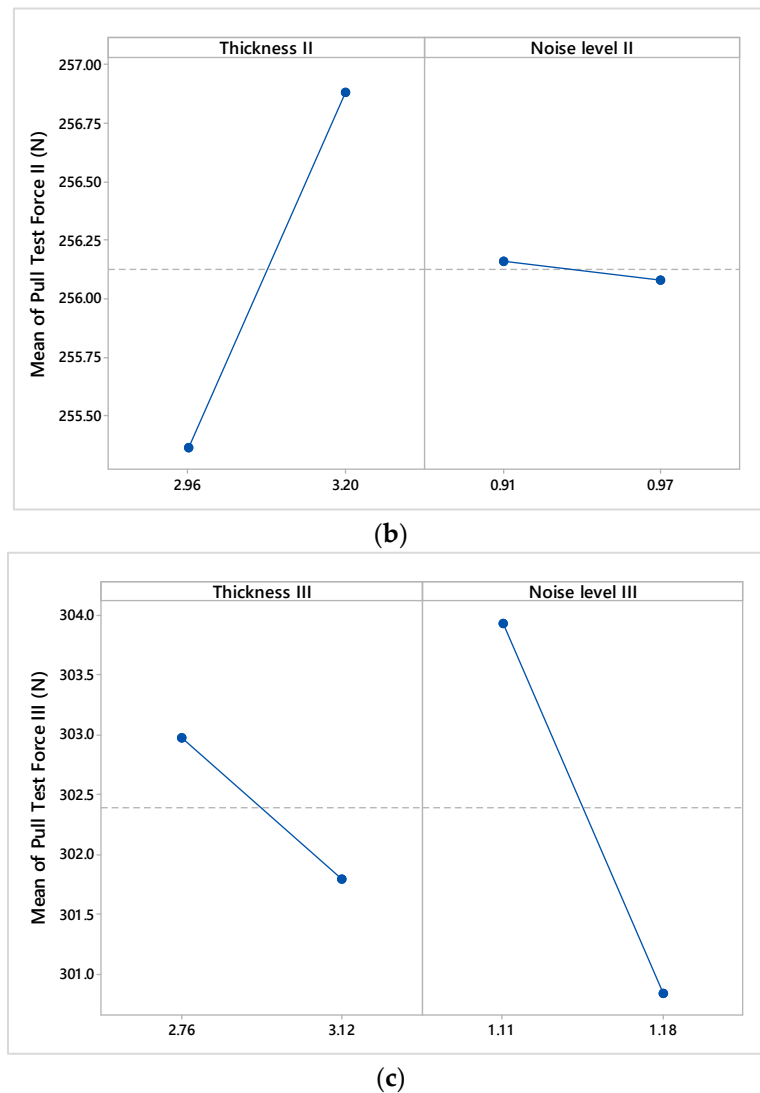


Figure 10. Main effects plot of analyzed factors: (a) main effects for pull test force I; (b) main effects for pull test force II; (c) main effects for pull test force III.

5. Results and Discussion

5.1. Evaluation of Perforation Quality in the Presence of Electromagnetic Noise

The pull tests conducted on the perforated materials were analyzed to determine the impact of electromagnetic noise on perforation quality. The tests revealed that, in the presence of electromagnetic noise, there were significant variations in the size and shape of the holes, as well as the presence of irregular edges.

The structural examination of the perforated material using the Gemini 500 Zeiss electron microscope (Zeiss, Jena, Germany) revealed the presence of defects such as excessive burns and deformations of holes' edges in areas exposed to strong electromagnetic fields. These defects can compromise the integrity and functionality of the airbag, highlighting the necessity of EMI control in the laser process.

5.2. Analysis of Tensile Test Results

The results of the tensile tests reveal distinct performance characteristics between samples categorized as NOK (Not OK) and those categorized as OK (Figures 11–13). Specifically, samples classified as NOK exhibited an average tensile strength of 409 N at a noise level of 0.8 V, and an average of 255 N at a nominal electromagnetic noise level of 1 V. In contrast, samples categorized as OK demonstrated an average tensile strength of 303 N when exposed to a noise level of 1.2 V. These findings underscore the sensitivity of tensile

strength to variations in applied noise levels, highlighting the need for a precise control and optimization of experimental parameters in material testing protocols.

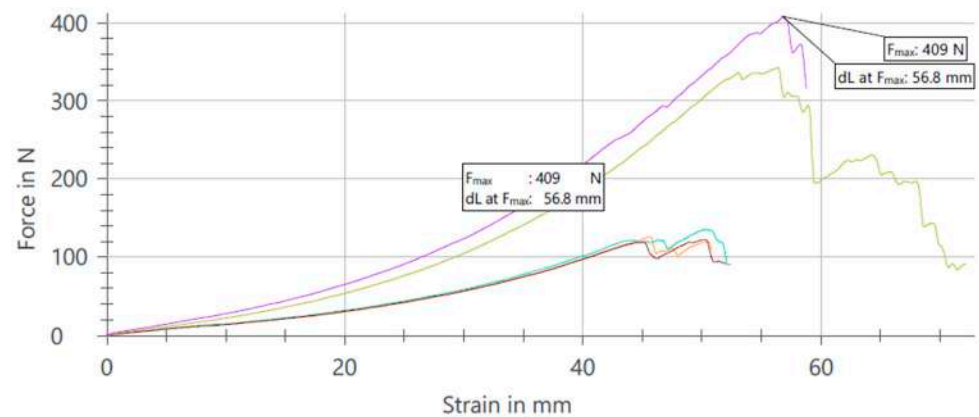


Figure 11. Analysis results after pull test with NOK values and noise set to 0.8 V.

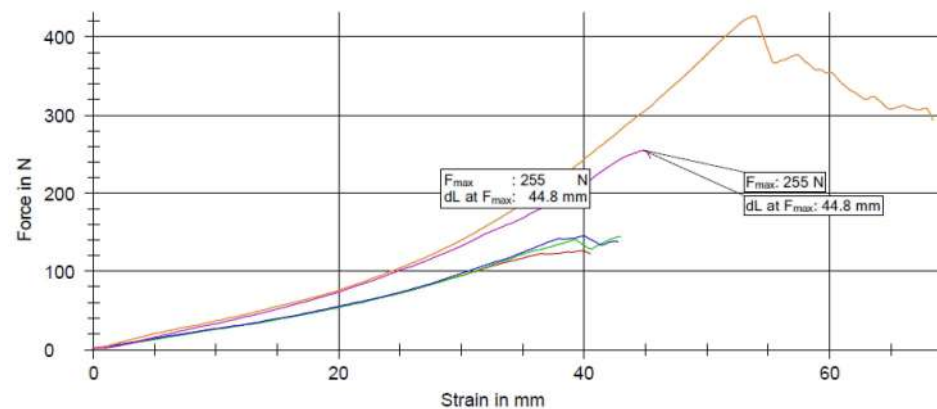


Figure 12. Analysis results after pull test with NOK values and noise set to 1 V.

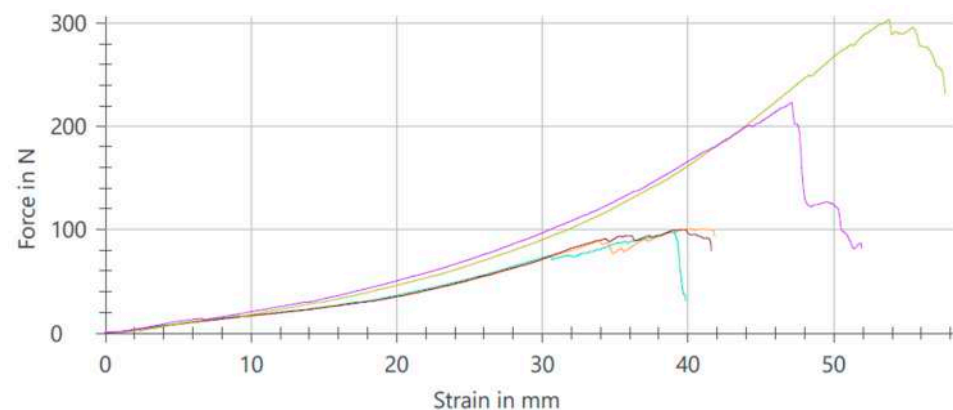


Figure 13. Analysis results after pull test with OK values and noise set to 1.2 V.

These results indicate that the tensile values are affected by the level of electromagnetic noise. At a noise level of 1.2 V, the tensile values are more consistent and closer to the optimal values, demonstrating that this level is favorable for achieving the desired quality of perforations.

5.3. Impact of Electromagnetic Noise on the Material

The 1.2 V noise level appears to favor greater consistency and stable quality of perforations compared to lower or higher noise levels (Figure 13). This noise level helps

maintain a balanced mechanical performance and reduces variability in the size and shape of perforations.

Under 1.2 V noise conditions, defects and deformations are minimized, ensuring better structural integrity of the perforated material.

5.4. Relationship between Noise and Mechanical Performance

The results suggest that an electromagnetic noise level of 1.2 V offers an optimal balance between mechanical performance and consistency of results. While lower noise levels (0.8 V) provide higher tensile values, they are more variable and less predictable. At 1.2 V, the perforated material shows superior stability, which is crucial for critical applications such as airbags.

The perforated material was subjected to strength tests in the presence of electromagnetic noise, using the ZwickRoell Z100 and INSTRON 5967 testing machines. The results showed a decrease in mechanical strength in areas affected by EMI, emphasizing the importance of minimizing electromagnetic interference to maintain the final product quality.

5.5. Process Optimization

Laser processing of textile components for airbags has a significant impact on their quality and performance. Laser technology allows high precision and consistency in material perforation, essential for ensuring the functionality and safety of airbags. However, the influence of electromagnetic noise can compromise these advantages, affecting the stability and accuracy of the laser process.

Using lasers in processing textile materials offers numerous advantages, such as the ability to achieve precise and uniform perforations and the efficiency of the process. However, the presence of EMI can introduce defects and variabilities that reduce the final product quality.

To improve the laser processing process and minimize the influence of electromagnetic noise, the following main recommendations can be mentioned:

- **Electromagnetic Shielding:** Continue using electromagnetic shielding equipment to maintain the optimal noise level at 1.2 V.
- **Experimental Setup Isolation:** Maintain the adequate isolation of the experimental setup to prevent unexpected variations in electromagnetic noise.
- **Power Supply Stabilization:** Ensure a stable power supply to consistently maintain the optimal electromagnetic noise level at 1.2 V.

During the laser perforation of the airbag's protective material, electrostatic energy is generated, which can impact the process. However, the primary objective of this procedure is to ensure the precise and efficient perforation of the material without compromising the functionality or safety of the airbag.

To prevent any adverse effects and ensure the reliability of the airbags in the event of an impact, specific measures are implemented. The electrostatic energy produced by the laser device can potentially affect nearby materials or electronic components under certain conditions. Therefore, measures are taken to minimize electrostatic interference and to safeguard the integrity of both the airbag system and the associated electronic components.

To enhance the micro-perforation process and control the level of electrostatic noise, adjustable tolerances are utilized. These tolerances can be configured through the laser's software, allowing parameters to be adjusted based on the material used for micro-perforation. This ensures that the perforation is carried out effectively without compromising the performance and safety of the airbag.

In this regard, the studies on influences of electromagnetic noise show that these factors must be detected, controlled, and mitigated.

6. Conclusions

Laser processing of textile components for airbags is a complex and crucial field for vehicle safety. By deeply understanding process parameters and the influence of external

factors such as electromagnetic noise, superior results can be achieved that comply with the industry stringent specifications. Continuing research and continuous improvement of the technologies and methodologies used will ensure the development of high-quality products and maximum safety for end-users.

In conjunction with the design of experiments' analysis, the differences among the analyzed factors were examined. The three noise levels appear to affect the pull test results compared to a target value of pull test force. The interaction effect is present because the different levels of the analyzed electromagnetic noise factors affect the response differently. Additionally, the plots of influence of electromagnetic noise levels compare to material thickness over pull test force results; it shows that there is a main effect present. Based on the analysis of factor effects, it can be mentioned that the noise levels have significant influence over the micro-perforation laser process.

The unacceptable results demonstrate significant variation in tensile values under the influence of electromagnetic noise. At a noise level of 0.8 V, the average tensile value is 407 N, suggesting better mechanical performance but with reduced consistency. At a noise level of 1 V, the average tensile value drops to 256 N, indicating a significant deterioration in the quality of the perforated material.

The acceptable results show that at a noise level of 1.2 V, the average tensile value is 303 N. Although the absolute value is lower than that at 0.8 V, the consistency and stability of the results are superior.

A detailed analysis of the tensile test results under the influence of electromagnetic noise indicates that a noise level of 1.2 V is optimal for achieving the desired quality of perforations in textile materials for airbags. This noise level provides a balance between mechanical performance and consistency of results, minimizing defects and ensuring the necessary structural integrity for vehicle safety. Controlling and maintaining this optimal electromagnetic noise level will significantly contribute to improving the quality and reliability of the final products.

Author Contributions: Conceptualization, A.-N.R., D.-I.D. and A.-E.D.; Data curation, A.-N.R.; Formal analysis, A.-N.R., D.-I.D. and A.-E.D.; Investigation, A.-N.R.; Methodology, A.-N.R.; Software, D.-I.D. and A.-E.D.; Supervision, A.-E.D.; Validation, A.-N.R. and A.-E.D.; Writing—original draft, A.-N.R., D.-I.D. and A.-E.D.; Writing—review and editing, A.-N.R., D.-I.D. and A.-E.D. All authors have read and agreed to the published version of the manuscript.

Funding: This research received no external funding.

Data Availability Statement: The data are contained within the article.

Acknowledgments: The authors are grateful to the Transilvania University of Brasov for technical and financial support.

Conflicts of Interest: The authors declare no conflicts of interest.

References

1. Dutta Majumdar, J.; Manna, I. *Laser Processing of Materials*; Springer Nature Switzerland AG: Cham, Switzerland, 2003; Volume 28. [[CrossRef](#)]
2. Dubey, A.K.; Yadava, V. Laser beam machining—A review. *Int. J. Mach. Tools Manuf.* **2008**, *48*, 609–628.
3. Steen, W.M.; Mazumder, J. *Laser Material Processing*, 4th ed.; Springer Nature Switzerland AG: Cham, Switzerland, 2010. [[CrossRef](#)]
4. Klein, T.; Vicaneck, M.; Simon, G. Forced oscillations of the keyhole in penetration laser beam welding. *J. Phys. D Appl. Phys.* **1996**, *29*. [[CrossRef](#)]
5. Guo, B.; Sun, J.; Hua, Y.; Zhan, N.; Jia, J.; Chu, K. Femtosecond Laser Micro/Nano-manufacturing: Theories, Measurements, Methods, and Applications. *Nanomanuf. Metrol.* **2020**, *3*, 26–67. [[CrossRef](#)]
6. Guo, Z.; Li, L.; Wang, Z.B.; Luk'yanchuk, B.S.; Hong, M. Optical resonance and polarization effects in femtosecond laser nanostructuring of metals: Application to the fabrication of 3D nanostructures. *Appl. Phys. Lett.* **2010**, *96*, 251502.
7. Paivasaari, K.; Laakso, P.; Laakso, P.; Sarnet, T. Fabrication of large area microstructures with a high-speed scanning multi-beam interference patterning technique. *J. Micromech. Microeng.* **2015**, *25*.
8. Stratakis, E.; Ranella, A.; Fotakis, C. Micro and nanostructuring of materials for biomedical applications using ultrafast lasers. *Laser Photonics Rev.* **2010**, *4*, 517–529.

9. Iyengar, V.V.; Wollman, S.H. Broadband and wide-angle antireflective surfaces based on conical microstructures. *Opt. Mater. Express* **2017**, *7*, 648–653.
10. Paivasaari, K.; Sarnet, T. Ultrafast laser processing for large area microstructuring. In Proceedings of the SPIE—The International Society for Optical Engineering, SPIE Photonics Europe, Brussels, Belgium, 15–18 April 2013.
11. Dusser, B.; Sagan, Z.; Soder, H.; Faure, N.; Colombier, J.P.; Jourlin, M.; Audouard, E. Controlled nano structuring of metals using femtosecond laser pulses. *Appl. Surf. Sci.* **2010**, *257*, 2250–2254.
12. Fowles, G.R. *Introduction to Modern Optics*, 2nd ed.; Dover Publications, Inc.: New York, NY, USA, 1989.
13. Bosi, M.; Attolini, G.; Negri, M. Nanowire heterostructures for optoelectronics. *J. Appl. Phys.* **2008**, *104*, 073105.
14. Yu, Z.; Raman, A.; Fan, S. Nanowire photovoltaic cells. *Opt. Express* **2010**, *18*, A366–A380. [[PubMed](#)]
15. Fan, P.; Yu, Z.; Raman, A.; Fan, S. Nanophotonic Light Trapping in Ultrathin Silicon Solar Cells. *Prog. Photovolt. Res. Appl.* **2011**, *19*, 217–233.
16. Smith, D.R.; Kroll, N. Negative Refractive Index in Left-Handed Materials. *Phys. Rev. Lett.* **2000**, *85*, 2933–2936. [[PubMed](#)]
17. Green, M.A. Third generation photovoltaics: Ultra-high conversion efficiency at low cost. *Prog. Photovolt. Res. Appl.* **2003**, *9*, 123–135.
18. Atwater, H.A.; Polman, A. Plasmonics for improved photovoltaic devices. *Nat. Mater.* **2010**, *9*, 205–213.
19. Bierman, D.M.; Lenert, A.; Chan, W.R.; Bhatia, B.; Celanovic, I.; Wang, E.N.; Soljačić, M. Enhanced photovoltaic energy conversion using thermophotovoltaic emitters. *Nat. Energy* **2016**, *1*, 16068.
20. Hu, L.; Chen, G. Analysis of optical absorption in silicon nanowire arrays for photovoltaic applications. *Nano Lett.* **2007**, *7*, 3249–3252.
21. Cui, Y.; Wei, Q.; Park, H.K.; Lieber, C.M. Nanowire nanosensors for highly sensitive and selective detection of biological and chemical species. *Science* **2001**, *293*, 1289–1292.
22. Li, X.; Zhang, Y. Graphene-based materials for thermoelectric energy generation. *Energy Environ. Sci.* **2014**, *7*, 1190–1214.
23. Yang, Z.P.; Ci, L.; Bur, J.A.; Lin, S.Y.; Ajayan, P.M. Experimental observation of an extremely dark material made by a low-density nanotube array. *Nano Lett.* **2008**, *8*, 446–451.
24. Schuller, J.A.; Barnard, E.S.; Cai, W.; Jun, Y.C.; White, J.S.; Brongersma, M.L. Plasmonics for extreme light concentration and manipulation. *Nat. Mater.* **2010**, *9*, 193–204.
25. Rusu, A.-N.; Dumitrascu, D.-I.; Dumitrascu, A.-E. Monitoring, Control and Optimization of Laser Micro-Perforation Process for Automotive Synthetic Leather Parts. *Processes* **2024**, *12*, 1275. [[CrossRef](#)]
26. Gibra Isaac, N. *Probability and Statistical Inference for Scientists and Engineers*, 1st ed.; Prentice-Hall: Hoboken, NJ, USA, 1973.
27. Taeger, D.; Kuhnt, S. *Statistical Hypothesis Testing with SAS and R*; John Wiley & Sons: Hoboken, NJ, USA, 2014. [[CrossRef](#)]
28. Mason, R.L.; Gunst, R.F.; Balding, D.J. *Statistical Design and Analysis of Experiments with Applications to Engineering Science*; John Wiley & Sons: Hoboken, NJ, USA, 2003.
29. Montgomery, D.C.; Runger, G.C. *Applied Statistics Probability Engineers*, 5th ed.; John Wiley & Sons: Hoboken, NJ, USA, 2011.

Disclaimer/Publisher’s Note: The statements, opinions and data contained in all publications are solely those of the individual author(s) and contributor(s) and not of MDPI and/or the editor(s). MDPI and/or the editor(s) disclaim responsibility for any injury to people or property resulting from any ideas, methods, instructions or products referred to in the content.

Article

Monitoring, Control and Optimization of Laser Micro-Perforation Process for Automotive Synthetic Leather Parts

Alexandru-Nicolae Rusu ¹, Dorin-Ion Dumitrascu ^{2,*} and Adela-Eliza Dumitrascu ¹

¹ Department of Manufacturing Engineering, Transilvania University of Brasov, 5 Mihai Viteazul, 500036 Brasov, Romania; alexandru.rusu@unitbv.ro (A.-N.R.); dumitrascu_a@unitbv.ro (A.-E.D.)

² Department of Automotive and Transport Engineering, Transilvania University of Brasov, 1 Politehnicii, 500036 Brasov, Romania

* Correspondence: d.dumitrascu@unitbv.ro

Abstract: This paper presents a comparative analysis of the laser operating power (P1 and P2) and synthetic leather thickness to achieve the optimal quality of components in the airbag area, produced through micro-perforation laser processing. Within the study, various laser power settings and material thicknesses were investigated to determine the combinations that ensure the best component performance. The experimental results indicate that setting the laser to 25% of its total power (P1, P2) of two kilowatts (kW) represents the optimal parameter setup to achieve parts of superior quality. This configuration is not significantly influenced by the material thickness, suggesting important versatility in practical applications. The overall results indicate the significant influence of the laser power level on micro-perforation processing. The normal analysis of means (ANOM) and factorial design (DOE) provide significant evidence for an interaction, highlighting that the effects of one laser power factor depend on the level of the other laser power factor. These findings are essential in improving production processes, as they allow for the manufacture of airbag components with high precision and consistency, minimizing the risks of material deformation or damage. Thus, not only is compliance with safety standards ensured, but the economic efficiency of the production process is also enhanced.

Keywords: synthetic leather; micro-perforation process; automotive parts; laser parameters; analysis of variance; factorial analysis; quality improvement



Citation: Rusu, A.-N.; Dumitrascu, D.-I.; Dumitrascu, A.-E. Monitoring, Control and Optimization of Laser Micro-Perforation Process for Automotive Synthetic Leather Parts. *Processes* **2024**, *12*, 1275. <https://doi.org/10.3390/pr12061275>

Academic Editors: Li Li, Wei Cai and Lingling Li

Received: 3 May 2024

Revised: 14 June 2024

Accepted: 19 June 2024

Published: 20 June 2024



Copyright: © 2024 by the authors. Licensee MDPI, Basel, Switzerland. This article is an open access article distributed under the terms and conditions of the Creative Commons Attribution (CC BY) license (<https://creativecommons.org/licenses/by/4.0/>).

1. Introduction

1.1. Literature Review

Laser processing technology is seen as an efficient method due to its lack of tool wear, fast processing speed, ease of performance, possibilities for flexible automation, high-quality products and contactless nature; it can be employed in various industrial applications, such as drilling, cutting, milling, polishing, etc. [1–3].

Laser processing can be categorized into thermodynamic and non-thermodynamic processes based on the laser pulse width. Thermodynamic processes involve continuous, long-pulse and short-pulse lasers with pulse widths greater than 10–11 milliseconds (ms), leading to heat transfer and diffusion phenomena, such as electron excitation, electron-phonon relaxation and phonon-phonon relaxation. These processes result in material melting, evaporation and removal through thermal effects, causing significant thermal damage to the edges of the laser-processed area. In contrast, picosecond and femtosecond lasers, with pulse durations shorter than the electron-lattice energy relaxation period, operate under a “cold processing” mechanism. During these ultra-short pulses, the laser energy is absorbed by the electrons before any energy coupling with the lattice, leaving

the lattice and electrons in a non-equilibrium state. This results in an instantaneous non-thermal phase change, where the material is ejected with the formed plasma before thermal diffusion can occur. This prevents thermal damage and produces clean, precise edges [4,5].

Femtosecond lasers are widely used in various fields. A femtosecond fiber laser for micro-hole drilling and cutting in ambient air was developed in [6]. Initially, the process was examined for both transparent materials (such as glass) and nontransparent materials (such as metals and tissues). The hole shapes and morphologies were characterized using optical and scanning electron microscopy (SEM). The results indicated the successful creation of debris-free micro-holes with excellent roundness and no thermal damage, achieving an aspect ratio of 8:1. Additionally, micro-hole drilling in both hard and soft tissues was accomplished without causing cracks or collateral thermal damage. The study then investigated trench micromachining and cutting in various materials, analyzing the influence of the laser parameters on the trench properties. The findings show that straight and clean trench edges can be produced without thermal damage.

The theoretical and experimental analysis of micro-hole arrays on coated fused silica using a femtosecond laser was developed in [7]. The authors discussed 3D microstructures to underline the advantages and the rapidity of the processing method using an ultrafast laser.

In the laser microfabrication applications field, the authors in [8,9] discussed the power output of picosecond and femtosecond ultrafast lasers, which typically ranges from tens to hundreds of watts, positioning them as primary contenders. This contrasts sharply with continuous lasers, which boast an average power rating of 10 kW. Recent advances in industrial ultrashort-pulse laser technology have led to a substantial rise in the average power levels, surging from a modest 10 watts to several kilowatts. These breakthroughs are anticipated to catalyze significant advancements across multiple aspects, including the processing efficiency, material thickness capabilities and surface area coverage. Moreover, these innovations are expected to enhance the distinguishing characteristics of ultrafast laser technology—notably, its unparalleled precision and quality in processing operations.

Studies referring to analyses across various materials emphasize the effects of the laser parameters on the trench properties. The findings show that straight and clean trench edges can be obtained without thermal damage [4].

The optimization of the processing outcomes was proposed in [10–12]. It is imperative to focus the laser beam precisely on the surface of the workpiece, ensuring that it converges to a single point without any deviation, a state referred to as zero defocus. This alignment guarantees that the laser beam lands directly on the material's surface to be processed, thus maximizing the processing efficacy. It is crucial to note that the power density reaches its zenith under these conditions. When the laser's focal plane is positioned above the surface of the workpiece, it is termed positive defocusing, while positioning it below the workpiece surface leads to negative defocusing. Variations in the focal length lead to energy dispersion and a consequent decline in processing quality, irrespective of whether the defocusing is positive or negative.

Zhang et al. [13] conducted a comparative analysis on the impact of laser irradiation on carbon fiber composite materials in both subsonic airflow and no-flow environments. Their results indicated that the presence of a tangential airflow contributed to a noticeable cooling effect within the processing area. As the air pressure increased, the airflow intensified, leading to more efficient heat dissipation and a consequent reduction in the heat-affected zone.

In a scientific study, Riveiro et al. [14] investigated the efficacy of assisted laser cutting using Ar gas across varying air pressures with a 3.5 KW CO₂ laser. Their findings demonstrated that the gas delivered through both coaxial subsonic nozzles and paraxial supersonic nozzles effectively dissipated the heat, resulting in a reduction in the heat-affected zone.

Furthermore, Yuki et al. [15] explored laser processing using nitrogen, argon and oxygen as auxiliary gases under consistent average power and scanning speed conditions. Nitrogen, with its higher specific heat capacity compared to argon, proved to absorb more

heat, thus limiting the expansion of the carbon fiber end face. Additionally, oxygen's inclusion facilitated deeper material incisions, addressing challenges associated with material removal in deeper layers due to lower laser energy.

In their study, Wang et al. [16] utilized a water-guided laser for the processing of a carbon-fiber-reinforced polymer (CFRP). Their findings indicated that the resultant cutting surface of the CFRP exhibited remarkable cleanliness and flatness when processed with a water-guided laser. Notably, minimal fused impurities were observed adhering to both the cutting surface and groove. Furthermore, enhancements were noted in the mitigation of surface heat-affected zones, material delamination phenomena and fiber expansion.

Leveraging the cooling potential of a paraxial water jet, Zhang et al. [17] strategically harnessed it to curtail the diffusion of excess heat generated during laser processing. A morphology analysis revealed a direct correlation between the reduction in the heat-affected zones and the flow rate of water through the system (B). This underscores the effectiveness of water jet assistance in not only facilitating prompt heat dissipation but also elevating the quality of carbon fiber cutting surface processing while concurrently diminishing carbonization.

1.2. Objectives and Scope of the Study

The production and testing of airbag parts involves the use of various specific equipment and technologies. In this context, the aim of this study is to analyze the laser micro-perforation process of airbag components considering the main influencing factors. The obtained results in the pull test are analyzed from the point of view of the influences of the laser power (P1 and P2) and the thickness of the material. The statistical analysis of the experimental data includes a goodness-of-fit test, regression analysis, analysis of variance (ANOVA) and multivariate and factorial analyses. All of these are applied to identify patterns, correlations and outliers within the dataset. Additionally, advanced visualization tools are utilized to emphasize the complex data relationships and trends, aiding in the interpretation of the results and the formulation of actionable insights.

The novelty in the laser micro-perforation process of textile materials refers to recent technological improvements that optimize both the process and the outcomes of this technique. The updated laser technology allows for the creation of extremely precise and uniform perforations, which are essential for applications where the technical characteristics are crucial. Laser micro-perforation systems are much faster, enabling mass production without compromising product quality, thereby making the process more efficient and cost-effective for manufacturers. Additionally, modern technologies offer advanced control over the laser parameters, such as the power, frequency and pulse duration, allowing for fine adjustments based on the type of material and the desired outcome.

This exhaustive investigation represents a significant step towards enhancing the reliability and consistency of airbag cutout laser processing methodologies. The comprehensive analyses and proposed remedial measures outlined herein underscore the collective commitment to quality assurance and process optimization within the automotive safety industry. It is imperative that stakeholders collaborate closely to ensure the seamless implementation of these measures, thereby fostering a culture of continuous improvement and excellence in manufacturing practices. By applying the specific methods, the following outcomes are expected.

- **Uniform and precise perforations:** The optimization of the laser parameters and rigorous control implementation should lead to uniform and precise perforations across the entire surfaces of synthetic leather parts.
- **Reduction in defects and waste:** Real-time process monitoring should enable the immediate detection and correction of any issues, thus reducing the quantity of damaged material and minimizing waste.
- **Increase in efficiency and consistency:** Through parameter optimization and continuous process control, a significant increase in operational efficiency and improved consistency in the quality of end products is anticipated.

2. Materials and Methods

The analyzed CO₂ laser micro-perforation process technology is presented in Figure 1.

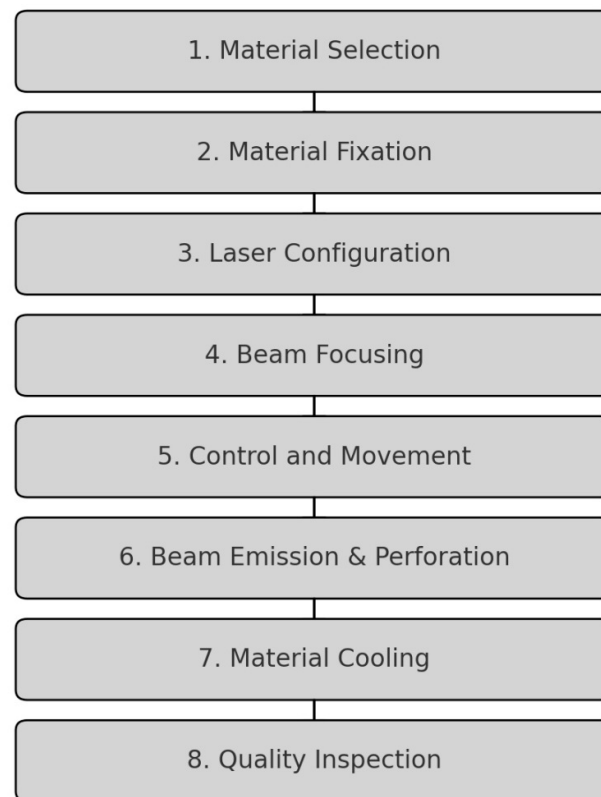


Figure 1. Laser micro-perforation flow process.

Material preparation: The materials used for airbags include robust technical textiles such as nylon or polyester, which are treated for high tear and wear resistance. The airbag material must be securely fixed on a work platform to prevent movement during perforation, ensuring precision perforations.

Laser configuration: The CO₂ laser used for the micro-perforation of airbag materials operates at a wavelength of 10.6 μm . This wavelength is effective for absorption by technical textile materials. The laser power varies depending on the thickness of the material and the perforation specifications, with typical powers ranging from a few watts to hundreds of watts.

Laser beam focusing: The optical system focuses the laser beam using lenses or mirrors to concentrate the beam into a small point. The size of the focused point determines the diameter of the micro-perforation, and the precise adjustment of the focus is essential to ensure high-quality perforations in airbag materials.

Control and movement: A computer controls the movement of the laser and the perforation pattern, allowing the precise programming of the size, shape and distribution of the perforations. The movement system, which may include stepper motors or servomotors, ensures the precise movement of the laser or the platform holding the material, essential in achieving uniform perforations in the complex airbag materials.

Micro-perforation process: The laser beam is emitted and absorbed by the material, causing the rapid evaporation of a small portion of the material and creating a perforation. In airbag materials, the perforations must be precise to ensure the proper and safe deployment of the airbag during an impact. Lasers can operate continuously or in pulses, with short, high-intensity pulses often preferred to minimize the heat-affected zone (HAZ) and increase the perforation precision.

Cooling and inspection: After perforation, the airbag material may need time to cool, especially if the process generates significant heat. Quality inspection is essential, with the perforated material being checked to ensure the size and uniformity of the perforations. Optical instruments or high-resolution cameras are often used for this inspection, thus guaranteeing compliance with the strict standards of the automotive industry.

Important parameters in the micro-perforation process for airbags: The laser power is crucial to ensure precise and uniform perforations in the technical textile materials of airbags. The power must be sufficient to vaporize the material but not so high as to degrade the edges of the perforation or cause excessive material damage.

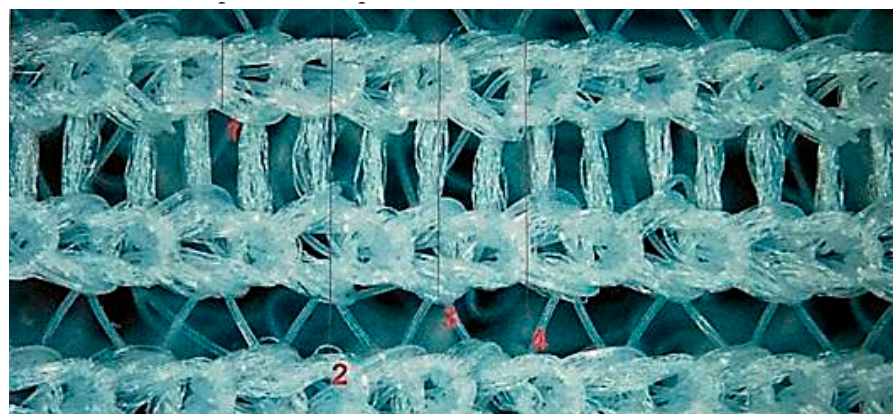
The pulse duration affects the precision of the perforations. Short pulses produce precise perforations and minimize the heat-affected zone (HAZ), essential to maintaining the structural integrity of the airbag material.

The movement speed of the laser affects the size and shape of the perforations. High speeds can produce smaller, shallower perforations, while slower speeds allow deeper penetration and larger perforations.

Beam focusing determines the size of the focused point, and precise focusing produces smaller, more precise perforations. The stability of the focus is crucial to ensuring uniform perforations across the entire airbag material.

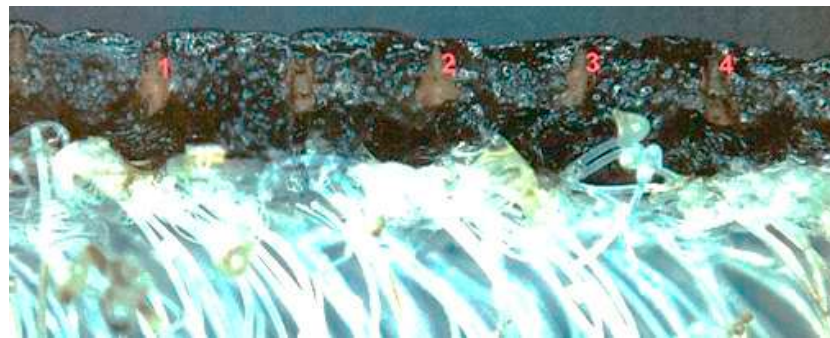
The material type influences the absorption of the laser. The technical textile materials used in airbags have specific absorption rates for the CO₂ laser wavelength, and materials with high absorption require less power for perforation. The thermal properties of the material, such as the thermal conductivity and heat capacity, influence the heat dispersion and the size of the HAZ. The following materials and technology were utilized for the laser micro-perforation process.

- Synthetic leather: The synthetic leather parts used in this study were selected to represent common materials utilized in the automotive component manufacturing industry for airbag production (Figure 2). The sample size was 50 parts for each analyzed parameter: the laser power and material thickness. For the factorial analysis, 950 samples were considered. The material used consisted of synthetic leather produced from polyvinyl chloride (PVC) with a nominal thickness of 1.2 mm. This was laminated with a spacer fabric with a nominal thickness of 2.99 mm, with a specified tolerance of ± 0.3 mm.



(a)

Figure 2. Cont.



(b)

Figure 2. Analyzed synthetic leather: (a) microstructure image of synthetic leather; (b) micro-holes after laser micro-perforation into skin. The scale bar is 500 μm .

- Laser process: The micro-perforation process was conducted using a high-precision laser system, enabling precise control of the perforation parameters, such as the power and operating speed (Figure 3).



Figure 3. Laser line.

The main components of the machine setup for laser micro-perforation include a CO₂ laser, mirrors, a laser beam and a gas nozzle. The most important parameters of the laser micro-perforation process are the focus, laser power (P1, P2), impulses, robot speed (ms) and tolerance of material deviation.

The laser utilized in the conducted experiments operated in pulsed mode, exhibiting a pulse duration of 200 femtoseconds (fs) and a repetition frequency of 2 kilohertz (KHz). This configuration facilitated precise control over the laser's output, providing high-intensity pulses conducive to experimental investigations.

The analysis stages consisted of testing based on the following.

- Material characterization: Preliminary tests were conducted to characterize the material properties, including the thickness, texture and temperature resistance, before commencing the micro-perforation process.
- Laser parameter setting: Critical parameters of the laser process, including the power, frequency and beam traversal speed, were optimized to ensure efficient and uniform material perforation.

- Real-time monitoring and control: During the micro-perforation process, monitoring and control systems were implemented to detect and rectify any deviations in the operating parameters, thereby maintaining the quality and consistency of the perforations.

2.1. Methodology

The investigative approach adopted herein involved a meticulously planned and executed series of experiments, orchestrated with precision to closely examine the intricacies of airbag cutout laser processing. The methodology was designed to simulate real-world production scenarios, ensuring that the findings were applicable and relevant to industrial practices. Airbag cutouts, a critical component in automotive safety systems, underwent laser processing precisely 24 h after adhesive application, mimicking the timeline encountered in actual manufacturing settings. However, the key aspect of this investigation lies in the identification of a significant challenge: the inadvertent use of left-hand drive (LHD) parameters for right-hand drive (RHD) components during laser processing. This systemic inconsistency has far-reaching implications, potentially compromising the quality and reliability of airbag cutouts, which are vital for passenger safety. The manifestation of nonconforming (NOK) outcomes during subsequent pull testing procedures underscored the urgency of addressing this issue, prompting a comprehensive examination of the underlying causal factors.

2.2. Laser Processing Investigation

The airbag cutout laser processing investigation detailed in this report represents a meticulous endeavor aimed at comprehensively understanding and rectifying the discrepancies encountered during the manufacturing process. With automotive safety as a paramount concern, the study meticulously delves into the nuanced intricacies surrounding the application of LHD and RHD parameters in laser processing techniques. The optimization of production methodologies within the automotive safety industry is not merely a matter of efficiency but a critical aspect in ensuring passenger safety and regulatory compliance. This investigation, therefore, serves as a critical work in the quest for excellence in automotive safety standards. Through rigorous experimentation and analysis, the study aims not only to identify areas of improvement but also to pave the way for innovative solutions that elevate the standards of airbag cutout manufacturing processes.

2.3. Experimental Design and Setup

The experimental design was meticulously crafted to ensure robustness and reliability in data collection. Airbag cutouts, sourced from diverse production batches, were carefully selected to capture the variability inherent in real-world manufacturing processes. Prior to laser processing, the cutouts underwent stringent quality control checks to ensure uniformity and consistency across samples. Adhesive application was carried out using state-of-the-art equipment, adhering to industry best practices to minimize variability. The laser processing parameters, including the power, intensity and speed, were systematically varied to evaluate their impacts on the processing outcomes. Additionally, environmental conditions such as the temperature and humidity were closely monitored and controlled to minimize external influences on the experimental results.

2.4. Collection and Statistical Analysis

Data collection during the experimental phase was conducted with meticulous attention to detail, employing advanced instrumentation and data logging techniques to capture a comprehensive range of process parameters.

The inferential analyses of the recorded experimental data were performed using the Minitab v17 software (Minitab LLC, State College, PA, USA). Considering a 95% confidence interval (CI) and a significance level of $\alpha = 0.05$, the normal distribution of the experimental data was qualitatively and quantitatively validated by applying the Anderson–Darling (AD) goodness of fit [18,19]. An analysis of means (ANOM) chart [20] for a normal distribution

was computed for different laser power levels (P1 and P2). We used an analysis of means for normal data and a two-way design to identify any significant interactions and main effects. The experiments were designed (DOE) [21,22] based on the process' particularities by choosing the main control factors that affected the micro-perforation characteristics, applying a full factorial design.

3. Statistical Analysis of Experimental Data

3.1. Goodness-of-Fit Test of Experimental Data

The pull test results and material thickness were statistically analyzed with a 95% confidence interval (CI) and significance level of $\alpha = 0.05$. The homogeneity of the experimental data was tested by assessing the goodness of fit with a probability plot (Figures 4 and 5). Additionally, the quantitative assessment was performed with a hypothesis test, such as the Anderson–Darling normality test.

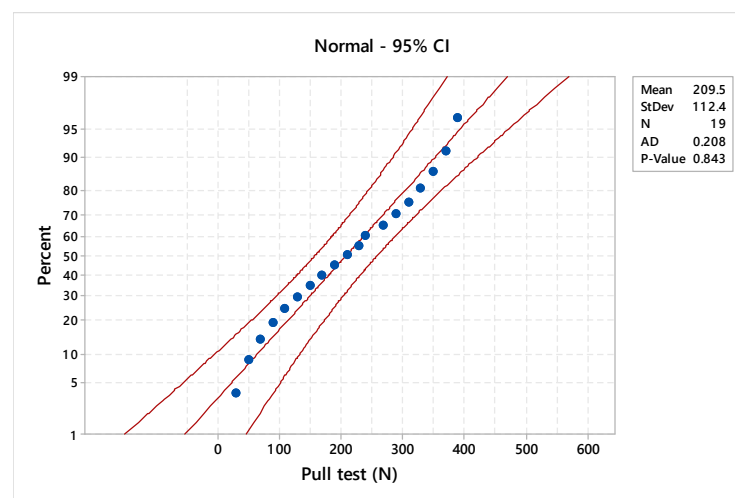


Figure 4. Probability plot of pull test results.

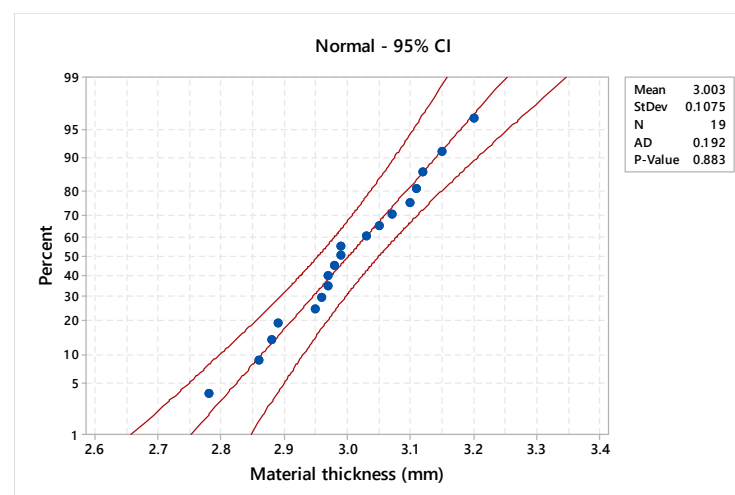


Figure 5. Probability plot of material thickness.

The results of the goodness-of-fit normality test are synthetically presented in Table 1. A parametric distribution analysis was considered in order to estimate the statistical parameters of the pull test and material thickness (Table 2).

Table 1. Anderson–Darling normality test.

Characteristic	AD	A-Squared	Correlation Coefficient	<i>p</i> -Value
Pull test (N)	0.208	0.21	0.990	0.843
Material thickness (mm)	0.192	0.19	0.992	0.883

Table 2. Descriptive statistics of analyzed characteristics.

Statistical Parameter	Pull Test (N)	Material Thickness (mm)
Mean	209.5	3.003
Standard Deviation	112.4	0.107
Minimum	30	2.78
1st Quartile	110	2.95
Median	210	2.99
3rd Quartile	310	3.10
Maximum	390	3.20
Skewness	0.014	−0.12
Kurtosis	−1.185	−0.27

Visually comparing the probability plots depicted in Figures 4 and 5, it can be concluded that the experimental data complied with a normal distribution. The points roughly follow the straight line, all of the points are within the lower and upper confidence boundaries, and the *p*-value is over 0.05.

The estimated mean of the pull test data is 209.5 (95% confidence intervals of 155.31 and 263.64), the standard deviation is 112.4 (95% confidence intervals of 84.91 and 166.18), and the median is 210 (95% confidence intervals of 127.28 and 292.72). Using a significance level of $\alpha = 0.05$, the Anderson–Darling normality test indicates that the pull test data follow a normal distribution.

In the case of the material thickness, the mean is 3.003 (95% confidence intervals of 2.951 and 3.054), the standard deviation is 0.107 (95% confidence intervals of 0.081 and 0.159), and the median is 2.99 (95% confidence intervals of 2.958 and 3.074). Moreover, it can be underlined that the estimated value of the Anderson–Darling statistic is 0.192.

The overall inferential analysis concludes that the pull test results and material thickness are from a normally distributed population.

3.2. Analysis of the Main Factors in the Laser Micro-Perforation Process

The assessment of the main influencing factors on the micro-perforation laser process is based on the analysis of means chart (ANOM) for a normal distribution. An experiment was performed to assess the effects of the most important factors: the level I laser power (P1), the level II laser power (P2), the pull test results and the material thicknesses. The ANOM results are illustrated in Figures 6 and 7.

In the case of first level of the laser power (P1), the pull test results indicate that the lower delimitation limit is 172.4 N and the upper limit is 246.7 N, with a mean of 209.5 N (Figure 6) and standard deviation of 74.2 N. Tested parts that had recorded values below the lower limit value were declared scrap.

The normal analysis of means chart for the P2 laser power (Figure 7) showed a lower delimitation limit of 161 N, an upper delimitation limit of 257.9 N and a mean of 209.5 N (Figure 3) with a standard deviation of 96.9 N.

The computed delimitation limits allow us to take appropriate measures to optimize the laser process. The indicated direction is to optimize the two laser powers, P1 and P2, to ensure the process' stability.

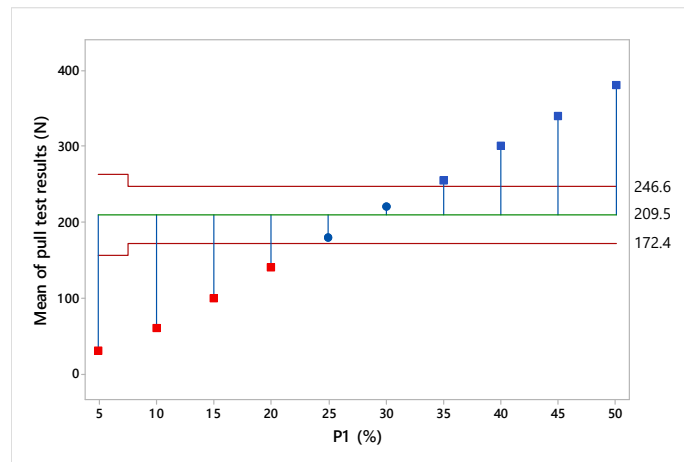


Figure 6. Normal ANOM for pull test results vs. P1 laser power.

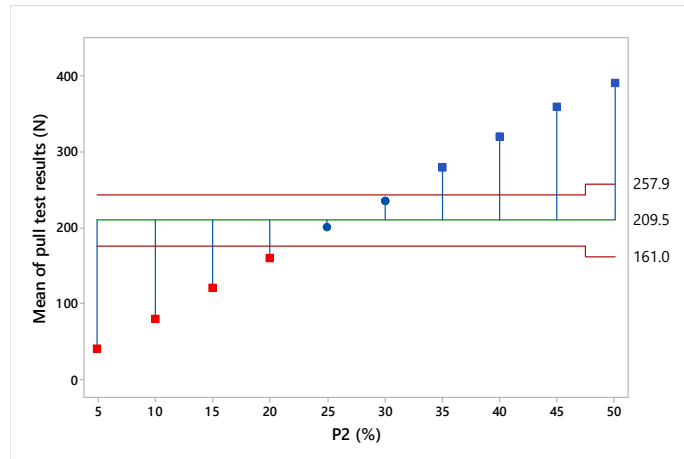


Figure 7. Normal ANOM for pull test results vs. P2 laser power.

The comparative analysis of the two laser powers emphasizes that the optimal level should be set around 0.25 W to ensure a material rupture force during testing. Additionally, quality limits can be easily determined from the comparative analysis: power of 0.20 W—beyond tolerance threshold; power of 0.21–0.24 W—within accepted limits; power > 0.25 W—higher precision, efficiency and stability (covers and removes material defects).

In order to highlight the interaction between the pull test results, laser power and material thickness and its effect on the micro-perforation process, a factorial analysis was designed (Figures 8 and 9). The magnitude and the importance of the effects were determined by applying the Pareto chart of the effects (Figure 10).

The interaction plot indicates that the material with the highest thickness depends on the P1 laser power, while the material with the lowest thickness depends on the P2 laser power. The difference between the P1 and P2 powers is given by the number of pulses. Specifically, a laser power fraction of 5–25% from the nominal laser power has a negative influence on the results of the pull test, while, for a laser power greater than 25%, the tested parts in the pull test are compliant.

In conjunction with an analysis of variance and design of experiments, we examined the differences among the level means for the three analyzed factors. The P1 and P2 laser powers appear to affect the pull test results compared to an overall mean of 209.5 N. A main effect is present because the different levels of the studied laser powers factors affect the response differently. Additionally, the graph for the material thickness shows that there is no main effect present.

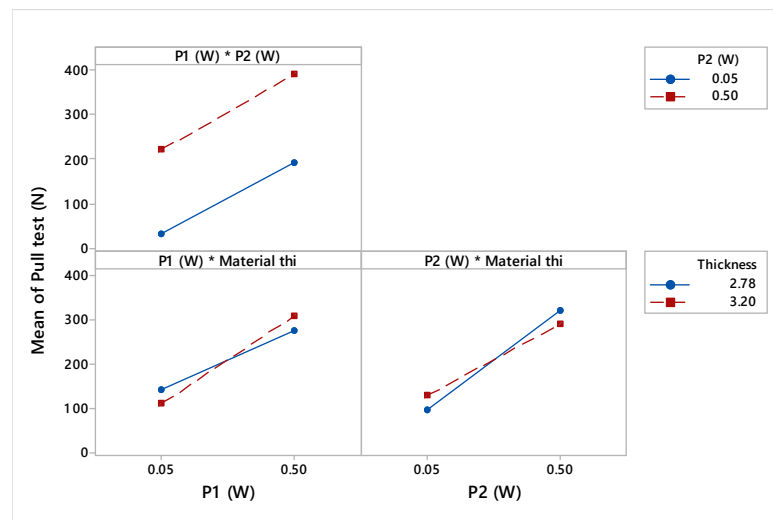


Figure 8. Interaction plot for pull test results.

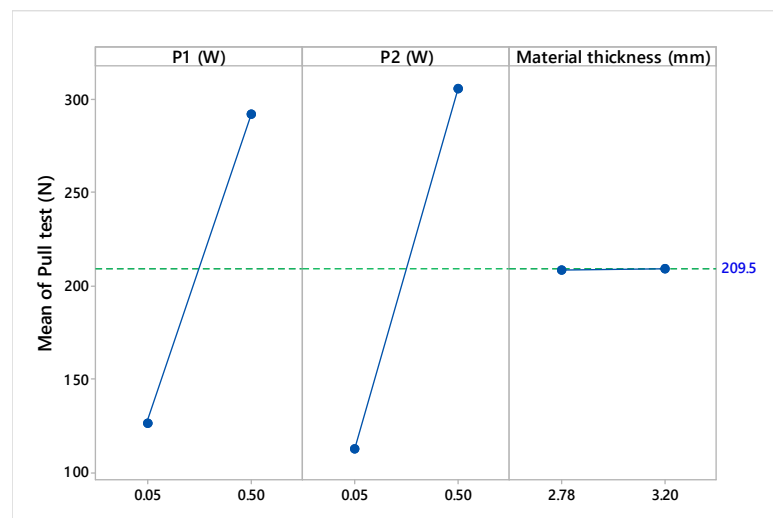


Figure 9. Main effects plot for pull test results.

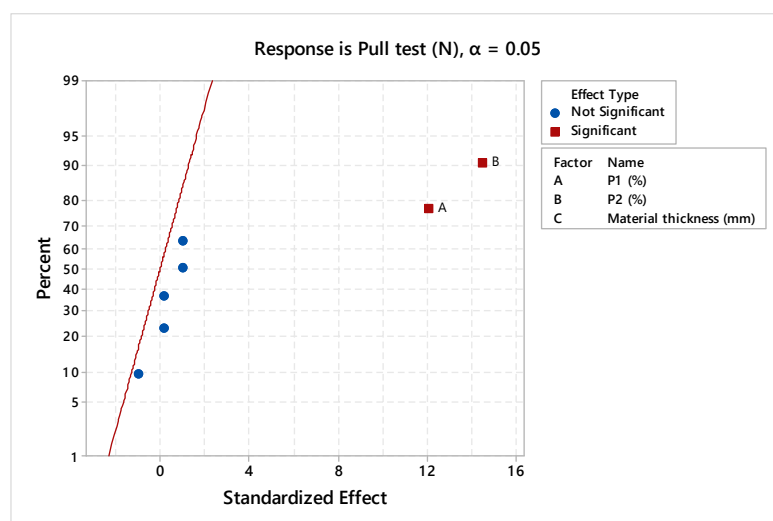


Figure 10. Micro-perforation factor effects.

The absolute effect values compared to the reference line show that the laser powers are statistically significant (Figure 10). Moreover, the standardized effects of the micro-perforation factors show a significant effect of the P2 (90%) and P1 (77%) laser powers.

4. Results and Discussion

4.1. Results and Summary

Nonconforming results (Figure 11): The statistical analyses revealed deviations from the established acceptance criteria during pull testing, indicative of underlying inconsistencies within the manufacturing process.

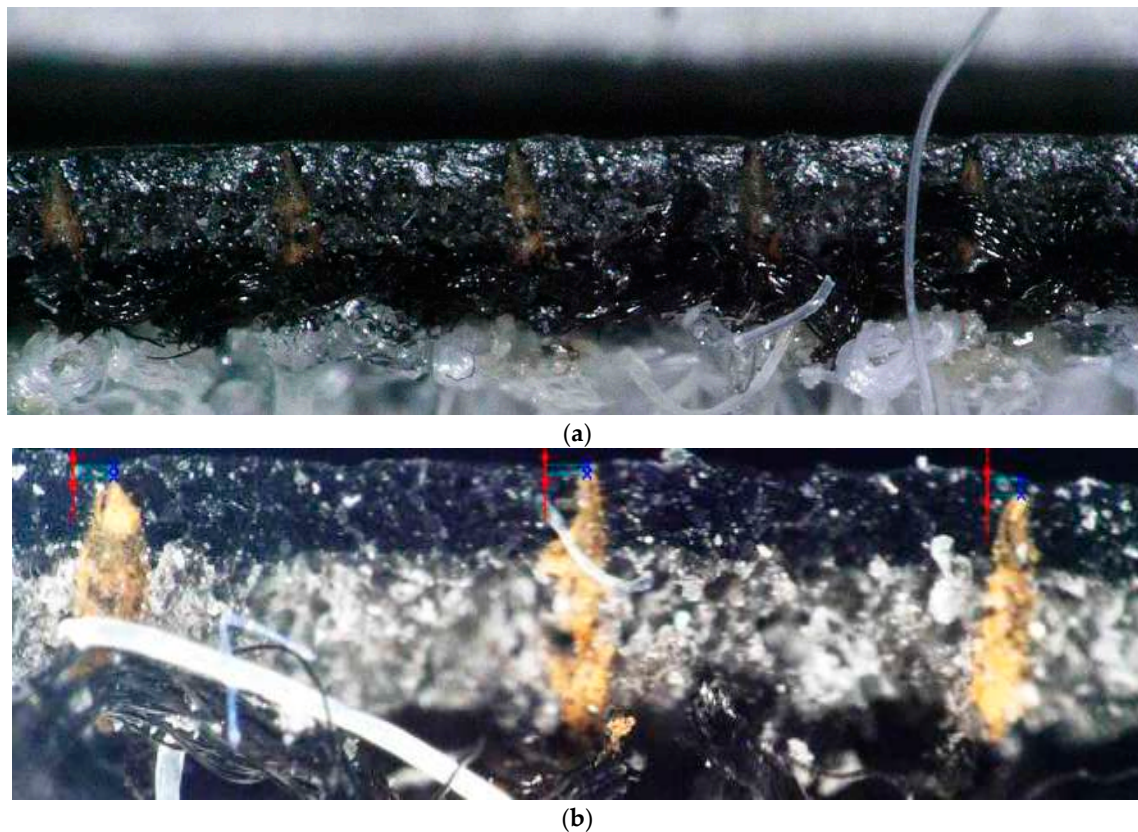


Figure 11. Microstructure images of nonconforming parts: (a) micro-holes in skin; (b) completed micro-perforation of micro-holes. The scale bar is 500 μm .

Post-pull-test values: Subsequent evaluations of the post-pull test revealed values within the predefined intervention thresholds, underscoring the need for further investigation to address the root causes.

Further action: This section delineates the ensuing steps, including additional testing protocols and proposed remedial measures aimed at rectifying the identified discrepancies and optimizing the manufacturing practices (Figure 12).

4.2. Proposed Measures and Next Steps

Laser processing with adhesive application on Bluemelt machine: Noteworthy consistency was observed within the specified tolerance limits, affirming the efficacy of this approach and providing valuable insights for future process refinements.

Cross-testing RHD parts on LHD nest: The validation experiments yielded pull test results consistent with the acceptance criteria, highlighting the potential interchangeability of the manufacturing parameters and informing standardized practices.

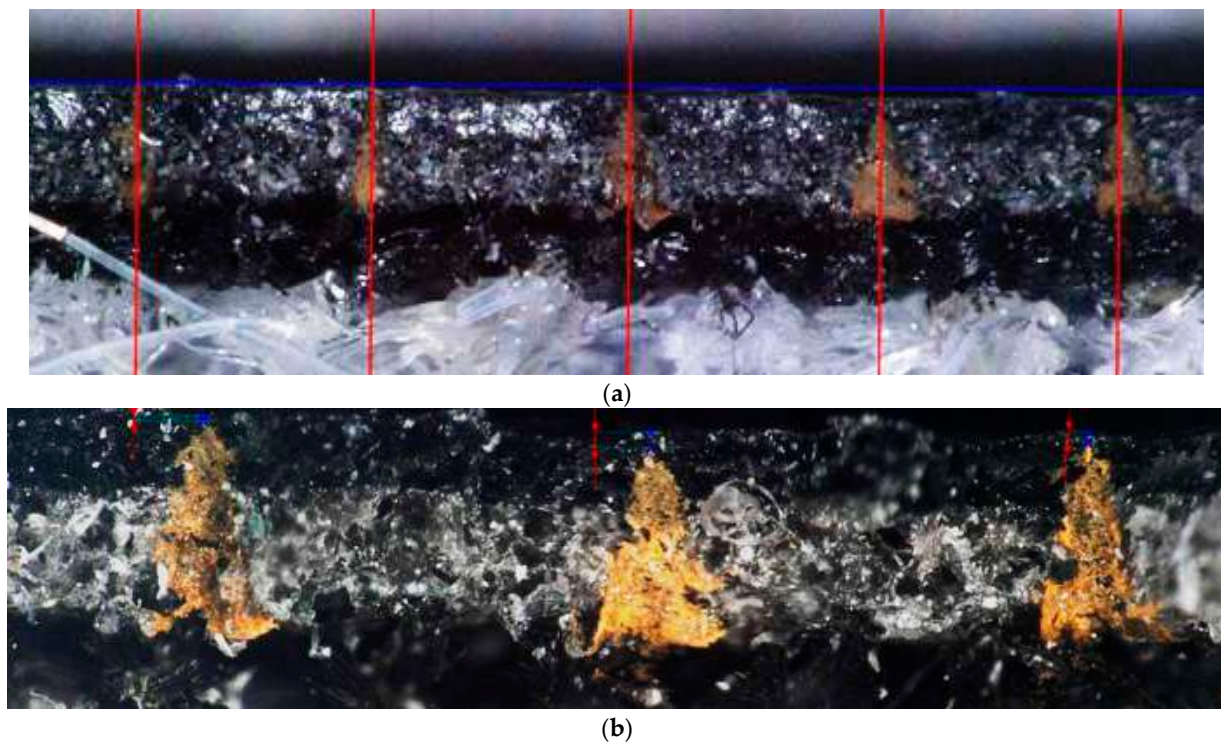


Figure 12. Microstructure images of conforming parts: (a) holes in skin; (b) completed micro-perforation holes. The scale bar is 500 μm .

New batch of material preparation: The rigorous assessment of the material batch's impact on the pull test tolerances can inform future manufacturing practices and enhance the process' predictability and repeatability.

Adhesive application and laser: The granular examination of the variances after adhesive application and laser processing can identify process optimization opportunities and minimize variability.

4.3. Detailed Analysis

Pull test influences: The in-depth analysis revealed the significant influences of the adhesive application techniques and spacer dimensions, necessitating meticulous control and calibration of the process parameters. The laser power needs to be set and optimized for both the P1 and P2 powers to ensure the coverage of defects from the previous process.

Parameter adjustments: The dynamic nature of the spacer thickness underscored the imperative for frequent iterations and standardization efforts to ensure consistent laser processing outcomes.

Continued research: The ongoing exploration of alternative laser processing scenarios, including variations in adhesive application techniques, is necessary to comprehensively delineate the process dynamics and inform iterative enhancements.

Glue application influence: The differential outcomes observed based on the adhesive application methodologies underscored the need for systematic evaluation and refinement to optimize the process parameters and ensure uniformity across adhesive types.

4.4. Proposed Enhancements

Spacer dimension standardization: The implementation of stringent protocols to standardize the spacer dimensions, minimizing the need for frequent parameter adjustments and enhancing the process' stability and predictability.

Laser line optimization: The precision calibration of the laser line positioning to ensure seamless alignment with the spacer fabric, facilitating consistent pull test results and mitigating variability.

Refinement of glue application: The systematic evaluation of the adhesive application methodologies to ascertain the optimal parameters conducive to uniform outcomes across different adhesive types and enhance the process' repeatability.

Contingency planning: The development of robust contingency plans to preemptively address potential machine-related issues, safeguarding the production continuity and efficiency.

Noise parameter adjustment: The fine-tuning of the noise parameters to optimize the process' stability and minimize adverse effects on the pull test outcomes, enhancing the overall process' reliability and repeatability.

4.5. Discussion

The investigation results indicate several significant findings and implications in the context of previous studies and working hypotheses. The detailed analysis of the airbag cutout laser process revealed substantial discrepancies in the application of LHD and RHD parameters, aligning with the initial working hypotheses. Additionally, other influences on the process, such as the adhesive application techniques and spacer dimensions, were identified.

Interpreting these results in the context of previous studies suggests that a more rigorous and systematic approach is needed to ensure consistency and reliability in the airbag cutout laser process. Compared to previous research, which has indicated similar challenges in laser processing for automotive applications, this investigation adds a new perspective by identifying and documenting detailed issues related to the incorrect use of the LHD and RHD parameters.

The implications of these findings are extensive and could significantly impact the production process across the automotive industry. Optimizing the airbag cutout laser process could lead to significant improvements in the quality and reliability of automotive safety components, thereby reducing the risk of failure and enhancing passenger safety.

Regarding future research directions, this investigation opens the door to several further studies. These include more detailed research into the influence of various process parameters on the final outcomes, exploring alternative adhesive application methods and assessing the impact of introducing new or improved technologies into airbag cutout laser processing.

These future research directions can contribute to the ongoing development of knowledge and practices in laser processing in the automotive industry and provide innovative solutions to improve the production processes and product quality.

Moreover, it is essential to consider the broader implications of autonomous vehicles beyond the manufacturing process. The widespread adoption of autonomous driving technologies has the potential to revolutionize urban mobility, reduce traffic congestion and minimize environmental impacts. By leveraging AI-driven autonomous vehicles, cities can reimagine transportation systems, optimize infrastructure utilization and enhance the overall quality of life for residents.

Furthermore, the ethical and societal implications of autonomous vehicles must be carefully examined. Issues such as liability, privacy and job displacement require thoughtful consideration and proactive measures to mitigate the potential risks and ensure equitable outcomes. Collaborative efforts between policymakers, industry stakeholders and the research community are essential to addressing these challenges and fostering public trust in autonomous driving technologies.

5. Conclusions

- The overall conclusion of the presented study is that the level of the laser power has a significant influence on the micro-perforation process.
- The analysis of the micro-perforation factors provides significant evidence for an interaction. The effect of one laser power factor depends upon the level of the other

laser power. Moreover, the statistically significant difference is highlighted by the design of experiments analysis and main effects plots.

- The laser micro-perforation process is optimal for a percentage of at least 25% of the laser power, with upper limits above 25% beneficial for both process stability and the material's resistance to the pull test. The analyzed parameters for the laser process, including the power (W) and material rupture resistance (N), are of paramount importance due to their critical characteristics (CC), significantly influencing the efficiency and quality of the process.
- The analyses of the experimental results provide valuable insights into the factors influencing the airbag cutout laser processing outcomes. The inappropriate use of LHD parameters for RHD components significantly contributed to process variability, resulting in nonconforming outcomes during pull testing. The correlations between the processing parameters and product quality underscore the importance of parameter optimization for consistent outcomes. To address this, standardized parameter sets tailored to specific component configurations are recommended, alongside enhanced quality control protocols including real-time monitoring. Future research may explore advanced laser processing techniques, like adaptive process control and machine learning algorithms, to optimize the efficiency and quality.

Author Contributions: Conceptualization, A.-N.R., D.-I.D. and A.-E.D.; data curation, A.-N.R.; formal analysis, A.-N.R., D.-I.D. and A.-E.D.; investigation, A.-N.R.; methodology, A.-N.R., D.-I.D. and A.-E.D.; resources, A.-N.R.; software, D.-I.D. and A.-E.D.; supervision, A.-N.R. and A.-E.D.; validation, A.-N.R. and A.-E.D.; writing—original draft, A.-N.R., D.-I.D. and A.-E.D.; writing—review and editing, D.-I.D. and A.-E.D. All authors have read and agreed to the published version of the manuscript.

Funding: This research received no external funding.

Data Availability Statement: The data are contained within the article.

Acknowledgments: The authors are grateful to the Transilvania University of Brasov for technical and financial support.

Conflicts of Interest: The authors declare no conflicts of interest.

References

1. Kannatey-Asibu, E. *Principles and Laser Materials Processing. Developments and Applications*, 2nd ed.; John Wiley & Sons, Inc.: Hoboken, NJ, USA, 2023.
2. Anming, H. *Laser Micro-Nano-Manufacturing and 3D Microprinting*; Springer Series in Materials Science; Springer Nature Switzerland AG: Cham, Switzerland, 2020; Volume 309.
3. Caristan, C.L. *Laser Cutting Guide for Manufacturing*; Society of Manufacturing Engineering: Dearborn, MI, USA, 2004.
4. Fischer, F.; Romoli, L.; Kling, R. Laser-based repair of carbon fiber reinforced plastics. *CIRP Ann. Manuf. Technol.* **2010**, *59*, 203–206. [[CrossRef](#)]
5. Hypsh, S. Femtosecond laser processing overcomes barriers for use in medical device manufacturing. *Adv. Mater. Process.* **2014**, *172*, 26–29. [[CrossRef](#)]
6. Huang, H.; Yang, L.-M.; Liu, J. Micro-hole drilling and cutting using femtosecond fiber laser. *Opt. Eng.* **2014**, *53*, 051513. [[CrossRef](#)]
7. Feng, G.; Li, G.; Wang, Z. Xiao Micro-hole Arrays and Net-like Structure Fabrication via Femtosecond Laser Pulses. In *Laser Micro-Nano-Manufacturing and 3D Microprinting*; Hu, A., Ed.; Springer Series in Materials Science; Springer Nature Switzerland AG: Cham, Switzerland, 2020; Volume 309, pp. 211–246.
8. Freitag, C.; Wiedenmann, M.; Negel, J.P.; Loescher, A.; Onuseit, V.; Weber, R.; Ahmed, M.A.; Graf, T. High-quality processing of CFRP with a 1.1-kW picosecond laser. *Appl. Phys. A* **2015**, *119*, 1237–1243. [[CrossRef](#)]
9. Onuseit, V.; Freitag, C.; Wiedenmann, M.; Weber, T.; Negel, J.P.; Löscher, A.; Ahmed, A.; Graf, T. Efficient processing of CFRP with a picosecond laser with up to 1.4 kW average power. In *Laser Applications in Microelectronic and Optoelectronic Manufacturing (LAMOM) XX*; SPIE: Bellingham, WA, USA, 2015; Volume 9350, pp. 107–113.
10. Weber, R.; Freitag, C.; Kononenko, T.V.; Hafner, M.; Onuseit, V.; Berger, P.; Graf, T. Short-pulse laser processing of CFRP. *Phys. Procedia* **2012**, *39*, 137–146. [[CrossRef](#)]
11. Lu, M.; Zhang, M.; Zhang, K.; Meng, Q.; Zhang, X. Femtosecond UV Laser Ablation Characteristics of Polymers Used as the Matrix of Astronautic Composite Material. *Materials* **2022**, *15*, 6771. [[CrossRef](#)]

12. Shehryar Khan, M.; Shahabad, S.I.; Yavuz, M.; Duley, W.W.; Biro, E.; Zhou, Y. Numerical modelling and experimental validation of the effect of laser beam defocusing on process optimization during fiber laser welding of automotive press-hardened steels. *J. Manuf. Process* **2021**, *67*, 535–544. [[CrossRef](#)]
13. Zhang, Y.Q.; Li, Z.; Yan, H.T. Damage characterization of carbon fiber/epoxy composite under laser irradiation and tangential flow. *High Power Laser Part. Beams* **2015**, *27*, 071014.
14. Riveiro, A.; Quintero, F.; Lusquiños, F.; Val, J.; Comesaña, R.; Boutinguiza, M.; Pou, J. Laser cutting of carbon fiber composite materials. *Procedia Manuf.* **2017**, *13*, 388–395. [[CrossRef](#)]
15. Yuki, H.; Sakai, K.; Shizuka, H. The effect of fiber laser machining parameters on thermal-affected zone of carbon fiber reinforced plastic. In *Advanced Materials Research*; Trans Tech Publications Ltd.: Bäch, Switzerland, 2016; Volume 1136, pp. 377–383.
16. Wang, J.X.; Wu, Y.W.; Zhang, G.Y.; Chao, Y.; Zhang, W.W. Experimental Research of CFRP Cutting by Using Water Jet Guided Laser Processing. *China Mech. Eng.* **2021**, *32*, 1608–1616.
17. Zhang, C.; Yuan, G.F.; Cong, Q.D.; Guo, B.C. Study of the water jet assisted laser cutting carbon fiber reinforced plastic (CFRP) composites. *Laser J.* **2018**, *39*, 68–71.
18. Gibra Isaac, N. *Probability and Statistical Inference for Scientists and Engineers*, 1st ed.; Prentice-Hall: Hoboken, NJ, USA, 1973.
19. Taeger, D.; Kuhnt, S. *Statistical Hypothesis Testing with SAS and R*; John Wiley & Sons: Hoboken, NJ, USA, 2014. [[CrossRef](#)]
20. NIST/SEMATECH. e-Handbook of Statistical Methods. Available online: <https://www.itl.nist.gov/div898/handbook/> (accessed on 27 April 2024).
21. Mason, R.L.; Gunst, R.F.; Balding, D.J. *Statistical Design and Analysis of Experiments with Applications to Engineering Science*; John Wiley & Sons: Hoboken, NJ, USA, 2003.
22. Montgomery, D.C.; Runger, G.C. *Applied Statistics Probability Engineers*, 5th ed.; John Wiley & Sons: Hoboken, NJ, USA, 2011.

Disclaimer/Publisher’s Note: The statements, opinions and data contained in all publications are solely those of the individual author(s) and contributor(s) and not of MDPI and/or the editor(s). MDPI and/or the editor(s) disclaim responsibility for any injury to people or property resulting from any ideas, methods, instructions or products referred to in the content.

RELIABILITY ESTIMATION OF TOWED GRADER ATTACHMENT USING FINITE ELEMENT ANALYSIS AND POINT ESTIMATION

Summary

The paper presents an analysis of the reliability of front blade, rear blade and frame of the towed grader as well as experimental validation of the results obtained from the finite element analysis. The analyzed prototype was designed for maintenance and repair of forest roads and equipped with two types of blades for cleaning and levelling the ground surface. Lifetimes of towed grader attachments can be estimated with high accuracy using three-parameter Weibull distribution. The values of the location parameter γ were determined by using the maximum values of the correlation coefficient, while the method of maximum likelihood was used for the point estimation of the parameters. Because higher values of the shape parameter had been obtained, the point estimation and estimation with confidence intervals of components lifetimes were performed. The analysis of the results indicates that the used assumptions may not fully take the complex stresses encountered in use into account.

Key words: towed grader, reliability estimation, finite element analysis (FEA), Weibull distribution, confidence interval

1. Introduction

An ambitious and rapidly growing rate of the earth moving machinery industry is achieved owing to the high performance construction machinery with complex mechanisms and the automation of the construction activities. Bulldozers, scrapers, graders, excavators and other machines are widely used for most arduous earth moving work in construction engineering. Thus, it is really necessary for the designers to provide not only equipment of maximum reliability but also of minimum weight and cost, keeping the design safe under all loading conditions by performing careful stress analyses of machines [1, 2].

Towed graders are designed for a variety of applications including earthworks for removing vegetation, grading, road building and maintenance, ditch and slope works, scarifying and snow removal [3, 4].

These types of machines are characterized by a good handling of an actively working body (blade) that is displaced horizontally, vertically and laterally. The maneuverability of the

blade and the creation of the needed force for the blade to penetrate the soil are the main requirements imposed on the towed grader to ensure its operational performance [5].

Most of the studies on reliability estimation of grader structural components have focused on the finite elements analysis (FEA), [1, 6-10].

FEA is the most powerful technique for calculations of strength of the structures working under some known load and boundary conditions [2]. The implementation of the FEA makes the identification of weak components of towed grader attachments possible because a strength analysis is performed.

A case study on the analysis and simulation of shock resistance of a grader blade was carried out by Yongjun et al. [11]. The authors determined that a crack on a grader blade often occurred during an impact. In order to avoid this failure, shock resistance of the blade was analyzed and the characteristic curve of the shock resistance of the blade was also obtained based on different types of impact acceleration. They also studied the FEA model, impacts of different types of obstacles were transferred into impact forces, and the impact characteristics of the blade were acquired rapidly based on the dynamic explicit finite element method.

In this paper, we propose a design solution for towed grader attachments, i.e. for two blades designed for maintenance and repair of forest roads, including an estimation of the grader reliability and experimental validation of the results obtained from the FEA. The main working part of the grader blade is the front blade, to which auxiliary ripping teeth and a bulldozer front blade can be mounted. The front blade can be used either as embankment or ditch digging equipment, depending on the change of the working position. The FEA analysis enables us to determine levels of stress and deformation on the grader frame, the front blade and the rear blade and to estimate the product lifetime. Based on the FEA results and considering the performance specification, the duration of exploitation, as well as the design and technological factors, the reliability of the towed grader attachments has been estimated using the most suitable statistical model for such an analysis. The reliability of the front blade, the rear blade and the frame was estimated by using the three-parameter Weibull distribution. The objective was to estimate the distribution parameters by two methods: point estimation and estimation with confidence intervals.

2. Design characteristics of the towed grader designed for maintenance of forest roads

The prototype of the analyzed towed grader was designed and built by the Institute of Research and Forest Management Bucharest, Laboratory for Forest Works Mechanization. Its main technical characteristics are as follows (Fig. 1a):

- main dimensions: length: 2,000-2,200 mm, width: 2,200-2,500 mm, height: 900-1,000 mm,
- weight: 550-600 kg,
- angle of the blades: 0°- 30°,
- blade height: 540-560 mm.

The front blade is made of steel sheet sleeve 8 mm thick in order to obtain the curvature for the transport of filler material. The blade has reinforcing ribs (gussets) at the back, arranged equidistant so as to stiffen the blade. At the bottom of the moldboard, there is a scraper knife made of manganese austenitic material with a relatively low hardness (250 HB - Brinell units) with high wear resistance, commonly termed the Hadfield steel.

Due to heavy wear that they are subjected to, scraper blades are spare parts.

At the upper part of the blade and decentered from the axis of symmetry of the blade, a bracing tube is welded to the rod of the hydraulic cylinder which controls the rotation of the blade. Also, at the top there is a metal box with a screw of special design that fastens bearing

bushes to the chassis. The special design screw mounted in the blade is fastened to the chassis with a nut and a cotter pin is inserted to prevent the nut from loosening.

The front blade has a length of 2,000 mm, which permits spreading and levelling the material in a single pass, which is completed by the second blade (the rear blade) arranged asymmetrically with respect to the front blade. This technological solution has been adopted to improve the load distribution on the two blades. In addition, the asymmetry to the attachment of the blades to the frame results in a working width of about 2,700 mm in the case when the blades are arranged perpendicular to the longitudinal axis of the chassis.

The rear blade has an identical design with the front blade, having the same kind of a longitudinal scraper knife (similar to the one on the front blade) at the bottom of the working area. The movement relative to the longitudinal axis is carried out separately by the first blade by means of the second hydraulic cylinder. It is possible that the grader works with one of the blades inclined at an angle and the second blade perpendicular to the direction of advance of the grader.

The blades are powered by two hydraulic cylinders. The blades work simultaneously with an overlap of 1,600 mm centered by the longitudinal axis of the chassis. In this manner, in a single pass of the grader, the blades, levelling the road surface, pass the surface twice. With the inclination of the blades operated by the hydraulic cylinders, the working width decreases with a sinusoidal projection, reaching the minimum value of 2,500 mm.

In the case when a forest road is repaired with gravel it will be necessary to obtain parallelism between the equipment frame and the road surface that must be repaired.

3. Finite element analyses of the subassembly of the towed grader

A 3D model of a towed grader (Fig. 1a) was performed by using the Pro-Engineering software, widely used in design and mechanical engineering. In the 3D modelling only the components that have a structural role in the operation and the most unfavorable position of the two blades, i.e. when they rotate through 30 degrees relative to the transverse axis of the machine, were taken into account. The hydraulic cylinders, which tilt the blade, were not modelled, but were simulated directly in the Ansys Workbench.

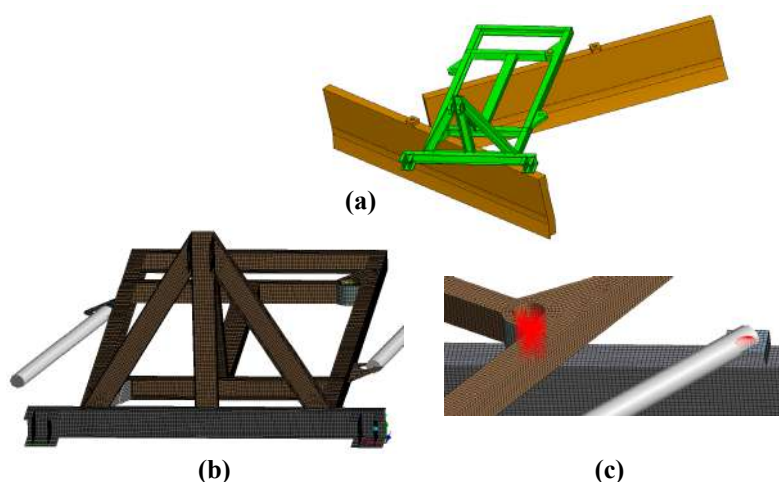


Fig. 1 Finite element modelling of the towed grader: (a) 3D model; (b) 2D towed grader frame; (c) the link between the blade and the frame and between the blade and the hydraulic cylinder

The FEA was performed by using the Ansys Workbench software. The 2D finite elements that simulate profiles and sheets as they are given in the model were assigned material properties including the thickness of each component.

The towed grader structure is made of square profiles, C profiles and plates. On the front frame there are two mounting brackets and a mounting bracket subassembly of the upper link. This structure is welded, non-removable and simulated with shell-type elements (Fig. 1b). The links between the welded components are achieved by using common joints, located between the finite elements of the weld area. Shell type 2D finite elements were used to simulate the blade. The welded blade sheets were connected by common nodes between the finite elements of the weld area. The pin around which the front blade rotates to the grader frame was modelled with a rigid element, linked to the two components, the blade and the frame, which rotates freely around the axis of the pin (Fig. 1c). The hydraulic cylinder was simulated by using a deformable beam type 1D element, which preserved the cylinder section properties. The links with the blade, i.e. with the grader frame were made by using rigid elements fixed in all degrees of freedom (Figs. 1b and 1c).

The finite element modelling of the towed grader has taken the following into account: the numerical modelling is to be as close to actual operating conditions as possible, the quality of items and the number of nodes and elements result in a finite element mesh.

When the levelling blade is calculated, the blade geometry is a portion of a cylinder having a radius of 3,100 mm, sectioned by two generators. The blade is considered to be embedded in the centre of the cylinder by means of a rigid member at its upper end. On the working surface of the blade the applied normal pressure is about 0.016727 MPa, representing a half of the traction force needed for the levelling process (36000 N).

For the purpose of obtaining the results from the numerical calculation that would be as close to reality as possible, all forces acting on the towed grader during operation will be taken into account (Fig. 2). The traction force produced by the tow tractor is $F_{tot} = 36,000$ N and it is exerted to each of the grader blade. When the structure is subjected to such stress, it was considered that the worst case is when each blade grader was charged with the same amount of material (ballast) over the whole surface. The force is applied normal to the working surface of the blade, angled at 30 degrees. Gravitational acceleration was applied to the whole system taking the grader mass into account. The constraints in the finite element model were all degrees of freedom, the clamping brackets and the mounting bracket subassembly of the upper link of the grader.

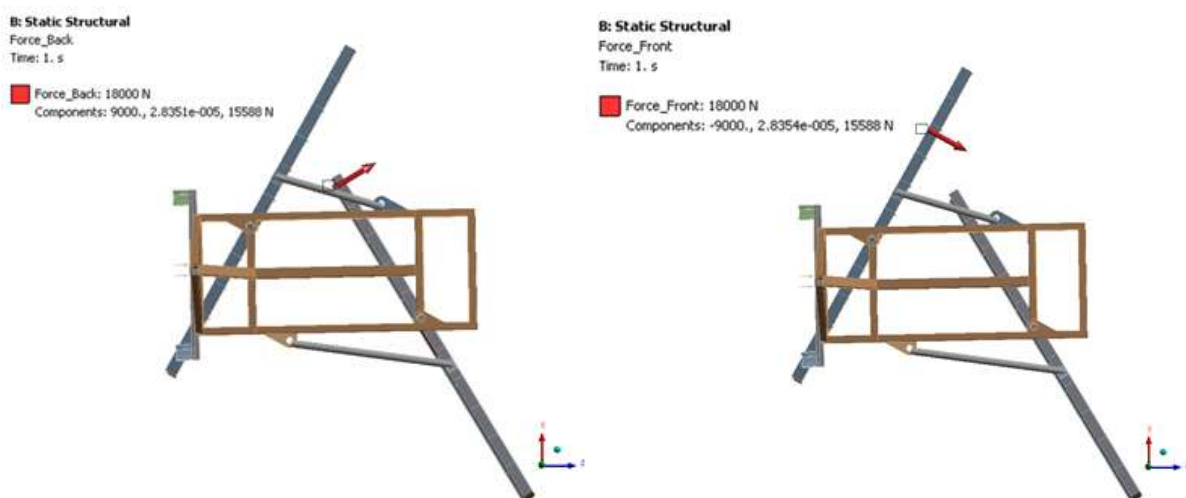


Fig. 2 The force decomposition in three directions of each blade

4. Reliability analysis of towed grader attachments

In order to estimate lifetime of the towed grader attachments, in the first stage we identified the most suitable statistical model for such an analysis. In this respect, the Anderson-Darling concordance test was used, applied on experimental data, $y_i, i = \overline{1, n}$ considering four statistical distributions used in the reliability analysis (Fig. 3).

Applying this concordance test to the four cases, the statistic estimation of the following parameter is carried out as follows [12]:

$$A_n^2 = n \cdot \int_{-\infty}^{\infty} \frac{[Q(y) - F(y)]^2}{F(y) \cdot [1 - F(y)]} \cdot dF(y). \quad (1)$$

The obtained value is a measure of the discrepancy between the empirical distribution, $Q(y)$, sampling values and the considered theoretical distribution, $F(y)$.

If, for the empirical distribution the relation is used:

$$Q[y_{(i)}] = \begin{cases} 0, & \text{for } Y < y_{(1)} \\ \frac{1}{n}, & \text{for } y_{(i)} < Y < y_{(i+1)}, \quad i = \overline{1, n-1}, \\ 1, & \text{for } Y > y_{(n)} \end{cases} \quad (2)$$

then, the Anderson-Darling test statistic results in [13]:

$$A_n^2 = - \sum_{i=1}^n \frac{2 \cdot i}{n} \cdot \{ \ln F(y_{(i)}) + \ln [1 - F(y_{(n+1-i)})] \} - n. \quad (3)$$

Using the experimental results obtained from the operation of the three attachments to the towed grader (the front blade, the rear blade and the frame), the calculated values of the Anderson-Darling statistics (Table 1) indicate that the Weibull distribution allows modelling of the lifetime of this equipment with the highest accuracy (Fig. 3).

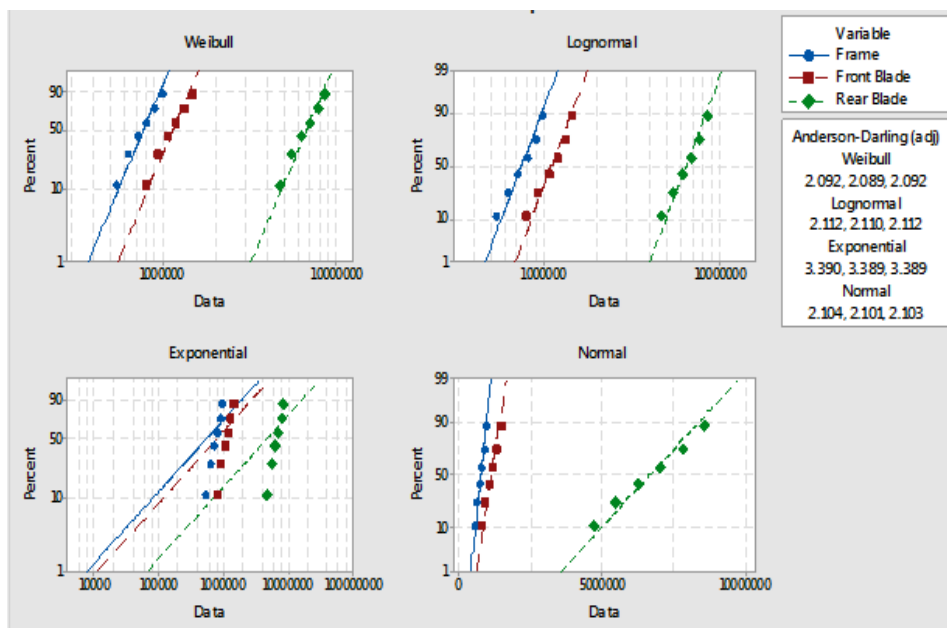


Fig. 3 Probability plot of the Anderson-Darling test for the frame, the front blade and the rear blade

The location parameter γ is estimated by using the correlation coefficient method and minimum lifetimes are determined experimentally (Table 2).

Table 1 The Anderson-Darling statistics

Distribution	Anderson-Darling statistic values, A_n^2		
	Frame	Front Blade	Rear Blade
Weibull	2.092	2.089	2.092
Log-normal	2.112	2.110	2.112
Exponential	3.390	3.389	3.389
Normal	2.104	2.101	2.103

The estimation method consists of determining the location parameter values, γ , under maximum conditions of the correlation coefficient values [14].

Table 2 The parameter estimation

Coefficient	Towed grader		
	Frame	Front Blade	Rear Blade
γ	315226.979	460147.983	2746288.329
ρ	0.99821	0.99839	0.99821

The results shown in Table 2 were obtained by using an application in the Mathcad software. Knowing the values of the location parameter, the obtained values are two-parameter Weibull distributed (Table 3).

Table 3 Lifetime estimation of the frame, the front blade and the rear blade.

Issue	Lifetime (cycle), $x_i, i = \overline{1, n}$		
	Frame	Front Blade	Rear Blade
1	224773.02	339852.02	1953711.67
2	314773.02	472852.02	2733711.67
3	404773.02	609852.02	3523711.67
4	494773.02	739852.02	4303711.67
5	584773.02	869852.02	5083711.67
6	674773.02	1009852.02	5873711.67

In order to estimate the reliability and unreliability functions, the probability density function and the hazard rate of the front blade, the rear blade and the frame of the towed grader, the statistical processing of experimental data allows us to determine the statistical parameters of distribution using specialized functions from the Minitab [15] and Mathcad software.

The point estimation method used is maximum likelihood. The estimated values of the shape and scale parameters of the two-parameter Weibull distribution are obtained as a solution to the equation system [12, 14, 16-21].

Because the sample size is very small, asymptotical properties of the maximum likelihood estimators cannot be applied in this case, and the estimations with confidence intervals were calculated on the basis of two random variables, independent of the sample size (n) and the type of test ($n = r$) for the complete test. The point estimation and the estimation with confidence intervals for the Weibull distribution parameters were determined based on the estimated lifetime presented in Table 3 and are shown in Table 4. The confidence level used is $1 - \alpha = 0.95$ and corresponding values of the random variables $v(r, n)$ and $k(r, n)$ were taken from [14].

Table 4 Parametric estimation of β with confidence interval

Parameter	Frame	Front Blade	Rear Blade
β	3.312	3.345	3.308
β unbiased mean estimate	2.475	2.500	2.472
β unbiased median estimate	2.786	2.814	2.782
β_L	1.125	1.137	1.124
β_U	5.221	5.273	5.214
η	503199.504	753268.187	4377022.514
η unbiased mean estimate	509353.318	762387.877	4430623.371
η unbiased median estimate	509302.572	762312.678	4430181.362
η_L	349418.523	524968.199	3037882.11
η_U	745295.925	1111319.82	6486304.749

Fig. 4 shows a comparison between values of the reliability indicators of the three attachments of the towed grader in the Weibull probability network.

High values of the shape parameters $\beta = 3.308$, $\beta = 3.312$ and $\beta = 3.345$ indicate that the normal distribution for reliability modelling can be used. The same conclusion can be drawn from the Anderson-Darling statistics analysis, as shown in Fig. 4.

The point estimation and the estimation with confidence intervals for normal distribution parameters were determined based on the estimated lifetime given in Table 3 and they are shown in Table 5. The confidence level used is $1 - \alpha = 0.95$.

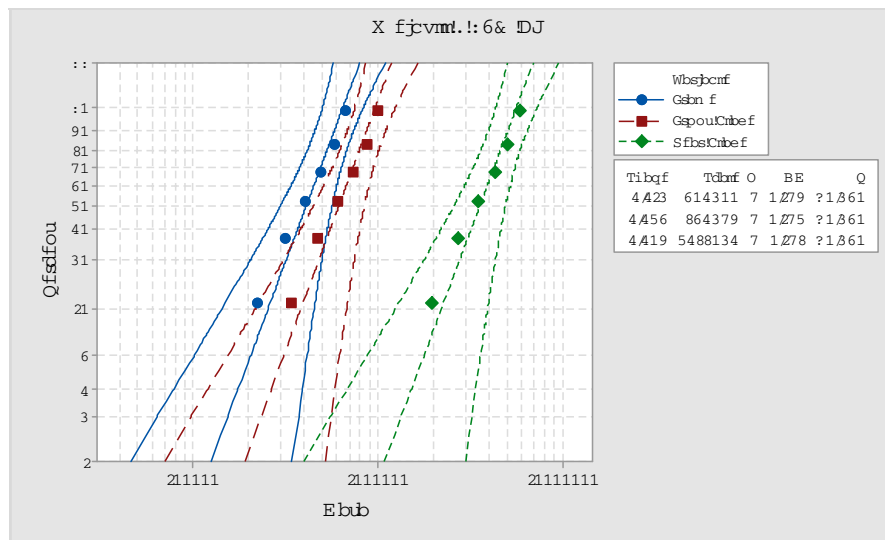


Fig. 4 Probability plot of the frame, the front blade and the rear blade for the Weibull distribution

Table 5 Parametric estimation of μ with confidence interval

Parameter	Frame	Front Blade	Rear Blade
μ	765000.00	1133833.33	6658333.33
μ_L	588301.71	871801.70	5119652.86
μ_U	941698.29	1395864.97	8197013.80
σ	168374.5824	249688.1388	1466198.031
σ_L	105100.7617	155857.3343	915212.544
σ_U	412957.8561	612388.622	3596017.801

Fig. 5 shows a comparison between values of the reliability indicators of the three attachments of the towed grader with confidence interval in a network having normal probability distributions.

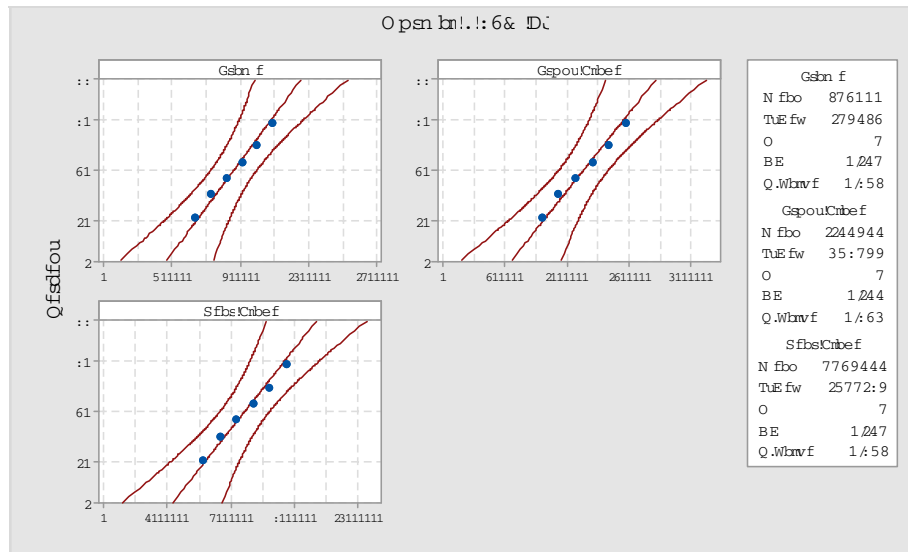


Fig. 5 Normal probability plot of the frame, the front blade and the rear blade

5. Results and discussion

The results obtained from the finite element calculations performed for the prototype of a levelling blade focus on deformation and stress levels. Since the blade is a structure made of welded steel plates, the assumptions for the analytical calculation were simplified. The finite element calculation was modelled based on the existing levelling blade and it took all the components, such as tables and gussets behind the blade, into account. Modern methods of calculation, widely used in the machine building industry and beyond, were used to check the blade size calculation. Due to the curvature of the blade, forces acting on the blade were broken down in each direction.

The calculated maximum displacement on the levelling blade is 0.4 mm and is located at the bottom of the blade, as shown in Fig. 6a. Also, blade positions (undistorted or deformed) are presented, indicating the deformation gradient (scaling factor 100). The maximum value of the equivalent stress (88.7 MPa) is obtained on the back of the blade, near the gusset-plate weld zone. It is noted that the stress value does not exceed the yield strength (365 MPa) of the material (Fig. 6b). From Figs. 6c and 6d it can be seen that the main stress acting on the blade is compressive stress. It is caused by the pressure applied to the blade surface, which compresses the gussets that are located behind the blade. For the calculation of the levelling blade a safety factor greater than 2, which is calculated by the finite element method using the ANSYS Workbench, is required. As can be seen in Fig. 6e, the minimum value of the safety factor is 4. The safety factor value is obtained in the area near the gusset-back blade plate weld zone. Forces acting on the two blades of the towed grader developing reaction forces in each direction are presented in Fig. 6f.

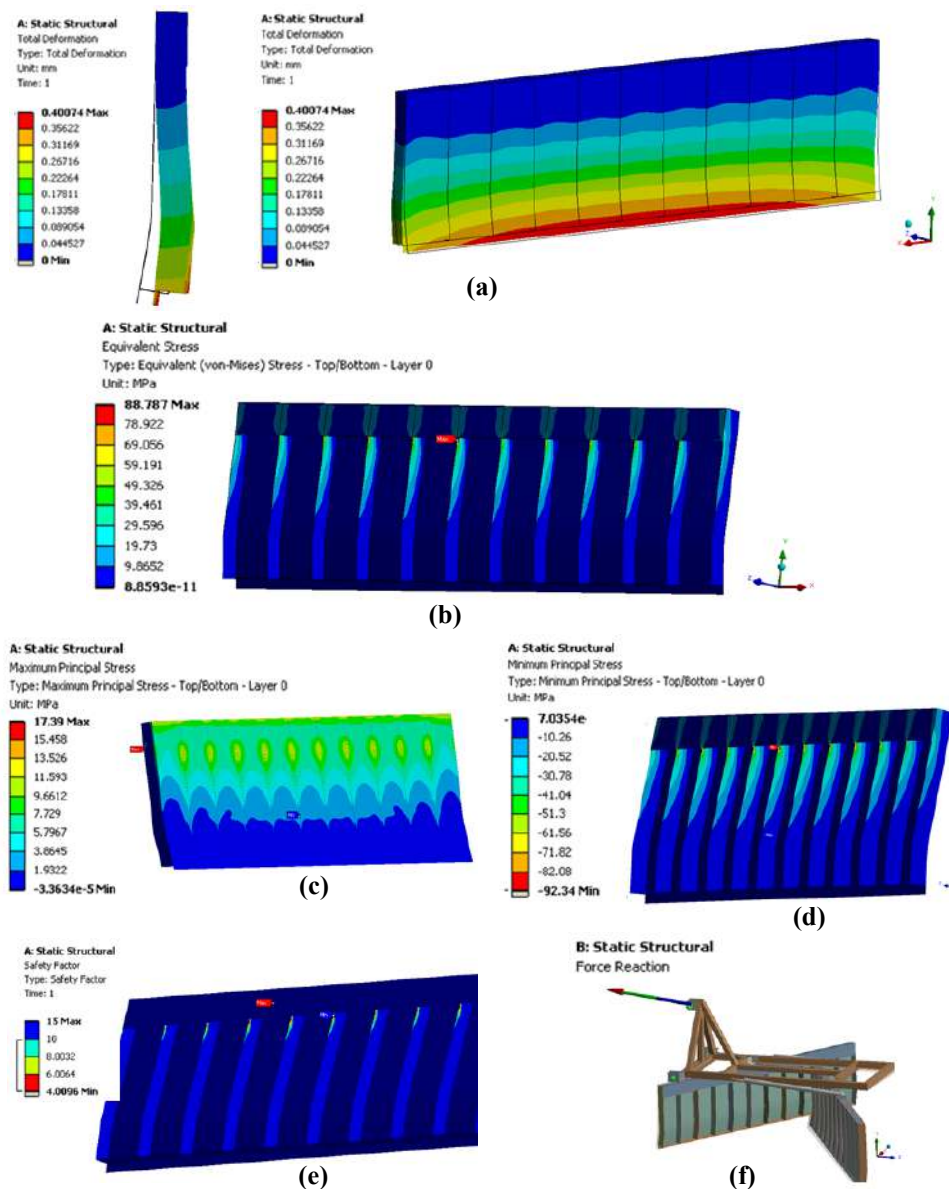


Fig. 6 Equivalent von Mises stresses, distribution of the safety factor and total reaction force

Due to the fact that the two blades are angled in opposite directions, the resultant force in the X direction is cancelled. The reaction force obtained in the Y direction is given by the mass of the vehicle and by the force component that causes stress on these two blades having the same direction. The higher force acts around the Z axis, in the direction of the movement of the tractor. The total resultant force is close to the maximum value of the towing force. The difference in the calculated total force in the extent from 31,342 N to 36,000 N can occur due to nonlinearities appeared in the model, numerical calculation errors specific to the calculation method, but also because of the way the connections between the components of the finite element model are made.

The maximum total displacement calculated on the towed grader is 46.6 mm and was located at the bottom of the blades, the point farthest from the grader blade attachment to the frame (Fig. 7). Fig. 7 shows the grader deformation in side view where the real grader deformation can be seen and the undistorted position is illustrated as wireframe on an enlarged scale of 5:1. Also, the frame displacement value is 26.3 mm.

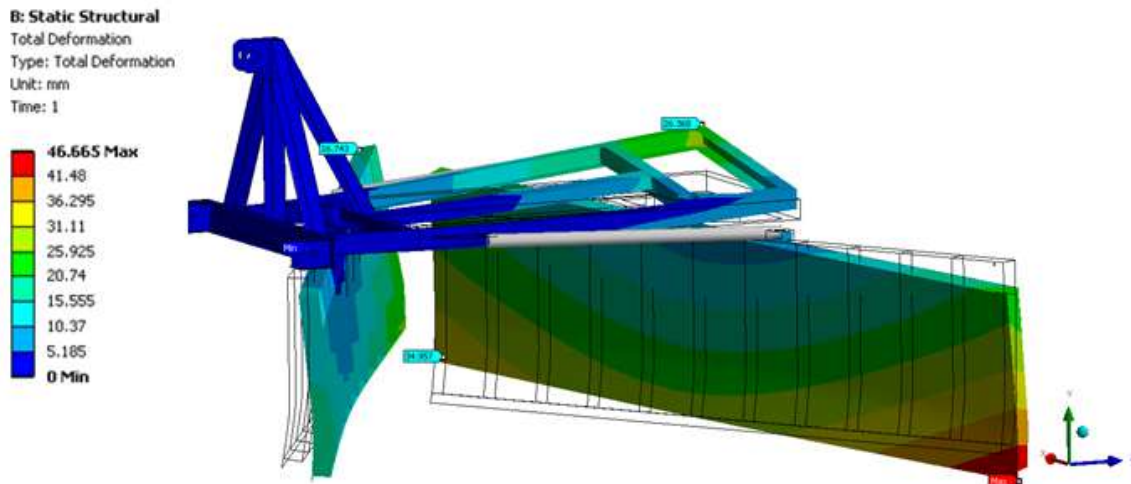
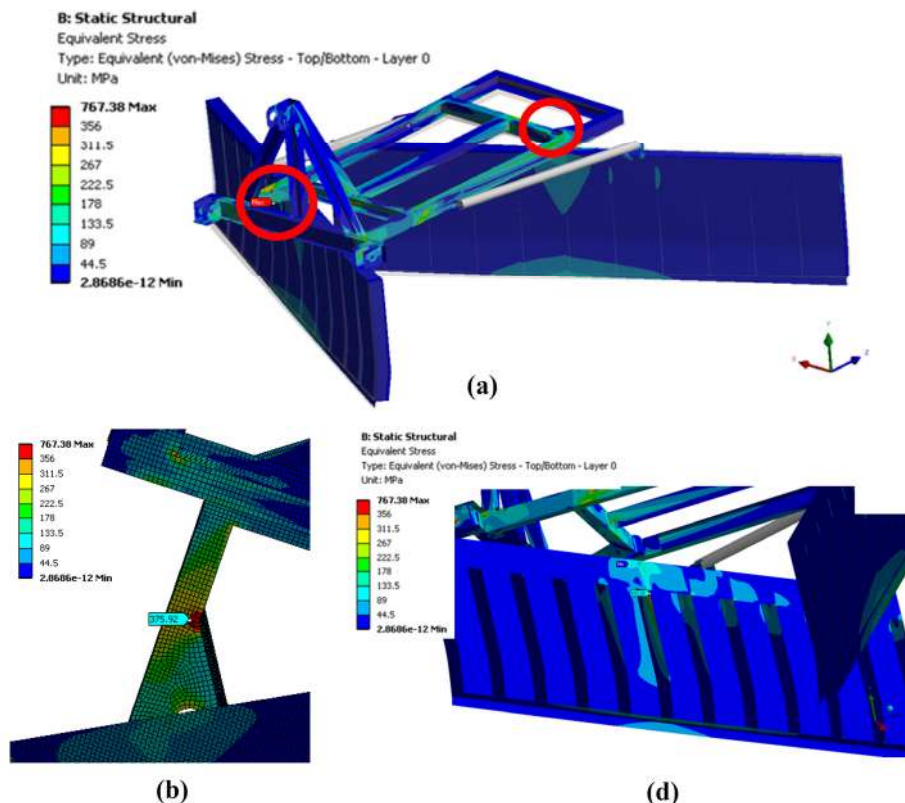


Fig. 7 Total shift of the towed grader

Von Mises equivalent stresses on the towed grader are shown in an overview in Fig. 8. The maximum stress (767 MPa) is obtained in the area in which the frame is welded to the plates forming a rotating hitch of the tilting blades (Fig. 8a). These values of stresses in the weld areas are not real, because in these areas, due to the transformations of the welded material during welding, mechanical properties of materials change. For this reason, the reading is made at a distance equal to the size of the weld. The real value of the maximum equivalent stress is about 376 MPa, measured in the area in which the frame is welded to plates forming the rotating hitch used for tilting the front blade (Fig. 8b). In this weld area the equivalent stress is about 305 MPa (Fig. 8c). In Figs. 8d and 8e the equivalent stress distribution on the two blades is shown. Maximum stresses are located near welds, in the middle part of the blade, right near the rotation couplings. Thus, on the front blade, the maximum stress is approximately 433 MPa (Fig. 8d) and on the rear blade it is about 374 MPa (Fig. 8e).



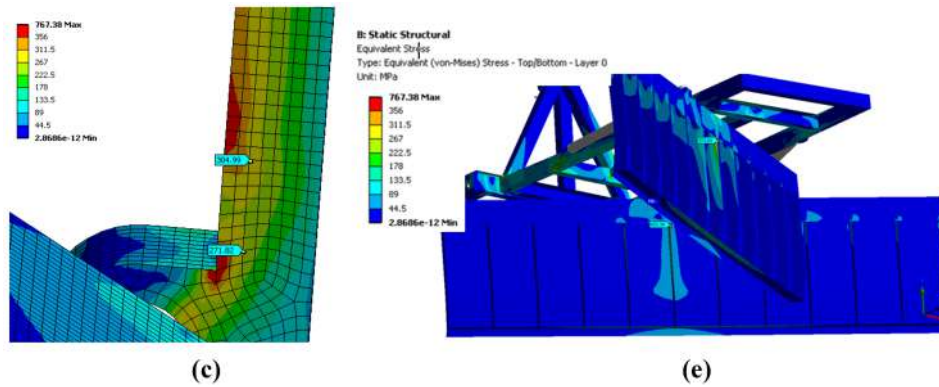


Fig. 8 Von Mises equivalent stress: (a) overview; (b) and (c) details in weld areas; (d) front blade; (e) rear blade

In terms of static loads acting on the towed grader, the maximum obtained stresses exceed the yield stress of material (356 MPa), but are below the breaking point of the material (441 MPa). Thus, the maximum stress on the grader frame is 376 MPa, on the front blade it is 433 MPa and on the rear blade it is 374 MPa. These results indicate that during operation or after a limited period of time the towed grader can undergo permanent plastic deformation without reaching the breaking point. Also, the results obtained from the durability calculation in the marked areas are synthetically presented. The minimum lifetime is about 5.4×10^5 cycles and the critical area is on the front side of the frame, in the area in which the frame is welded to the plates that form the rotating hitch for tilting the blade. The front levelling blade has a minimum life of 8×10^5 cycles and this refers to the areas in which the gussets are welded to the plates which form the blade. Minimum lifetime of the rear blade is 4.7×10^6 cycles.

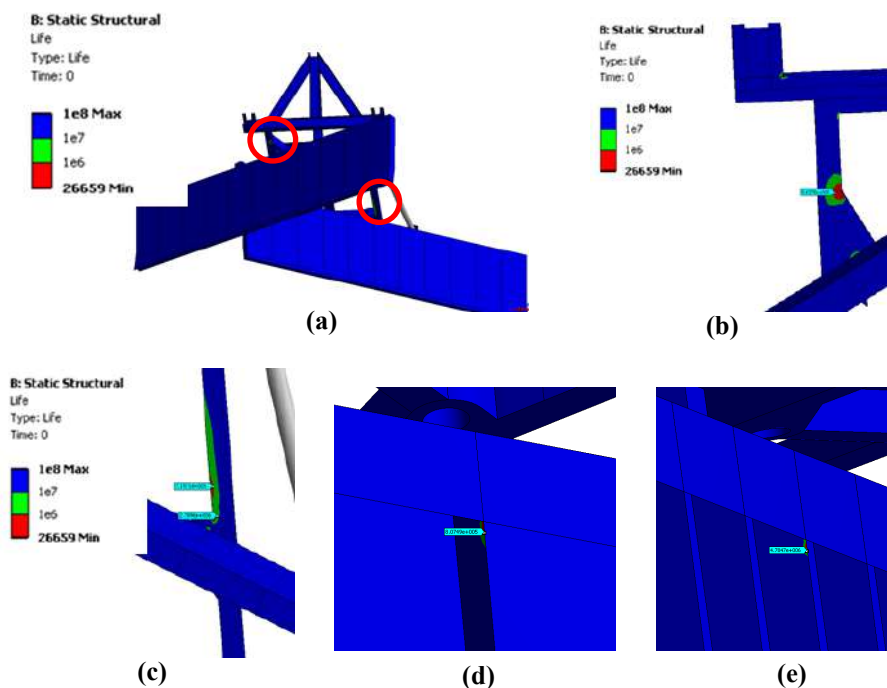


Fig. 9 Estimated lifetime: (a) general view; (b) and (c) area in which the frame is welded to plates forming rotating hitch for tilting two blades; (d) lifetime of the front blade; (e) lifetime of the rear blade.

The reliability of the towed grader subassemblies can be modelled by using the Weibull distribution model. In Table 6 and Fig. 10 analytical expressions of reliability functions for the three analyzed subassemblies are specified and values of the main reliability indicators are estimated based on the experimental results collected from the operation of these attachments. The value of the location parameter γ indicates the minimum lifetime of each subassembly,

estimated in real operating conditions. Reliability distribution plots for the frame, the front blade and the rear blade are presented in Fig. 10.

Table 6 Reliability indicators

Subassembly	The main reliability indicators			
	$R(t)$	γ	μ	σ
Frame	$e^{-\left(\frac{x-315227}{503200}\right)^{3.312}}$	315227.0	765000.0	168374.6
Front blade	$e^{-\left(\frac{x-460148}{753268}\right)^{3.345}}$	460148.0	1133833.3	249688.1
Rear blade	$e^{-\left(\frac{x-2746288}{4377023}\right)^{3.308}}$	2746288.0	6658333.3	1466198.0

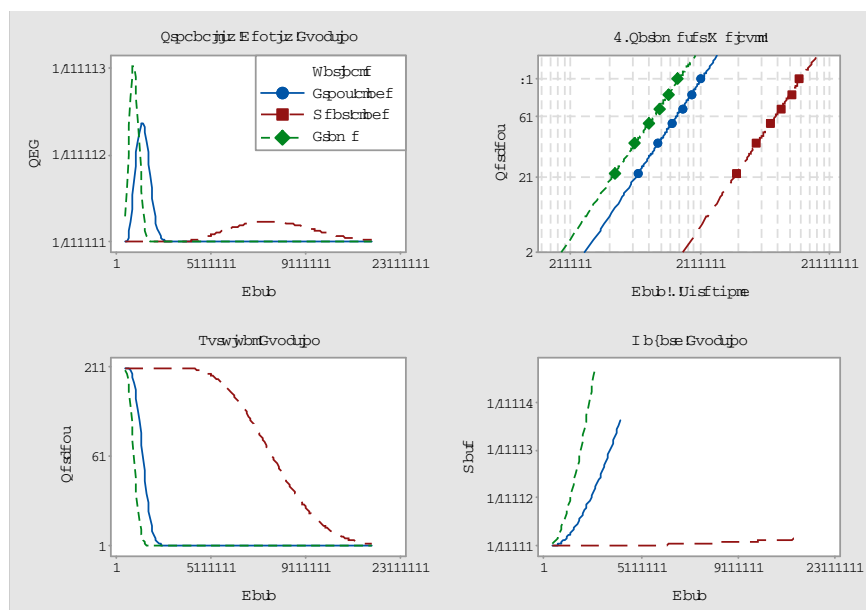


Fig. 10 Reliability distribution overview plot for front blade, rear blade and frame

6. Conclusions

In this paper, a reliability analysis of a prototype of a towed grader equipped with two blades and designed for maintenance and repair of forest roads is presented. Lifetime of the front blade, the rear blade and the frame was estimated and the FEA was validated through experimental studies. Based on the performed FEA modelling on the towed grader attachments, the following conclusions can be drawn:

- The maximum displacement obtained on the towed grader is 46.6 mm; on the rear blade it was obtained on the corner farthest from the point of rotation;
- The maximum stress obtained on the frame is 376 MPa, and it is located in the area in which the frame is welded to the plates forming the torque needed for the inclination of the blade. On the front levelling blade, the maximum stress is 433 MPa, and on the rear levelling blade the maximum stress is 374 MPa. The stress values obtained on the towed grader exceed the material yield strength (356 MPa), but they are lower than its breaking limit (441 MPa);
- The determined minimum lifetime is $5.4e5$ lifecycles in the area in which the frame is welded to the plates forming the torque needed for the inclination of the blade. On

the front levelling blade, the lifetime is $8e5$ cycles. These values do not fit the theory of fatigue which states that if the number of cycles exceeds $1e6$, lifetime is unlimited. On the rear levelling blade, lifetime amounts to $4.7e6$ cycles, which exceeds the duration of $1e6$ cycles, and this is not a problem as long the lifetime complies with the stress cycle determined by the calculation.

The reliability analysis carried out for the towed grader attachments, based on the data collected from actual operating conditions allows us to draw the following conclusions:

- Reliability modelling of high accuracy can be achieved when the three-parametric Weibull distribution model is used;
- The value of the estimated minimum lifetime in actual operating conditions is lower than the value determined by the FEA method. These results indicate that the made assumptions may not have fully taken the complex stresses encountered in use into account.
- From Fig. 4 it can be concluded that the reliability values of the frame and the blade assemblies are close to each other, whereas the reliability value of the rear blade is much higher compared to the first two attachments.
- A high value of the shape parameter allows us to use normal distribution in the reliability analysis. This has offered the possibility of point estimation and estimation with confidence intervals of the average lifetime of the three component systems, as well as the estimation of the standard deviation of their lifetimes.
- Knowing the parameter values of the statistical distribution and the values of the main reliability indicators allows us a more useful approach to conducting preventive maintenance activities and their realistic planning.

Acknowledgement

The authors are grateful to the Transilvania University of Brasov for financial support. The analyzed equipment was provided by I.C.A.S. Bucharest and we would like to thank for their support and participation during data collection.

REFERENCES

- [1] Motka, C. P. and Momin, R. I. (2015). Development of backhoe machine by 3-D modelling using CAD software and verify the structural design by using finite element method. *International Journal for Innovative Research in Science & Technology* 8, 49-52.
- [2] Patel, B. P. and Prajapati, J. M. (2011). A review on FEA and optimization of backhoe attachment in hydraulic excavator. *International Journal of Engineering and Technology* 3, 505-511.
- [3] Hawthorne Cat (2015). Cat Motor Graders www.hawthornecat.com/cat_motor_graders
- [4] TEREX (2015). Heavy duty motor graders. Motor graders product range, www.terex.com/construction/en/idc03/groups/webcontent/@web/@con/documents/web_content/ucm03_081012.pdf
- [5] Debeleac, C. and Nastac, S. (2012). Comparative analysis between operational performances of motor grader equipment's. *The Annals of "Dunarea De Jos" University of Galati- Mechanical Engineering* XIV, 87-90.
- [6] Meck, K.-D. and Zhu, G. (2008). Improving mechanical seal reliability with advanced computational engineering tools. Part 1: FEA. *Sealing Technology* 1, 8-11, [https://doi.org/10.1016/S1350-4789\(08\)70023-0](https://doi.org/10.1016/S1350-4789(08)70023-0)
- [7] Gaspar, B., Naess, A., Leira, B. J. and Guedes Soares C. (2011). Efficient system reliability analysis by finite element structural models. In *ASME 30th International Conference on Ocean, Offshore and Arctic Engineering: Structures, Safety and Reliability* 2, 693-702. <https://doi.org/10.1115/OMAE2011-49950>
- [8] Bing, L., Meilin, Z. and Kai, X. (2000). A practical engineering method for fuzzy reliability analysis of mechanical structures. *Reliability Engineering and System Safety* 67, 311-315.

- [9] Nayak, A. O., Ramkumar, G., Manoj, T., Kannan, M. A., Manikandan, D. and Chakravarthy, S. (2012). Holistic design and software aided finite element analysis (FEA) of an All-Terrain Vehicle. *Journal of Mechanical Engineering Research* 4, 199-212. <https://doi.org/10.5897/JMER12.009>
- [10] Kiam Beng Yeo, Wai Heng Choong and Wen Yen Hau. (2014). Prediction of propeller blade stress distribution through FEA. *Journal of Applied Sciences* 14, 3046-3054. <https://doi.org/10.3923/jas.2014.3046.3054>
- [11] Yongjun, P., Liang, H., Qiliang, W. and Mingmin, C. (2010). Dynamic impact response analysis and simulation on grader blade. In *International Conference on Mechanic Automation and Control Engineering (MACE)*, Wuhan, 6001-6004, <https://doi.org/10.1109/MACE.2010.5536846>
- [12] Montgomery, D. C. and Runger, G. C. (2011). *Applied statistics probability engineers*. 5th ed. New-York: John Wiley & Sons, Inc.
- [13] NIST (2013). Anderson-Darling Test *Engineering Statistics Handbook*, www.itl.nist.gov/div898/handbook/eda/section3/eda35e.htm
- [14] Morariu, C. O. (2010). *Probabilities and applied statistics. Vol. I.*, Transilvania University Publishing House, Brasov.
- [15] Frost, J. (2013). How to identify the distribution of your data using Minitab, <http://blog.minitab.com/blog/adventures-in-statistics/how-to-identify-the-distribution-of-your-data-using-minitab>
- [16] Montgomery, D. C., Runger, G. C. and Hubele, N. F. (2011). *Engineering statistics*. 5th ed. New-York: John Wiley & Sons, Inc.
- [17] Stodola, J. and Stodola, P. (2009). Operation reliability and diagnostics of mechanical systems. *Transactions of Famena* 33(1), 47-56
- [18] Murthy, D. N. P., Xie, M. and Jiang, R. (2004). *Weibull Models*. Wiley Series in Probability and Statistics, New Jersey: John Wiley & Sons.
- [19] Bartkute, V. and Sakalauskas, L. (2008). The method of three-parameter Weibull distribution estimation. *Acta et Commentationes Universitatis Tartuensis de Mathematica* 12, 65-78.
- [20] Comandini, M., Olmi, G. and Freddi A. (2007). Fatigue performance of shot-peened gears investigated by experimental and numerical methods. *Transactions of Famena* 31(2), 1-10.
- [21] Nagatsuka, H., Kamakura, T. and Balakrishnan, N. (2013). A consistent method of estimation for the three-parameter Weibull distribution. *Computational Statistics & Data Analysis* 58, 210-226, <https://doi.org/10.1016/j.csda.2012.09.005>

Submitted: 23.11.2016

Accepted: 09.3.2017

Dorin-Ion Dumitrascu
Cristin Olimpiu Morariu
Adela-Eliza Dumitrascu
(corresponding author)
dumitrascu_a@unitbv.ro
Transilvania University of Brasov,
Department of Manufacturing
Engineering, 29 Eroilor Street,
500068 Brasov, Romania
Doina Valentina Ciobanu
Transilvania University of Brasov,
Faculty of Wood Engineering,
29 Eroilor Street,
500068 Brasov, Romania

The influence of the gasoline octane number on a turbocharged engine performance

Dumitrascu Dorin Ion

Department of Automotive and Transport Engineering, "Transilvania" University of Brasov, Eroilor Street, No. 29, 500036, Brasov
ROMANIA

Abstract: - This paper aims to analyze the differences in power performance of a turbocharged engine in the case of fueling with two types of gasoline, regular and premium. Generally, on turbocharged gasoline engines higher octane fuels are typically recommended. A gasoline with higher octane number, typically, will boost performance in the case of supercharged or turbocharged engines, considering and adequate engine's mapping, too. Nowadays, the oxygenated compounds are used to increase the octane number, ethanol being one of them, as a renewable source of energy. Thus, the gasoline characteristics are directly related to the power and environmental performance of the engine.

Key-Words: - gasoline type, octane number, power, turbocharging, ethanol, dynamometer.

I INTRODUCTION

Fuel type and quality, in terms of physical and chemical properties became essential for engine's power performances and emissions. These aspects were pushed forward by the EU regulations regarding emissions.

Thus, the internal combustion engines evolved, adopting a series of strategies in order to improve their efficiency and reduce the pollutant emissions. So, these solutions were: downsizing combined with supercharging or/and turbocharging, lean burn, higher compression ratios, variable compression ratios. All these technical solutions also involve the improvement of fuels properties in order to avoid abnormal, destructive operating regimes, such as knock, which consists in autoignition of portions of the unburned mixture ahead of the flame front. Then one or more specific regions in the end gas are compressed to a high pressure and temperature that generate spontaneously autoignition. This abnormal combustion – knock – limits engine's compression ratio and boost pressure and therefore engine performance and efficiency.

The tendency to knock depends on:

- ✓ constructive and functional parameters such as engine design and operating values which influence end-gas temperature, pressure and duration, before flame front arrival;
- ✓ antiknock property of the gasoline is defined by the fuel's octane number which is an indicator of a gasoline's resistance to autoignition.

It became obvious the dependency between engine operating parameters, "compression level" and gasoline octane number. Considering this aspect, the higher the octane number, the better the resistance to autoignition and knock.

II METHODOLOGY

In this section are presented the aspects regarding the engine characteristics and test bench. For the test were used two types of gasoline: regular RON 95 and premium RON 100.

A. The vehicle & engine

The test was performed with a Ford Focus equipped with an EcoBoost gasoline direct-injection turbocharged 1.6-liter four-cylinder engine, power 134 kW, at 6000 rpm. The EcoBoost 1.6 L features double overhead belt-driven camshafts and variable intake and exhaust valve timing

B. The dynamometric MAHA LPS 3000 test bench

The research was carried out on the dynamometric MAHA LPS 3000 stand. The dynamometer consists of:

- ✓ communication desk with PC;
- ✓ a remote control;
- ✓ a roller set.

The LPS 3000 is available in various versions for performance testing of cars. Depending on the

version, wheel power from 260 kW to 520 kW with a max. test speed of 260km/h can be tested. The dyno load simulation is done with an eddy-current brake.

The LPS 3000 enables engine power measurements to be made on cars with Otto and diesel engines. Testing of four-wheel drive vehicles

is possible if the LPS 3000 is equipped with the appropriate roller set and the corresponding control electronics. A cooling air fan which is connected to the communication desk and is operated via the radio remote control.



Fig.1 The dynamometric MAHA LPS 3000 test bench

III THE RESULTS OBTAINED WITH THE TWO TYPES OF GASOLINE

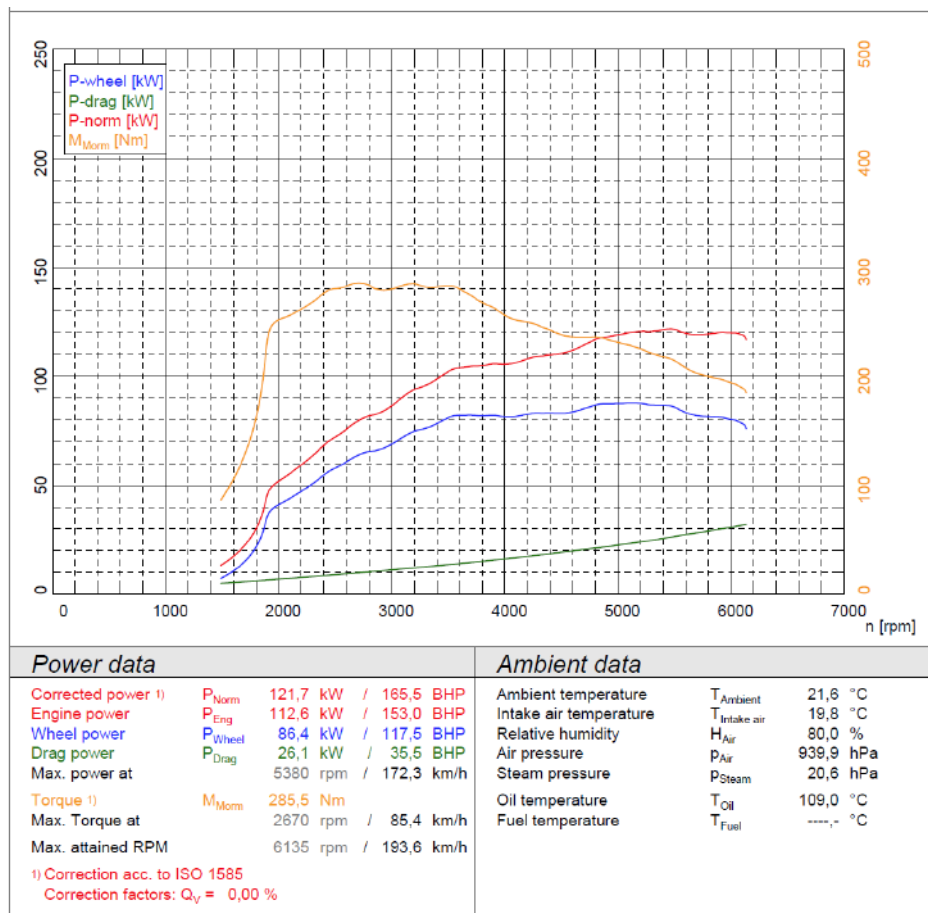


Fig. 2 Tests results for 95 RON gasoline.

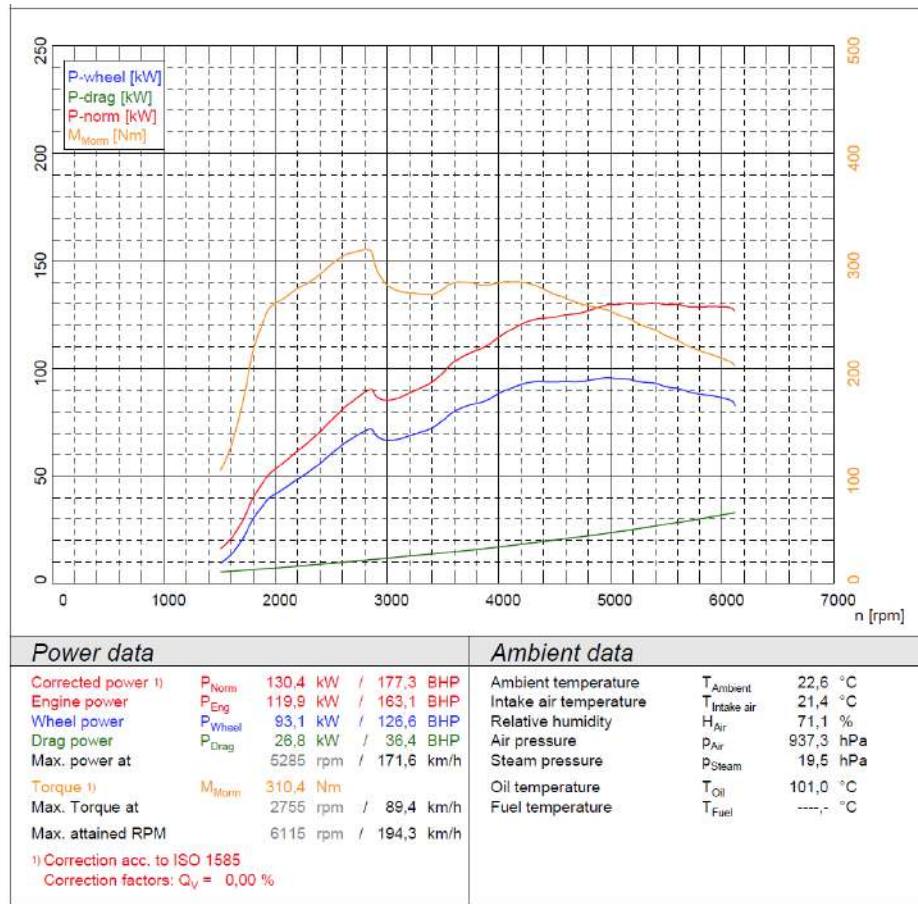


Fig. 3 Tests results for 100 RON gasoline.

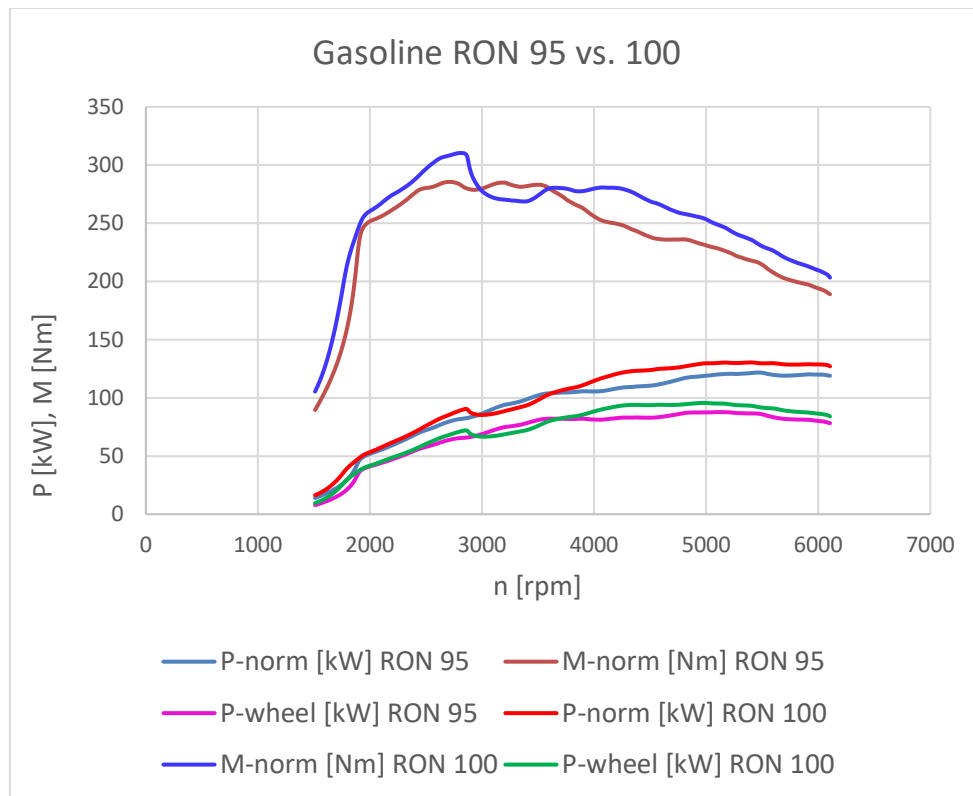


Fig. 4 Comparative analyses for 95 and 100 RON gasoline.

During the test all the characteristic parameters, such as the power and torque curves, have to be recorded and comparatively assessed.

In figure 2 and 3 are presented the results obtained for the for the two types of gasoline (RON 95 and 100) and in figure 4 is represented the comparative analyses between them.

The tests were performed in the fourth gear of the gearbox where the power and torque are maximum.

IV CONCLUSIONS

As it can be seen from diagrams the maximum engine power was 112,6 kW for 95 RON gasoline and 119,9 kW for 100 RON gasoline, an increase of about 6%, and this above 5000 rpm.

In the speed range between 2000 and 3000 rpm the differences between the registered power values for the two types of gasoline are insignificant, the curves overlapping almost the entire interval. In this case a higher-octane level doesn't increase the vehicle performance.

In the speed range between 3000 and 3500 rpm the power values for 95 RON gasoline are superior compared to 100 RON gasoline, the usage of a superior octane number decreased the engine energetical performance.

Only after the speed of 3600 rpm the power values become superior in the case of the 100 RON gasoline, in other words after this speed, the 100 RON gasoline makes its presence felt. Between 3600 rpm and 6000 rpm the engine power level become superior, compared with the case of 95 RON gasoline.

Maximum torque and maximum speed were obtained at about the same points for both types of gasoline, these aspects can be seen on the related diagrams.

In the case of this type of turbocharged engine, higher octanes can improve performance and can reduce emissions during some average to severe duty operations, above 3600 rpm. However, under normal driving conditions, it will do little to nothing for the vehicle performance.

Extrapolating the research results, it can be concluded that in a large number of cases a higher-octane level may not necessarily increase the vehicle's performance, but only paying extra for premium gasoline. This is especially true for naturally aspirated engines, which clearly do not have a mapping that can capitalize the benefits of a higher-octane number.

This can be contradicted, for example, by the corresponding increase of the compression ratio

value for the naturally aspirated engines, in order to increase their performance and efficiency.

REFERENCES:

- [1] John B. Heywood, *Internal Combustion Engine Fundamentals*, Second edition, McGraw-Hill Education, 2018, 978-1-26-011611-3.
- [2] Hua Zhao, *Advanced Direct Injection Combustion Engine Technologies and Development: Gasoline and Gas Engines*, Woodhead Publishing in Mechanical Engineering, 2014.
- [3] Konrad Reif, *Gasoline Engine Management Systems and Components*, Springer Vieweg, 2015, ISBN 978-3-658-03964-6.
- [4] George E. Totten, *Fuels and Lubricants Handbook: technology, properties, performance and testing*, ASTM International, 2003.
- [5] Rolf Isermann, *Combustion Engine Diagnosis, Model-based Condition Monitoring of Gasoline and Diesel Engines and their Components*, Springer Vieweg, 2017, ISBN 978-3-662-49467-7.
- [6] A. J. Martyr, M. A. Plint, *Engine Testing, The Design, Building, Modification and Use of Powertrain Test Facilities*, Butterworth-Heinemann is an imprint of Elsevier, 2012, ISBN-13: 978-0-08-096949-7.

Anghel Chiru · Nicolae Ispas
Editors

CONAT 2016 International Congress of Automotive and Transport Engineering

Editors

Anghel Chiru
Department of Automotive
and Transportation Engineering
Transilvania University of Brasov
Brasov
Romania

Nicolae Ispas
Department of Automotive
and Transportation Engineering
Transilvania University of Brasov
Brasov
Romania

ISBN 978-3-319-45446-7 ISBN 978-3-319-45447-4 (eBook)
DOI 10.1007/978-3-319-45447-4

Library of Congress Control Number: 2016953012

© Springer International Publishing Switzerland 2017

This work is subject to copyright. All rights are reserved by the Publisher, whether the whole or part of the material is concerned, specifically the rights of translation, reprinting, reuse of illustrations, recitation, broadcasting, reproduction on microfilms or in any other physical way, and transmission or information storage and retrieval, electronic adaptation, computer software, or by similar or dissimilar methodology now known or hereafter developed.

The use of general descriptive names, registered names, trademarks, service marks, etc. in this publication does not imply, even in the absence of a specific statement, that such names are exempt from the relevant protective laws and regulations and therefore free for general use.

The publisher, the authors and the editors are safe to assume that the advice and information in this book are believed to be true and accurate at the date of publication. Neither the publisher nor the authors or the editors give a warranty, express or implied, with respect to the material contained herein or for any errors or omissions that may have been made.

Printed on acid-free paper

This Springer imprint is published by Springer Nature
The registered company is Springer International Publishing AG Switzerland

Advanced Automotive Assembly Line Trends as Tools in Optimizing Production Line Performance	592
<i>Hariton Poparad</i>	
Cleaning Methods for Flux Pollution Measurement in Automotive Coolant Loop Components	599
<i>Hervé Bourgeois and Claire Demarcq</i>	
Design and Development of Chassis Along with Novel Under Run Protection Devices for Commercial Vehicles with the Use of an Innovative Approach Resulting in Lighter Weight of the Vehicle	610
<i>Ashesh Anil Shah and Himanshu Arora</i>	
The Quality Management Principles and Their Incidence Within ISO 9001: 2015	620
<i>Laurentiu Aurel Mihail</i>	
Product Quality Control Optimization for Selection of Measurement and Control Devices	629
<i>Constantin Buzatu and Iulian Alexandru Orzan</i>	
Improvement of the 8D Analysis Through a System Based on the “Internet of Things” Concept Applied in Automotive Industry	635
<i>Viorel Nicolae, Laurențiu Mihai Ionescu, Nadia Belu, and Știrbu Luminița Elena</i>	
A Case Study Regarding the Implementation of Six Sigma in an Assembly Process for the Automotive Parts	643
<i>Dorin-Ion Dumitrascu, Adela-Eliza Dumitrascu, and Anghel Chiru</i>	
Advanced Transport Systems and Road Traffic	
Analysis of the Influence of One-Way Streets on the Urban Road Networks Connectivity	653
<i>Daniela Florea, Dinu Covaciu, and Janos Timar</i>	
Cooperative Smart Intersection as an Enabler of Advanced Traffic Management Systems	668
<i>Laura Coconeá, Gonzalo Alcaraz, and Renato Augusto Lira de Andrade</i>	
Bus Routing Safety for the Transportation of Children to School	676
<i>Eleni Chalkia, Jose Maria Salanova Grau, Evangelos Bekiaris, Georgia Ayfandopoulou, Chiara Ferarini, and Evangelos Mitsakis</i>	
Improving the Road Traffic Regulation in the Area of Roundabout Intersections Function of the Traffic Streams Size	684
<i>Elena Neagu, Andrei Alexandru Boroiu, Ionel Vieru, and Alexandru Boroiu</i>	

A Case Study Regarding the Implementation of Six Sigma in an Assembly Process for the Automotive Parts

Dorin-Ion Dumitrascu, Adela-Eliza Dumitrascu^(✉), and Anghel Chiru

“Transilvania” University of Brasov, Brasov, Romania
{d.dumitrascu,dumitrascu_a,achiru}@unitbv.ro

Abstract. This paper aimed to investigate the process of six-sigma implementation in an assembly process for vehicle parts. The Six Sigma objectives consists in reducing the occurrence of specific defects, scratches and deformation of the assembled doors, saving material and reducing costs for internal repairs. By implementation of Six Sigma, it was possible to improve the DPMO indices (Defects per Million Opportunities) with 70 percent and to analyze the quality characteristics considered critical for the monitored process, in order to determine the performance level of the product. The results indicate that with proper implementation of Six Sigma methodology it can be achieved a positive impact on the quality parts by reducing defects, improving the flexibility of the assembly process and customers’ satisfaction, too.

Keywords: Assembly process · Six Sigma methodology · Defects per Million Opportunities (DPMO) · Capability analysis

1 Introduction

Six Sigma is a strategy of continuous quality improvement for an organization that is used in many fields. In general, Six Sigma is a methodology to improve the process by reducing the defects of products, minimizing the process variation and improving the capability of manufacturing processes. The Six Sigma objectives are focused on increasing the profit and reducing the costs, by minimizing the defective rate of performed products [1, 2].

Due to the diversity of industrial products and competitive environment, organizations have searched strategies to improve the processes and products quality such as total quality management (TQM), ISO certification, Six Sigma, etc.

Six Sigma is the new statistical approach for total quality management, a global approach aimed to improve customer satisfaction, which is not the same as quality improvement. Based on this improved customer satisfaction, Six Sigma is increasing source of profitability for the organization cumulating the following effects [3]:

- a decrease of scraps, work correction and generally the non-quality costs;
- an improvement of machine availability and synthetic yield rate;
- better market segments, considering product quality improvement.

One of the basic principles of Six Sigma is to reduce the process variability, which derives in particular from:

- variability of materials;
- procedures variability;
- variability of the condition where production process evolves.

Six Sigma has two major perspectives. One is a statistical perspective, the other is the business perspective. From the statistical point of view, the term Six Sigma is defined as having less than 3.4 defects per a million of produced items or a success rate of 99.9997 %, where sigma is a term used to represent the average of process variation. From a commercial perspective, Six Sigma is defined as a business strategy used to improve business profitability, to increase effectiveness and efficiency of all operations in order to meet the customer needs and expectations or to exceed them [4, 5].

Six Sigma promotes a philosophy of excellence and it is based on using two methods: DMAIC and DMADV [6, 7].

DMAIC method consists of the following steps: definition phase, measurement phase, analysis stage, stage and phase control improvement; it is applied when you want to improve products/services or existing processes.

DMADV method consists of the following steps: defining stage, measurement phase, analysis phase, design phase/stage and verification phase useful when you want to design new products or processes for a specific imposed capability.

In this paper is presented a study consists on implementation of Six Sigma methodology using DMAIC method in order to improve the assembly process. By implementation of Six Sigma methodology it allows us to identify the effective way to find out the critical points of the analyzed process. For analyzed process, which initially is carried out with open doors in assembled state on the vehicle, there are a number of defects (deformation of the assembled doors and paint scratches) that need repairing or even the parts are rejected. The main objective is to improve the assembly process by decreasing the number of defective units with a percent of minimum 70 %.

2 Implementation of Six Sigma. Case Study

2.1 Define Phase

The objective of Six Sigma is to reduce the number of rejects due to specific problems that appear during the doors assembly process on the vehicle, by reducing the occurrence of specific defects (door scratches and sheet shocks).

Thus, the following targets are defined with related indicators:

- Improving the number of DPMO (Defects per Million Opportunities) by 70 %, so reduction with the same percentage of the number of defective units, reported to a million opportunities of developing these defects;
- Increasing the number of positive results at the car body and paint;
- Saving materials;
- Cost savings due to internal repairs.

2.2 Measure Phase

In the second phase are presented measurements undertaken for further analysis of how internal failure occurs, reported proportional for the four doors assembled motor vehicles (for two models of the car body). Thus, for the first model body is observed that most failures occur on the back door on the left side, followed by the right front door and then by the other two doors, in the same proportion (Fig. 1). It can be concluded that failures occur approximately at the same proportion on each door, resulting the idea that the corrective actions that will be reached after applying optimization of the entire cycle will be applied to all four doors.

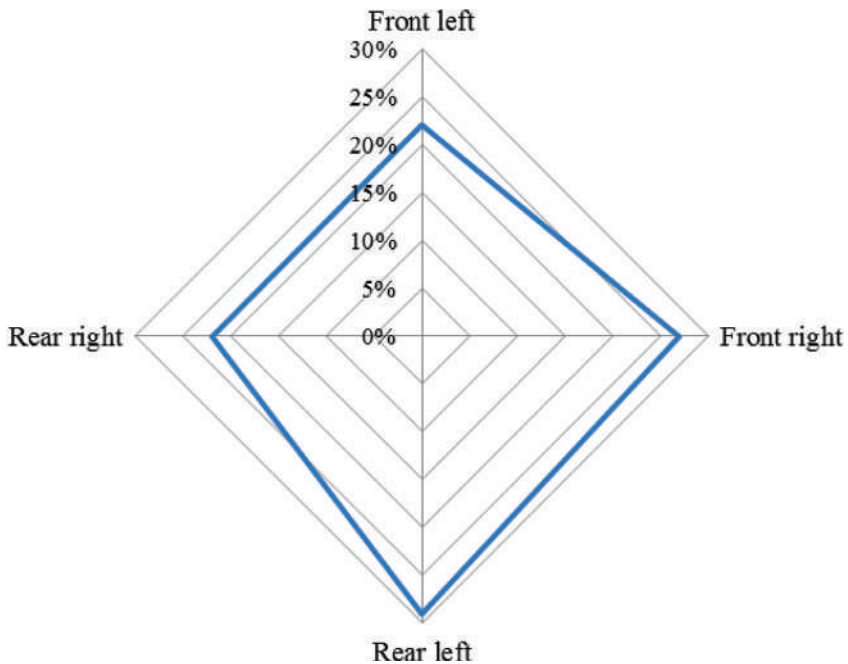


Fig. 1. Defects distribution for assembled doors of the analyzed type I car body

For the second examined car body model, it is observed that most failures occur at the front door on the right side, followed by the back door on the right side and the other two doors on the left side (Fig. 2). From here comes the same conclusion, according to which the optimal corrective solution will be applied to all four doors.

In order to determine the performance of the products, there are monitored the quality characteristics considered critical for the analyzed process, defects caused during assembling process: paint scratches and sheet shocks per 1000 products.

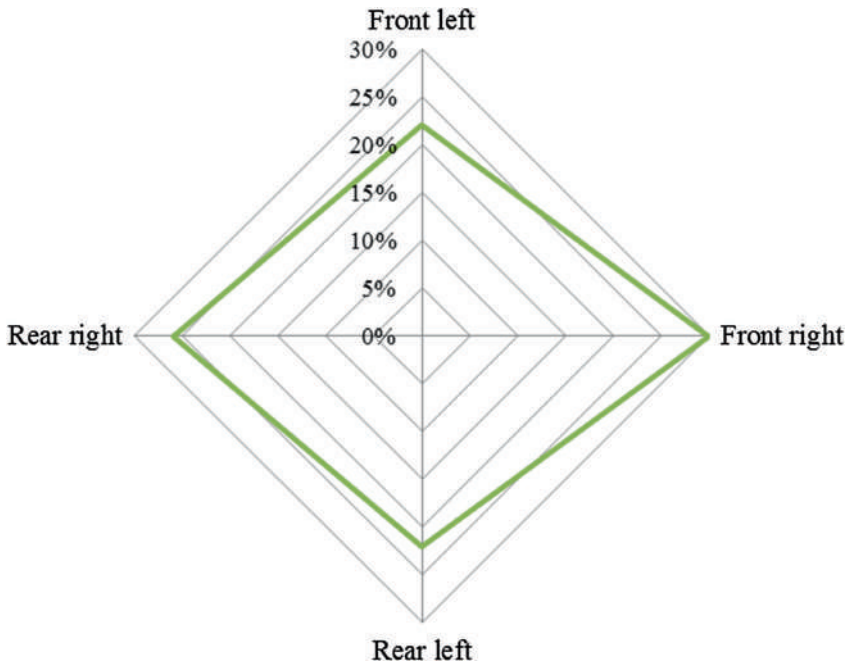


Fig. 2. Defects distribution for assembled doors of analyzed type II car body

2.3 Analyze Phase

Due to previously recorded data, there are identified the possible causes that generated the unfavorable recorded situation. It is analyzed the defect by drawing up a cause-effect diagram and as generating potential sources are included (Fig. 3):

- environment - workplace design, inadequate lightening;
- measurements - Cpk process capability indices;
- material - processed material strength (in a state of semi and finished parts), resistance of the paint layer, the protective elements of the door;
- labor force - improper assembly and usage of tools, lack of training, failure procedures;
- methods - improper design of the workplace, how to adjust the edges;
- machine tools - door handles transporters, improper maintenance of devices, faulty design of the conveyor.

The main causes that produce the irregular flow are faulty assembling process and inadequate equipment usage (as causes related to the labor force) and the doors conveying and transfer systems (as causes related to machine tools).

2.4 Improvement Phase

Process improvement consists in the use of an optimized transfer device to ensure disassembly of the vehicle doors, in order to avoid the appearance of defects related to

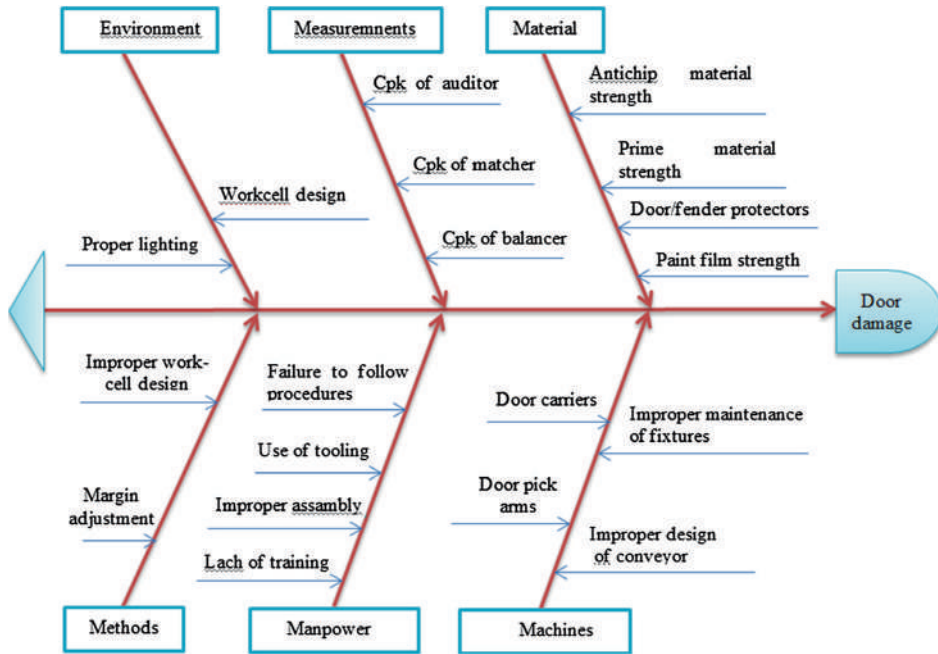


Fig. 3. Case-effects diagram of the assembly process

the previous mode of organization of assembling the inside components. This device allows not only a fence door, but its proper grip due to its overall dimensions and weight.

As an effect of applied corrective measures, the process performances by product quality point of view it was monitored for three months. Figure 4 shows that the defects percent records a significant decrease.

Monitoring the occurrence of defects on the assembly line, it is seen predominantly low levels, with a steep decrease slope, corresponding in time, immediately after implementation of the corrective solutions. The proposed and implemented optimization has led to a record level of DPMO by 1098, related to a defective fraction of 4.4. Compared to the initial state, it results an improvement of more than 85 % of the process, for the monitored critical quality characteristics.

2.5 Control Phase

The analysis of the samples dependency for means of monitored defects specific to initial and optimized stages it is detailed in Fig. 5.

The *t* test for determining the samples dependence is a statistical technique that is used to compare two populations if the two samples are correlated. Data were recorded before (*def b*) and after implementation of improvement actions (*def a*).

The analysis of process capability for monitored defects specific to initial and optimized stages are presented in Figs. 6 and 7.

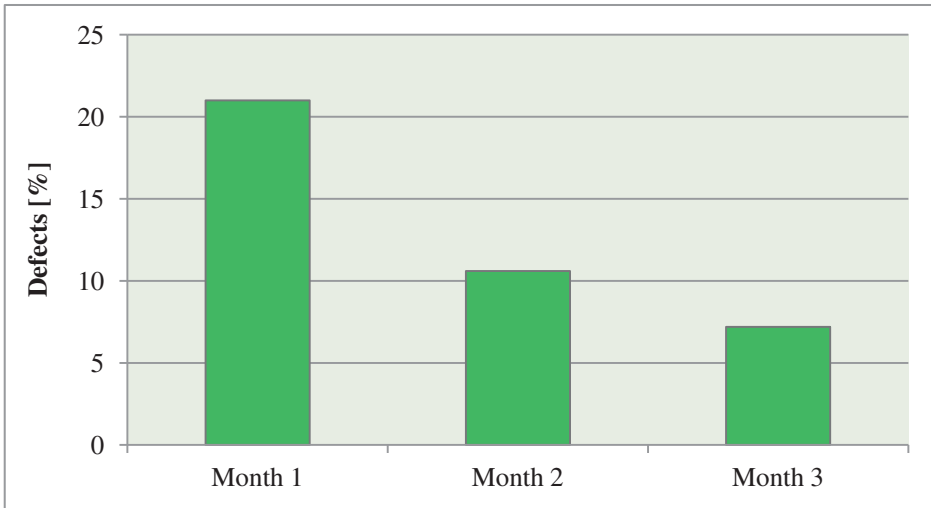


Fig. 4. Monitored process performance

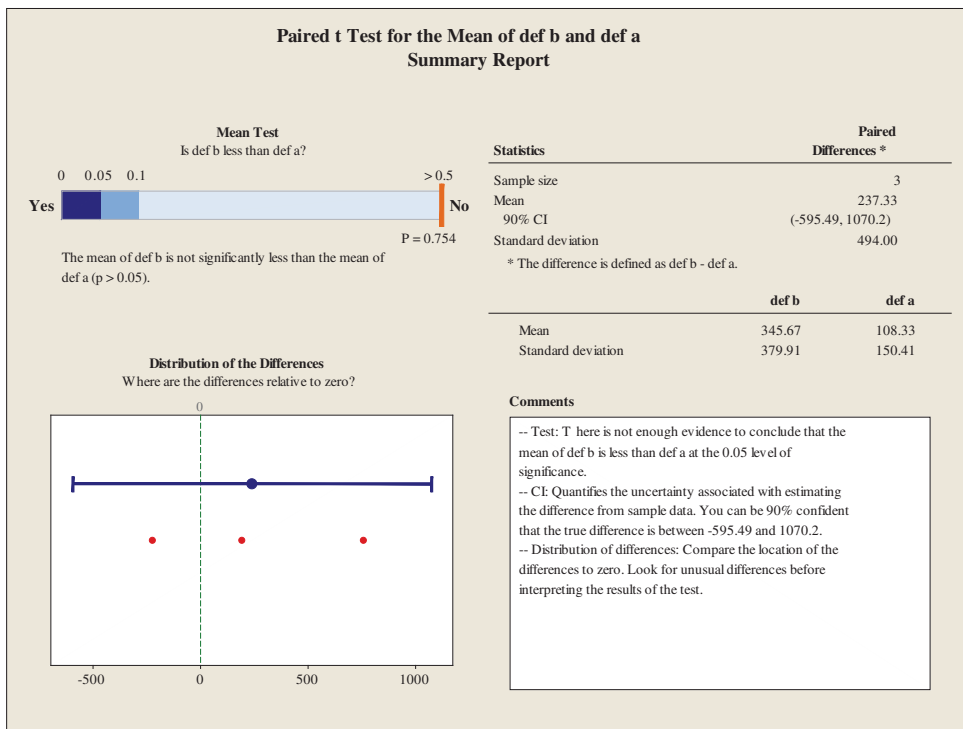


Fig. 5. Distribution for means differences applying t test

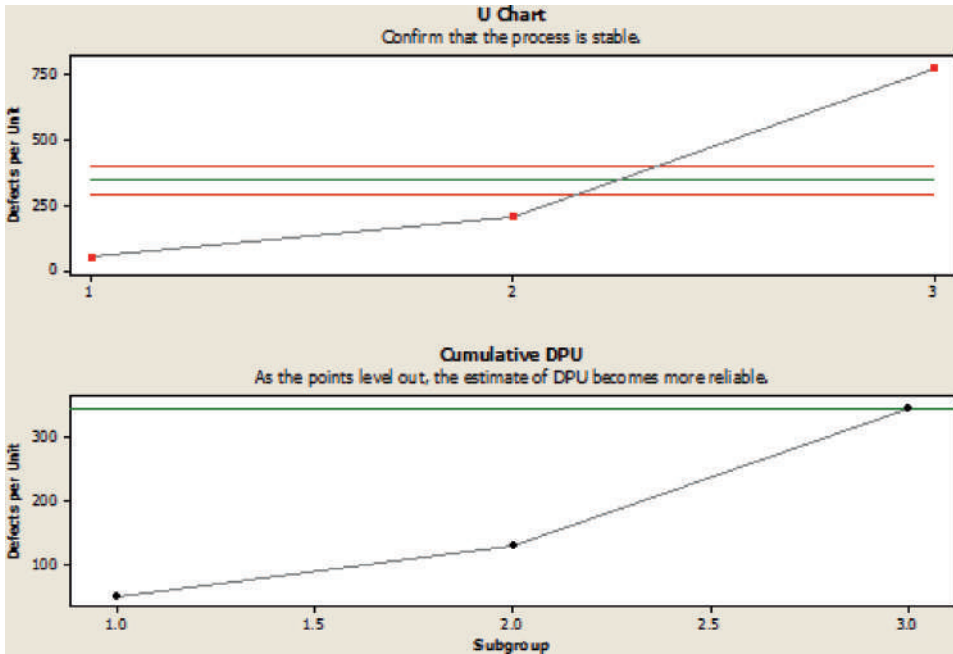


Fig. 6. Poisson capability analysis for *def b*

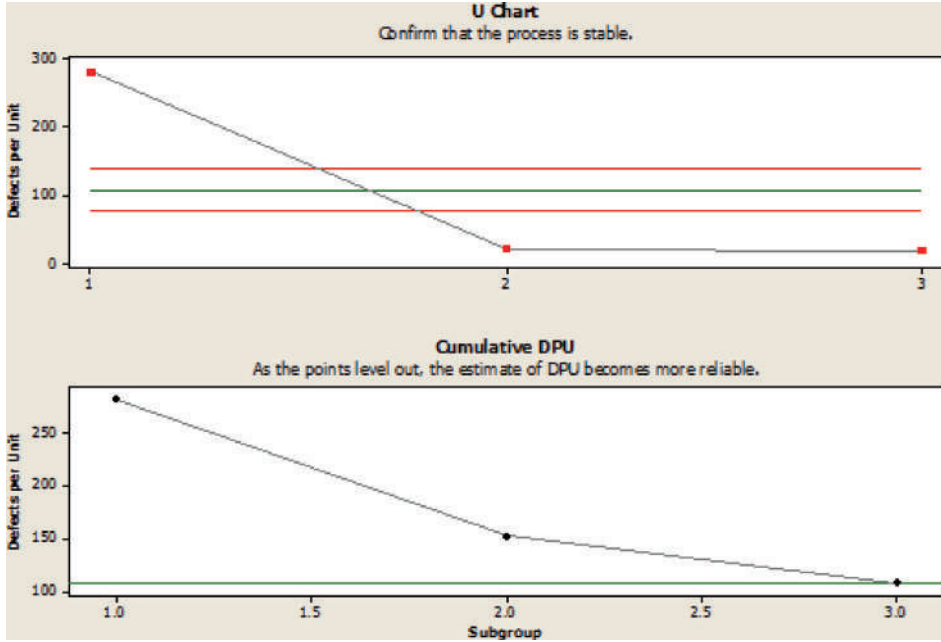


Fig. 7. Poisson capability analysis for *def a*

3 Conclusions

The implementation of Six Sigma methodology offers measurable parameters of process performance and valuable conclusions of the consequence of statistical analysis.

By implementing a permanent change for the transfer system and transport inter-doors, disassembled for a vehicle, in order to make the installation of interior components, it is removed completely the possibility of an error, a fact detected by a 100 % control of the machined parts.

From the statistical point of view, it can be seen that improvements have been implemented effectively.

After implementing the corrective actions, it can be mentioned that improvements applied to the analyzed process led to:

- significant reduction of losses by improvement of more than 85 % of the assembly process for the monitored critical quality characteristics;
- improving the assembly flexibility by taking into account aspects of ergonomics in the workplace;
- operational efficiencies growth;
- increase labor efficiency.

References

1. Chang, S.-I., Yen, D.C., Chou, C.C., Wu, H.C., Lee, H.P.: Applying six sigma to the management and improvement of production planning procedure's performance. *Total Qual. Manag. Bus. Excellence* **23**(3), 291–308 (2012)
2. Pyzdek, T.: *The Six Sigma Handbook: A Complete Guide for Green Belts, Black Belts, and Managers at all Levels*. McGraw- Hill, New York (2003)
3. Virgil, P.: The new statistical approach to total quality management. Six Sigma (in Romanian: Noul demers statistic în managementul calității totale. Six sigma). "Valahia" University of Targoviste (2015). http://www.ecr-uvt.ro/informatii_noutati/pdf/Sesiune_de_comunicari_J.M.JURAN/6_sigma.pdf
4. Baral, L.M.: Integrating of knowledge management concepts with six sigma methodology (in Romanian: Integrarea conceptelor managementului cunoașterii cu metodologia Six Sigma). Doctoral thesis, "Lucian Blaga" University of Sibiu (2014)
5. Park, S.H.: Six sigma for quality and productivity promotion. *Asian Productivity Organization*, pp. 37–38 (2003). ISBN: 92-833-1722-X
6. ISO 13053-1: ISO guideline on quantitative methods in process improvement- six sigma- part 1: DMAIC methodology (2011)
7. ISO 13053-2: ISO guideline on quantitative methods in process improvement- six sigma- part 2: tools and techniques (2011)



Editor

Vladimir Marascu-Klein



Advances in Production, Automation and Transportation Systems



Proceedings of the 6th International Conference on Manufacturing Engineering, Quality and Production Systems (MEQAPS '13)

Proceedings of the 4th International Conference on Automotive and Transportation Systems (ICAT '13)

Brasov, Romania, June 1-3, 2013

Scientific Sponsors



Advances in Production, Automation and Transportation Systems



ADVANCES in PRODUCTION, AUTOMATION and TRANSPORTATION SYSTEMS

Proceedings of the 6th International Conference on Manufacturing
Engineering, Quality and Production Systems (MEQAPS '13)
Proceedings of the 4th International Conference on Automotive and
Transportation Systems (ICAT '13)

Brasov, Romania
June 1-3, 2013

Scientific Sponsors:



Transilvania University
of Brasov



University
of Craiova



University Politehnica
of Bucharest



Stefan cel Mare
University of Suceava



Constantin Brancusi
University of Targu-Jiu



Megatrend University
of Belgrade



University Lucian Blaga
of Sibiu



Constanta Maritime
University

ADVANCES in PRODUCTION, AUTOMATION and TRANSPORTATION SYSTEMS

Proceedings of the 6th International Conference on Manufacturing Engineering, Quality and Production Systems (MEQAPS '13)

Proceedings of the 4th International Conference on Automotive and Transportation Systems (ICAT '13)

**Brasov, Romania
June 1-3, 2013**

Published by WSEAS Press
www.wseas.org

Copyright © 2013, by WSEAS Press

All the copyright of the present book belongs to the World Scientific and Engineering Academy and Society Press. All rights reserved. No part of this publication may be reproduced, stored in a retrieval system, or transmitted in any form or by any means, electronic, mechanical, photocopying, recording, or otherwise, without the prior written permission of the Editor of World Scientific and Engineering Academy and Society Press.

All papers of the present volume were peer reviewed by no less than two independent reviewers. Acceptance was granted when both reviewers' recommendations were positive.
See also: <http://www.worldses.org/review/index.html>

ISSN: 2227-4588
ISBN: 978-1-61804-193-7

ADVANCES in PRODUCTION, AUTOMATION and TRANSPORTATION SYSTEMS

**Proceedings of the 6th International Conference on Manufacturing
Engineering, Quality and Production Systems (MEQAPS '13)**

**Proceedings of the 4th International Conference on Automotive and
Transportation Systems (ICAT '13)**

**Brasov, Romania
June 1-3, 2013**

Some Problems Regarding Side Impact with a Fixed Cylindrical Vertical Obstacle	373
<i>M. Clinciu, A. Chiru, S. Zamfira, Tr. Bolfa, St. Ciunel</i>	
Experimental Study on Determining a Relationship for Calculating the Effective Torque for a Spark Ignition Engine with Ceramic Elements	377
<i>Ioan Radu Sugar, Mihai Banica</i>	
Research on Increase Liter Power Spark Ignition Engines by Isolating Combustion Chamber	381
<i>Ioan Radu Sugar, Lucian Adrian Butnar</i>	
Iterative Experimental Procedure for Determining of Heat Transfer Coefficient of Catenary's Contact Line Wire	385
<i>Constantin Florin Ocoleanu, Ioan Popa, Gheorghe Manolea</i>	
The Energetical and Ecological Performances of D.I. Diesel Engine Fueled with Biodiesel	389
<i>Dumitrascu Dorin Ion, Benea Bogdan Cornel</i>	
Authors Index	395

THE ENERGETICAL AND ECOLOGICAL PERFORMANCES OF D.I. DIESEL ENGINE FUELED WITH BIODIESEL

DUMITRASCU DORIN ION, BENEA BOGDAN CORNEL

Automotive and Transport Engineering Department

“Transilvania” University of Brasov

1 Politehnicii Street, Brasov

ROMANIA

d.dumitrascu@unitbv.ro, b.benea@unitbv.ro, <http://www.unitbv.ro>

Abstract: - Biodiesel, due to its renewable feature, greenhouse gas emission reduction became an attractive alternative to replace fossil diesel fuel in order to fulfill future demands for sustainable transport development. The physical and chemical properties of biodiesel make it suitable to be used in pure form (B100) or may be blended with petroleum diesel at different concentration.

The aim of this paper is to present some aspects regarding the energetical and ecological performances obtained with a compression ignition engine fueled with biodiesel.

Key-Words: - biodiesel, renewable, emission, performance, sustainable, compression ignition engine

1 Introduction

Biodiesel is a fuel composed of mono-alkyl esters of long-chain fatty acids derived from vegetable oils or animal fats, for use in compression ignition engines.

Biodiesel, a clean-burning alternative fuel, is considered to be the most appropriate in this category of fuels that can be used without major problems in compression ignition engines.

Compared to petroleum diesel, biodiesel is characterized by:

- energy content is about 10% less on a mass basis;
- reduced level of some exhaust emissions (although it may, in some conditions, increase others);
- lower / no sulfur content;
- lower heating value;
- no aromatics content;
- oxygen content up to 11%;
- higher cetane number;
- higher flash point;
- higher freezing temperature;
- higher viscosity;
- less toxic;
- superior lubricity;
- biodegradable;
- tends to deteriorate some types of natural rubber of which are made the fuel system parts found in some older engine.

Considering these aspects, it results that some characteristics, such as higher cetane number, superior lubricity, sulfur and aromatics content, flash point, etc. are advantages of biodiesel, while others, including flow proprieties at low

temperature, lower heating value, higher viscosity, corrosion properties are inconveniences.

2 Experimental Research Data

During the experimental phase, it was used pure petroleum diesel fuel and blended with biodiesel obtained from sunflower oil and waste oil. The proportion of biodiesel used during experiments was 10%.

2.1 The engine

The experimental research was made on a Renault turbocharged direct injection common rail diesel engine (K9K P 732), which has the following characteristics: in line 4-cylinder engine with a compression ratio of 18.8:1, displacement of 1.461 liters (bore =76 mm, stroke =80.5 mm), water cooled.

2.2 Experimental test bench

The engine was mounted on a Horiba Titan T250 test stand that is optimized for steady state and transient testing of light and heavy duty gasoline and diesel engines.

The main characteristics of the Horiba Titan T250 test stand are:

- Maximum torque [Nm]: 400
- Maximum speed [rpm]: 8000
- Moment of Inertia [kgm²]: > 0.15
- Dynamometer: Dynas₃ HT250

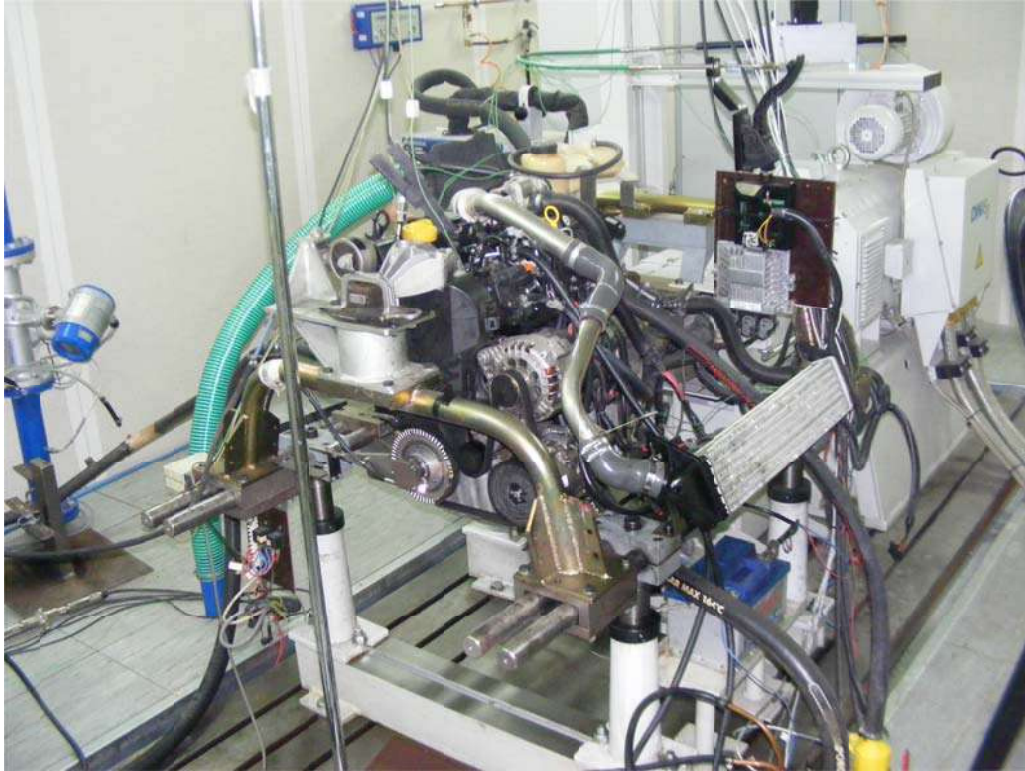


Fig. 1. The engine mounted on Horiba Titan T 250 stand



Fig. 2. AVL 415S Smoke meter

For soot emission measurement was used the AVL Smoke meter 415S which is an automatic measurement system; a controlled volume of exhaust gases is passed through a filter paper. The filtered soot causes blackening on the filter paper which is detected by a photoelectric measuring head and evaluated in the microprocessor to calculate the result in FSN or mg/m^3 [4].

Exhaust emissions were determined by the Pierburg Hermann, tip HGA 400 analyser.

3 Results and comments

In table 1, 2 and 3 are presented the results obtained with the engine running at full load. In this tables can be observed the values for torque, power and

emissions that characterized the energetical and ecological potential of biodiesel blended with

petroleum diesel fuel compared to pure petroleum diesel fuel.

Table 1. Pure Petroleum Diesel Fuel

Speed	Power	Torque	Soot	CO	CO ₂	O ₂	HC	NO _x
[rpm]	[kW]	[Nm]	[mg/m ³]	[%]	[%]	[%]	[ppm]	[ppm]
1200	13.47649	107.2292	166.56	5.25	14.7	17.11	143	418
1700	29.37798	164.9864	89.59	1.25	15.6	16.87	141	883
2200	41.49626	180.1189	39.24	0.86	15.1	16.9	111	838
2700	63.83509	225.7622	30.25	0.8	14.5	16.23	89	1137
3200	69.4686	207.306	40.5	0.78	14	16.75	95	1168
3700	71.63496	184.8818	63.46	0.8	14.1	16.38	80	1248

Table 2. B10 - sunflower oil

Speed	Power	Torque	Soot	CO	CO ₂	O ₂	HC	NO _x
[rpm]	[kW]	[Nm]	[mg/m ³]	[%]	[%]	[%]	[ppm]	[ppm]
1200	12.7691	101.5908	144.32	2.35	12.7	20.52	39	978
1700	29.00575	162.8987	74.25	0.23	12.6	20.26	40	874
2200	42.14181	182.9082	32.46	0.06	12.1	19.97	35	898
2700	64.44046	227.9237	28.47	0.04	11.4	20.24	40	1173
3200	69.11801	206.2719	32.47	0.04	12	20.02	46	1165
3700	71.87303	185.4877	40.43	0.04	11.4	20.08	64	1198

Table 3. B10 - waste oil

Speed	Power	Torque	Soot	CO	CO ₂	O ₂	HC	NO _x
[rpm]	[kW]	[Nm]	[mg/m ³]	[%]	[%]	[%]	[ppm]	[ppm]
1200	12.67961	100.8999	126.74	2.28	13.1	20.26	80	978
1700	29.21389	164.0858	67.14	0.23	13	19.93	79	910
2200	42.20342	183.1791	31.93	0.06	12.6	19.49	67	916
2700	64.22325	227.1576	27.41	0.04	11.5	19.21	62	1140
3200	69.39461	207.0703	29.94	0.04	11.6	19.02	42	1149
3700	71.62849	184.8628	44.41	0.04	11.2	19.09	41	1211

The evolution of torque and power relative to engine's speed is illustrated in figure 3. The level of emissions for engine's full load is represented in figure 4 to 7.

Figure 3 shows a proximate evolution of torque and power at full load for a B10 and pure petroleum diesel fuel.

Figure 4 and 5 indicate that HC and CO₂ emissions decrease in case of biodiesel blends (10% in our case). This effect is determined by the oxygen content in biodiesel, which generates a more complete oxidation in the combustion chamber.

NO_x emissions are increased with biodiesel especially at low to medium speed, but at high speed (3200-3700 rpm) the difference is insignificant, obtaining even a higher value for pure petroleum

diesel fuel. An increased level of NO_x could be explained through high oxygen content of biodiesel.

The soot level is decreased in case of B10 for all speeds (figure 7).

4 Conclusion

In terms of energetical performances, in case of B10 it can be observed that power and torque had an appropriate evolution, without notable differences.

Regarding the ecological side, the usage of biodiesel blended with pure petroleum diesel fuel generally reduces most of emissions in compression ignition engines. The exception is represented by the NO_x emission that is increased at some speed levels.

In conclusion it can be mentioned that B10 does not affect the energetically performance of the

engine, while by the ecologically point of view, it generally represents an improvement.

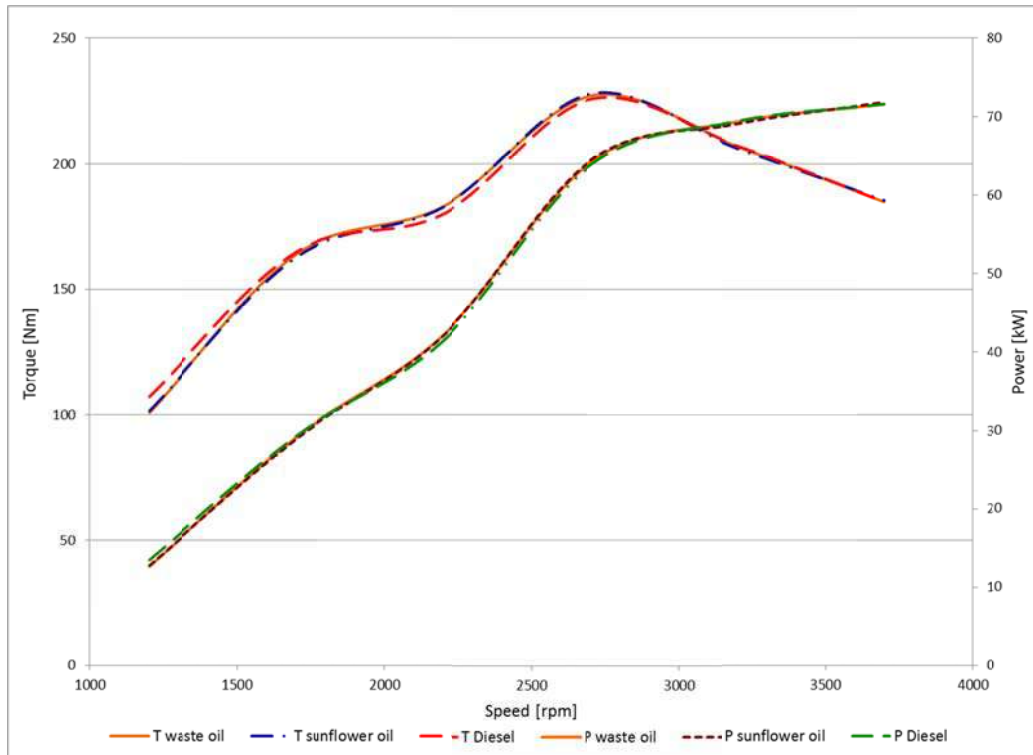


Fig. 3. Power and torque variation

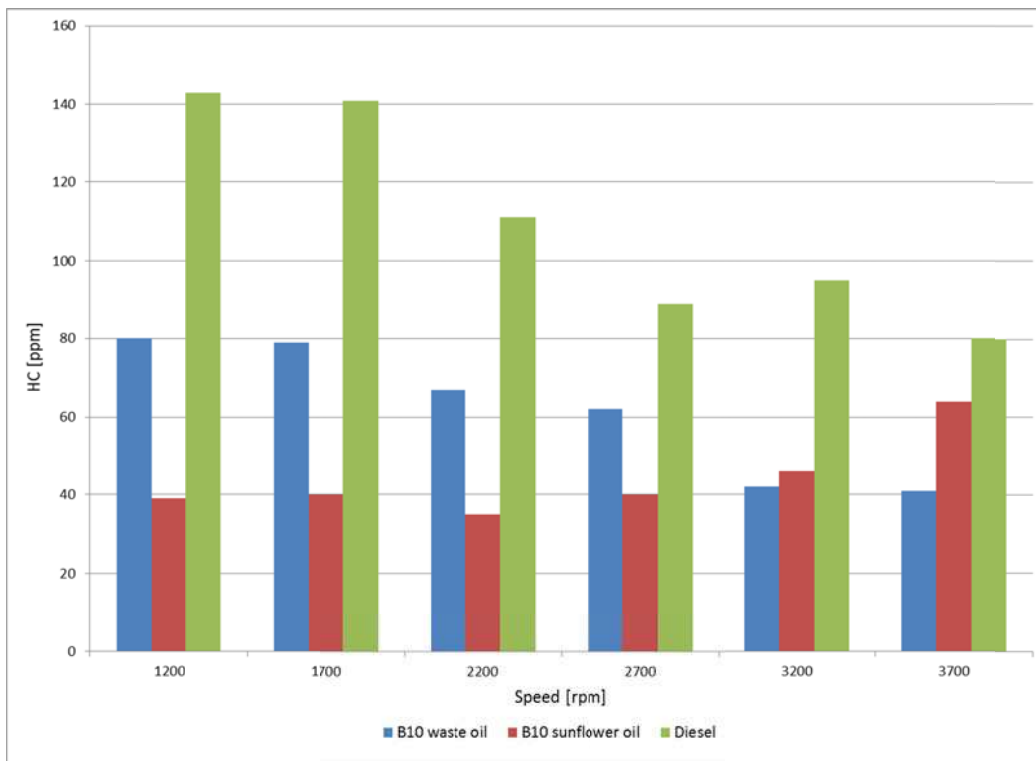


Fig. 4. HC emission

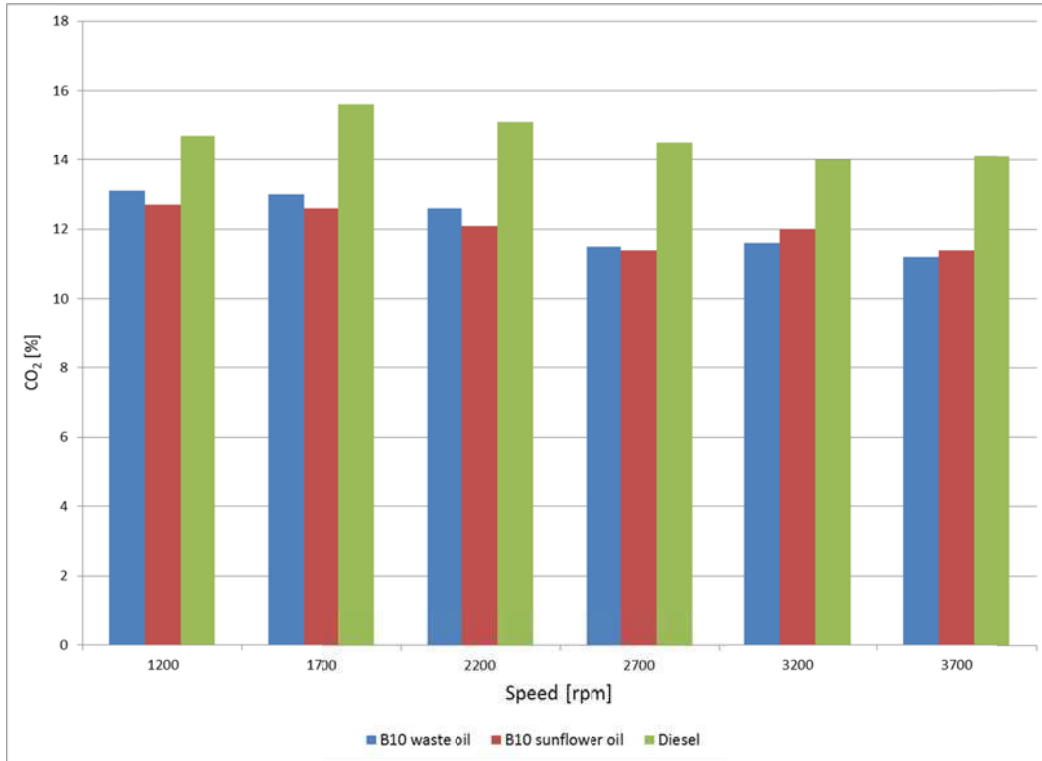


Fig. 5. CO₂ emission

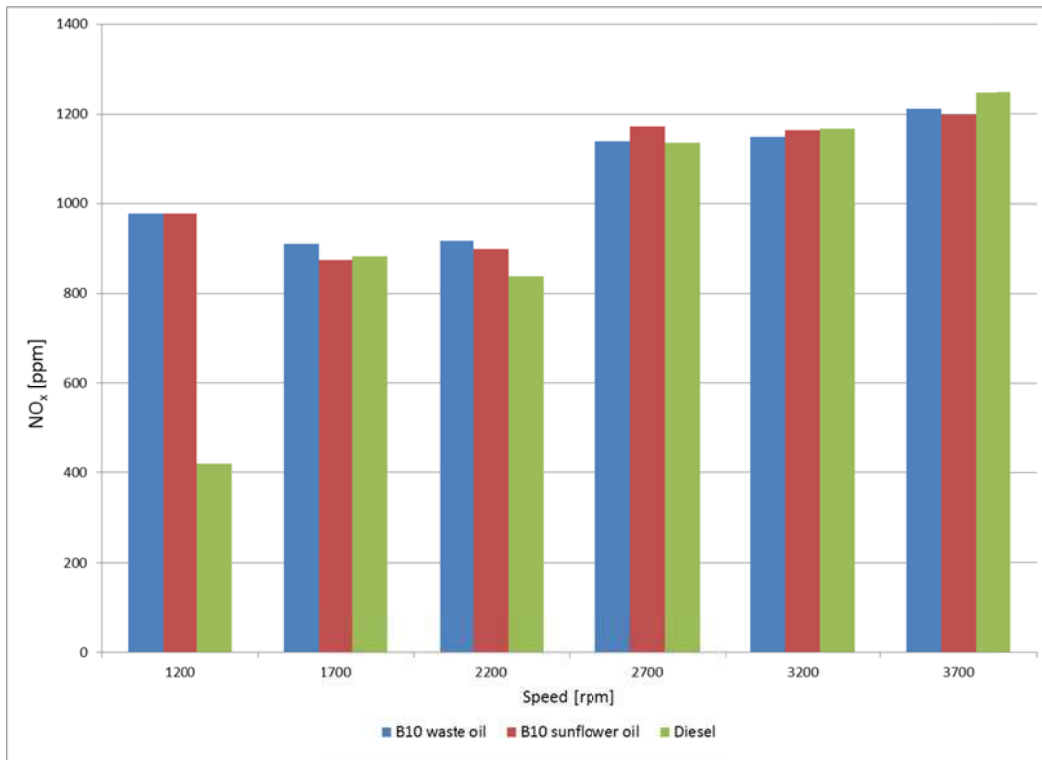


Fig. 6. NO_x emission

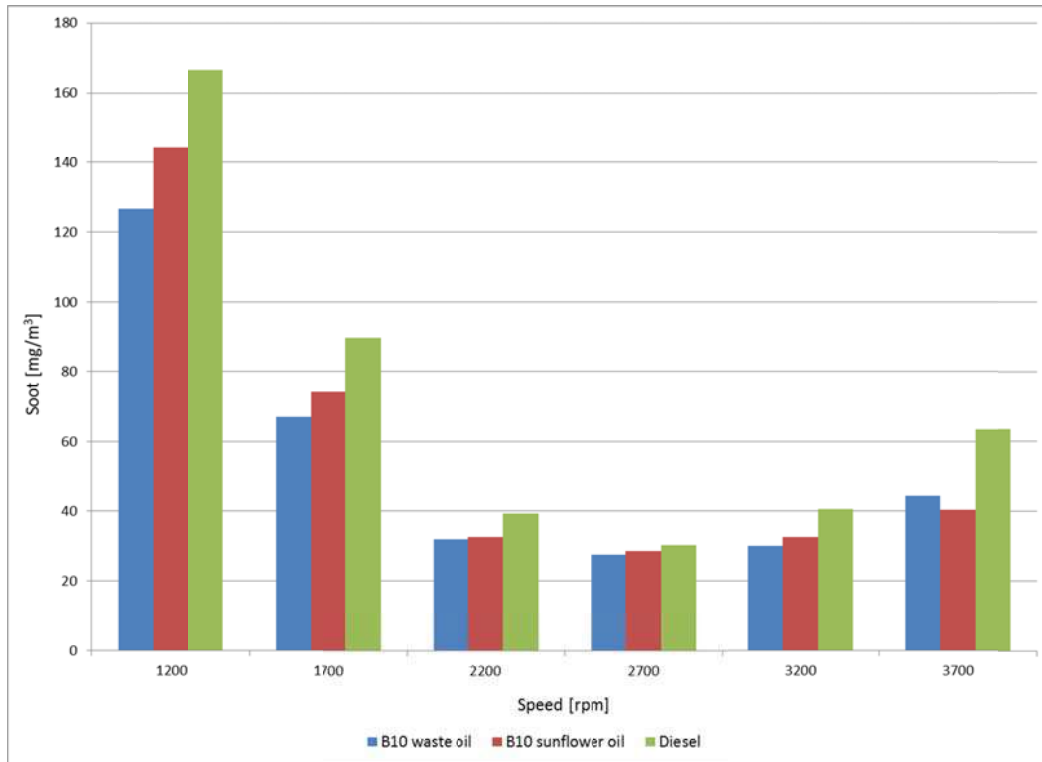


Fig. 7. Soot emission

Another aspect that must be taken into account is the material compatibility. The alternative fuel, as biodiesel, even blended can create unexpected problems in some fuel system parts such as: natural rubber hoses, gaskets, O-rings and metallic components.

References:

- [1] W. Addy Majewski, M. K. Khair, *Diesel emissions and their control*, SAE International, 2006.
- [2] H. Zhao, *Advanced direct injection combustion engine technologies and development, volume 2: Diesel engines*, Woodhead Publishing, 2010.
- [3] www.biodiesel.org.
- [4] www.horiba.com.
- [5] www.ebb-eu.org.
- [6] alternativefuels.about.com.



Editors: Sorin VLASE, Niitsu YASHUSI

**The 4th International Conference
Advanced Composite Materials Engineering
COMAT 2012
and
2nd International Conference
Research & Innovation in
Engineering**



Associazione Italiana
per l'Analisi delle Sollecitazioni

**Under Italian Society for
Experimental Stress Analysis
(AIAS)**

2

18 - 20 October 2012, Braşov, Romania

Elaborated and revised by Violeta MUNTEANU

Contents COMAT 2012
Volume 2

1. C. Casavola, L. Lamberti, C.I. Pruncu, WEIGHT MINIMIZATION OF TRUSS STRUCTURES WITH BIG BANG BIG CRUNCH.....	343
2. C.N. DRUGA, STAND FOR TESTING EXPERIMENTAL TOTAL HIP PROSTHESIS - electrical control circuits -.....	351
3. C.N. DRUGA, MODELING BY FEM OF A TOTAL HIP PROSTHESIS.....	355
4. S. Ciunel, D.L. Popa, O.V. Campian, A COMPARATIVE STUDY FOR TWO TYPES OF FRAME USED FOR DUMMY NECK IMPACT TESTING DEVICE.....	361
5. S. Ciunel, D.L. Popa, V. Campian, MATHEMATICAL MODEL OF THE DUMMY NECK INCLUDED IN A FRONTAL IMPACT TESTING SYSTEM.....	367
6. C. Buzatu, B. Lepadatescu, I. D. Bancila, CHOICE OF MATERIAL FACTOR IN ENSURING THE MACHINED SURFACE ROUGHNESS THROUGH SUPERFINISHING PROCESS.....	373
7. C.D. Stănescu, L. Căiniceanu, T. Burlan, RESEARCH ON THE IMPROVEMENT OF THE TECHNICAL CHARACTERISTICS OF HIGH POWER AUDIO SPEAKER.....	378
8. G. Buciu, D.L. Popa, D. Grecu, D. Niculescu, R. Nemes, VIRTUAL COMPARATIVE STUDY ON THE USE OF NAILS AT THE FIXATION OF TIBIAL FRACTURES USING FINITE ELEMENT METHOD.....	381
9. G. Buciu, D.L. Popa, D. Grecu, D. Niculescu, R. Nemes, COMPARATIVE ANALYSIS OF THE THREE NEW DESIGNS OF TIBIAL NAILS WHICH ELIMINATE THE USE OF ORTHOPEDIC SCREWS.....	387
10. C.C. Boricean, I.C. Rosca, P. Grigore, MONITORING AND IDENTIFYING VIBRATION SOURCES OF ROLLING BEARING AND HYDRODYNAMIC BEARING TURBOCHARGERS.....	393
11. C.C. Boricean, I.C. Rosca, P. Grigore, OIL INFLUENCE OVER DYNAMIC STABILITY OF ROLLING BEARING AND HYDRODYNAMIC BEARING TURBOCHARGERS.....	399
12. C.C. Boricean, I.C. Rosca, D. Buzea, ASPECTS REGARDING GENERAL VIBRATIONAL BEHAVIOR OF DIESEL ENGINES.....	403
13. M. Lupu, O. Florea, C. Lupu, QUALITATIVE STUDY OF THE STRUCTURAL INFLUENCE OF THE FORCES ON THE STABILITY OF DYNAMICAL SYSTEMS.....	408
14. N. Pandrea, N.D. Stănescu, P.P. Teodorescu, ANALYSIS OF A QUADRILATERAL CHEBYSHEV'S MECHANISM USING THE MINIMAX APPROXIMATIONS.....	414
15. N.D. Stănescu, STUDY OF THE STABILITY FOR A NONLINEAR QUADRATIC SUSPENSION OF A HALF OF AUTOMOBILE.....	419
16. C. Petrianu, M. Ință, D. Manolea, LASSER CUTTING PROCESS – INFLUENCE OF ASSISTING GAS PRESSURE ON SURFACE ROUGHNESS AT MILD STEEL CUTTING.....	427
17. I. Serban, N. Ispas, G. Bobescu, C. Arama, THE EXPERIMENTAL RESEARCH OF THE COMBUSTION ENGINE PISTON PIN STRESS.....	433

18. I. Serban, N. Ispas, G. Bobescu, C. Arama, THEORETICAL INVESTIGATIONS ABOUT THE INFLUENCES OF THE PISTON PIN STRESS ON THE COMBUSTION ENGINE PERFORMANCES.....	439
19. P. Vasiluta, N. Cofaru, D. L. Popa, MATHEMATICAL MODEL FOR THE TOTAL SOLAR RADIATION DETERMINATION AT THE SOIL LEVEL...	444
20. P. Vasiluta, N. Cofaru, D. L. Popa, INTERACTIVE AUTOLISP SOFTWARE FOR AUTOCAD MADE TO CALCULATE THE TOTAL SOLAR RADIATION DURING A DAY STARTING FROM LATITUDE AND LONGITUDE VALUES FOR A GIVEN POSITION.....	450
21. Ž. Arsenić, MODELLING OF THE FRICTION AND WEAR CHARACTERISTICS OF SEMI-METALLIC FRICTION MATERIALS FOR COMMERCIAL VEHICLE DISC BRAKES.....	456
22. C. Voican, C. Stanescu, FLEXIBLE SERVICE BINDING IN DISTRIBUTED AUTOMATION AND CONTROL SYSTEM.....	460
23. C. Voican, SERVICE ORIENTATION IN DISTRIBUTED AUTOMATION AND CONTROL SERVICE.....	465
24. D. Buzea, L. Kopacz, C. Husar, L. Ungureanu, COMPARATIVE ANALYSIS ON VIBRATION ATTENUATION OF RUBBER AND WIRE ROPE ISOLATORS.....	470
25. D. Buzea, L. Kopacz, C. Soimaru, C. Husar, EIGEN MODES IDENTIFICATION FOR HYBRID WIRE ROPE ISOLATORS.....	475
26. D. Stoica, THE EXISTENT BUILDINGS STOCK VULNERABILITIES AND THE POSSIBLE RETROFITTING STRATEGIES.....	482
27. I. Enescu, B. Lepădătescu, D. Enescu, THE STUDY OF TENSIONS IN THE INNERS BEARINGS.....	488
28. I. Enescu, B. Lepădătescu, D. Enescu, THE STUDIES OF THERMOELASTIC CONTACT FOR DETERMINATION THE FIELDS OF TEMPERATURES AND THERMAL TENSIONS IN BEARINGS INNERS (STATIONAR REGIM)	491
29. P.S. Făgăraș (Haba), IMPROVEMENT THE FREE THROWS IN BASKETBALL GAME.....	494
30. P.S. Făgăraș (Haba), DYNAMIC MODEL OF THE FREE-THROW IN BASKETBALL GAME.....	499
31. F. Constantin, INSTRUMENT FOR DETECTING CRITICAL FREQUENCY.....	505
32. F. Popescu, I.V. Ion, THE STUDY OF A SEPARATING AND REATTACHING FLOW TOPOLOGY.....	508
33. I.S. Radu, CHARACTERIZATION OF PERFORMANCE COATINGS USING THE MULTI-CRITERIA ANALYSIS METHOD.....	512
34. J. Timar, C. Cofaru, D. Florea, D. Covaciu, M.D. Stanciu, NOISE MAPPING OF A MAIN ROUTE IN BRAȘOV CITY	517
35. L. Hynčík, L. Kovář, T. Dziejowski, P. Baudrit, VIRTUAL HUMAN MODELS FOR INDUSTRY.....	522
36. V. Sandu, C. Bejan, EXPERIMENTAL MEASURES FOR MEETING STANDARDS OF DIESEL ENGINE VISIBLE EMISSIONS.....	528
37. C. Astalosch, I.T. Soare, C.G. Atanasiu, PARAMETRICAL OPTIMIZATION OF EXTRUSION PROCESS FOR AUTOMOTIVE COMPONENTS MADE FROM PP/TPV-E USING CFD METHODS.....	535

38. C. Astalosch, C.G. Atanasiu, GEOMETRICAL OPTIMIZATION OF AN EXTRUSION TOOL USED FOR AUTOMOTIVE DOOR'S SEALING SYSTEM USING CFD METHODS.....	541
39. G.N. Radu, I. Comanescu, M. Popescu, STUDIES ON THE VALUATION OF THE WORKING SAFETY OF THE GANTRY CRANES USING VIBRATORY ANALYSIS.....	550
40. G.N. Radu, I. Comanescu, M. Popescu, STUDIES REGARDING THE STATE OF STRESS AND STRAIN IN WINDBRACING BARS OF THE GANTRY CRANES. THE DYNAMIC ANSWER AT THE DISPLACEMENT OF THE CRANE'S CARRIAGE UNDER CONSTANT LOAD.....	554
41. A. Burnariu, R. Necula, B.P. Gálfi, I Száva, I. Šamotá, THE EVALUATION OF RELATIVE DISPLACEMENTS WITH VIC METHOD IN OSTEOSYNTHESIS OF TROCHANTERIC FRACTURES.....	558
42. A.C. Cucu, NEW COATINGS AND FINISHING METHODS FOR TOP PISTON RINGS OF DIESEL ENGINES TO REDUCE FRICTIONAL LOSS AND TO ENSURE ADEQUATE BEHAVIOUR UNDER MOST DIFFICULT REGIMES OF OPERATION.....	564
43. L. Kalmár, R. Hellmann, T. Régert, Z. Varga, NUMERICAL INVESTIGATION OF HEAT TRANSPORT PROCEDURE CAUSED BY HIGH POWERED UV LED.....	569
44. T.E. Bolfa, C.S. Bit, PROBLEMS SPECIFIC TO MATERIALS OF CAGES USED FOR BEARINGS FROM AERONAUTICS INDUSTRY.....	577
45. T.E. Bolfa, C.S. Bit, PROBLEMS SPECIFIC TO BLADE JUNCTION TO HUBS FOR WIND TURBINES.....	583
46. T.E. Bolfa, C. S. Bit, THE BEHAVIOR OF THE BEARINGS AT HIGH SPEED.....	586
47. G. Szeidl, L. Kiss, A NONLINEAR MECHANICAL MODEL FOR HETEROGENEOUS CURVED BEAMS.....	589
48. L. Dumitrescu, A. Matei, I. Manciulea, COMPOSITES ACRYLIC COPOLYMERS –WOOD WASTE.....	597
49. A. Gabor, M.V. Munteanu, DETERMINING THE SELF FREQUENCIES OF THE MAIN COMPONENTS FOR A VARIABLE COMPRESSION RATIO ENGINE.....	601
50. D.D. Truşcă, D.I. Dumitraşcu, EXPERIMENTAL RESEARCH REGARDING NIGHT VISIBILITY IN ROAD TRAFFIC.....	604
51. M.V. Guiman (Duţă), M.V. Munteanu, MODELING OF JOINTS FOR MULTIBODY SYSTEMS.....	610
52. C.S. Bit, T.E. Bolfa, CONSIDERATIONS CONCERNING FATIGUE CRACKS IN MECHANICAL STRUCTURES.....	614
53. C.S. Bit, T.E. Bolfa, FATIGUE CRACKS AND MICROSTRUCTURAL CONSTITUENTS.....	618
54. C.S. Bit, T.E. Bolfa, STRESS INTENSITY FACTOR IN BENDING.....	622
55. D.I. Dumitraşcu, D.D. Truşcă, VEHICLE-PEDESTRIAN ACCIDENT RECONSTRUCTION.....	626
56. A.E. Stanciu, R. Purcarea, METALLOGRAPHIC AND MICROSCOPIC ANALYSIS OF FIBERGLASS COMPOSITE MATERIAL, AFTER TENSILE TEST.....	630

57. A.E. Stanciu, R. Purcarea, M.V. Munteanu, S. Vlase, H. Teodorescu – Draghicescu, THEORETICAL AND EXPERIMENTAL DETERMINATION OF PROPERTIES FOR COMPOSITE MATERIAL TYPE ROVING SUBJECTED TO BENDING.....	634
58. A.E. Stanciu, D. Cotoros, M. Baritz, MICROSCOPIC ANALYSIS FOLLOWING BENDING OF MAT AND ROVING TYPE COMPOSITE MATERIAL.....	638
59. Č. Mitrović, N. Petrović, D. Bekrić, V. Dragović, I. Mileusnić, CHARACTERIZATION OF MICRO-STRUCTURES OF COMPOSITE OF SMALL WIND TURBINE BLADE FOLLOWING STRUCTURAL TESTING UP TO FAILURE.....	642
60. I. Ștefan, A. Olei, C. Nicolicescu RESEARCH ON MECHANICAL ALLOYING EFFECTS ON MAGNETIC PROPERTIES OF BARIUM FERRITE TYPE M.....	650
61. A.B. Muntean, A. Chiru, P. Grigore, STUDIES ON INFLUENCES OF FUEL INJECTION PARAMETERS ON POLLUTANT EMISSION OF DIESEL ENGINE, USING VIRTUAL ENVIRONMENT TOOL.....	656
62. P. Grigore, A. Gabor, M.V. Munteanu, I. Todor, INFLUENCE OF VARIABLE COMPRESSION RATIO REGARDING STRESS STUDY OF INTERNAL COMBUSTION ENGINES COMPONENTS.....	661
63. A.B. Muntean, A. Chiru, C. Soimaru, THE IMPACT OF DIFFERENT INJECTION SYSTEM PARAMETERS ON THE GEOMETRICAL FEATURES OF THE DIESEL SPRAY JET.....	667
64. P. Grigore, M.V. Munteanu, ENGINE OPTIMIZATION MECHANISM IN TERMS OF USING VARIABLE COMPRESSION RATIO.....	671
65. P. Grigore, A.B. Muntean, M.V. Munteanu, EXPERIMENTAL RESEARCH OF TOTAL DEFORMATION AND EQUIVALENT STRESS FOR INTERNAL COMBUSTION ENGINES COMPONENTS.....	677
66. A. Gabor, P. Grigore, A METHOD TO DETERMINE THE SELF FREQUENCIES OF A CRANKSHAFT FROM A SINGLE CYLINDER ENGINE WITH VARIABLE COMPRESSION RATIO.....	683



VEHICLE-PEDESTRIAN ACCIDENT RECONSTRUCTION

D.I. Dumitrașcu¹, D.D. Trușcă¹

¹ Transilvania University, Brașov, ROMANIA, d.dumitrascu@unitbv.ro, truscadan@gmail.com

Abstract: Traffic accident involving pedestrians are much different compared to other types of road events. This is certainly due to the different masses in contacts (average mass of a vehicle is 1200 kg and a pedestrian has 80 kg) and different speeds. The result of this collision is easy to predict: the pedestrian always has to suffer. Traces resulting from this type of accident are very important.

Vehicle-pedestrian accident reconstruction viability depends on the accuracy with which are extracted and recorded, during the primary investigation at the scene, the two samples: location of the vehicle and pedestrian impact and where pedestrian remained after the accident. If these elements are missing, which allowed the direct identification, should be searched and recorded other collateral evidence necessary to establish precisely the first two.

Keywords: pedestrian, simulation, dynamics, collision, vehicle

1. INTRODUCTION

A peculiarity of collisions with pedestrians is the time available for pedestrians on one side and the driver on the other side regarding the best decision to avoid the accident.

If a pedestrian crosses the street and gets hit from the left side, his knee bends properly to the shape of the vehicle bumper. Friction force between pedestrians shoe and road surface, keeps shoe on road initially, while the vehicle gives off a force that pushes forward the knee.

This mechanism can cause a fracture of the lower leg bone and cause pedestrian to rotate left, around its center of gravity, up above the hood or the roof, depending on the speed of impact. There is a transfer of mass from his right leg to left one, preventing, in most cases, a fracture of the right leg that is farthest from the vehicle's bumper and behind the initial impact.

The way that pedestrian rotates toward and over the vehicle and lands on the pavement on the road or on sidewalk area is another significant step of the dynamics of accident that requires a detailed analysis.

In the case of an impact of the pedestrian's head with the windscreen, in the crack area may remain hair, fragments of tissue and blood.



Figure 1: Impact with vehicle windscreen

The impact with the pedestrian body generally produces deformation of the car hood. It is necessary to corroborate trauma, primarily of swollen areas located on pedestrian upper body, like the shoulder or elbow or such as those of the hip or knee. Bumper causes the impact at lower leg pedestrian and by comparing the distance from the ground to the lesion with the height of known bumper, it can be established the contact area.

2. DYNAMICS OF PEDESTRIAN-VEHICLE ACCIDENT

From the made measurements to determine the distance of visibility, is chosen for the case study, the simulation of an accident with a pedestrian dummy dressed in yellow in a particular traffic situation.

For the simulation it was chosen a regular car traveling on a road at night, when at one point hits pedestrian traveling on the same lane in the opposite direction.

Pedestrian is drunk and moves irregularly. The chosen car is a Peugeot 206 that runs with a speed of 90 km/h, with low beam and when driver notifies the pedestrian, breaks vigorously. Yellow was chosen because it was determined from made measurements that it reflects a lot of light and is visible from the driver distances. The road is not heavily traveled, being out of town.

Pedestrian has the following characteristics: mass 75 kg, height 1.72 m, speed 4 km/h.

The objectives of the paper were:

- Dynamics of the accident;
- Place of impact in relation to the road surface
- Pedestrian observation distance by the driver in the following circumstances: with or without oncoming vehicle;
- Collision avoidance ways.

2.1. Collision simulation

Accident reconstruction was performed by using specialized software PC Crash 9.1.



Figure 2: Position of Peugeot 206 when the driver notified the state of danger (about 70m from the pedestrian)

Starting from the set speed $\approx 90 \text{ km/h} = 25 \text{ m/s}$, it can be calculated the braking space:

$$S_f = \frac{v \cdot t_r}{3.6} + \frac{v \cdot t_i}{3.6} - \frac{\varphi \cdot g \cdot t_i^2}{12} + \frac{(v - 1.8 \cdot \varphi \cdot g \cdot t_i)^2}{254.2 \cdot \varphi_b} = 45m \quad (1)$$

where: t_r - reaction time (= 1 s); t_i - the time required to achieve maximum deceleration from the braking start (0.2 s); φ - coefficient of adhesion = 0.7.

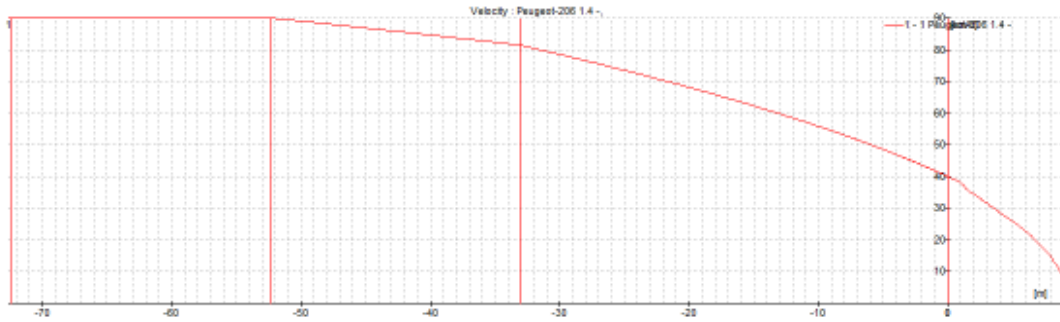


Figure 3: Peugeot 206 speed variation

Average referral distance for pedestrians dressed in yellow, as measured data is about 70m. Following notification exposure to danger, after covering the distance of 25 m corresponding reaction time of 1 s, at night time, the driver does push the brake pedal, resulting in braking printing marks on the road. The time to reach maximum deceleration of -6.87 m/s^2 from the start of braking, for a coefficient of adhesion of 0.7, is 0.2 seconds and vehicle continues to move for approximately 5m. Total braking space is about 46 meters. Pedestrian was hit after the vehicle has braking about 40 m.

The impact was characterized by:

- First contact between car and pedestrian was between the victim's right leg and bumper of the vehicle;
- The impact among the victim's head and the boundary between the hood and windscreen get materialized through the windscreen crack and bruises to the head of the victim;
- slip on the hood and pedestrian separation after completing by the vehicle of a distance of approximately 3.5 m;
- pedestrian slip on asphalt for a distance of about 4.3 m.

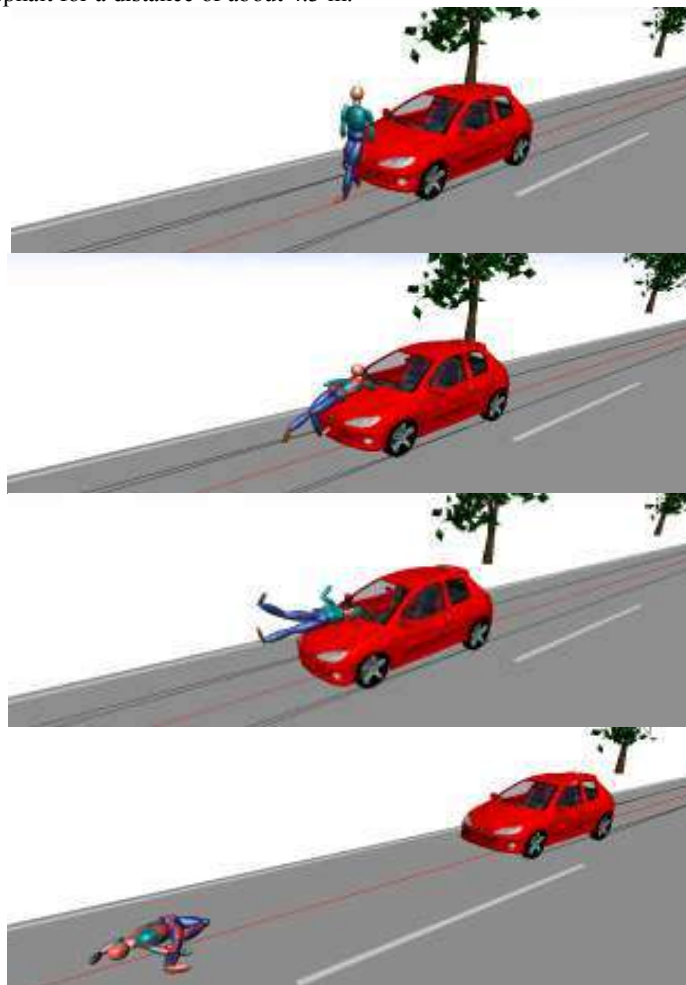


Figure 3: Pedestrian impact stages

The accident was simulated in condition of having an oncoming vehicle or the driver is moving with the low beam. The average distance for a pedestrian is 70 m. Under these conditions the accident cannot be avoided at this distance.

As shown in the table 1, the accident could have been avoided at the speed of 82.8 km/h.

If there is no oncoming traffic and it is used the high beam, the pedestrian would be visible from a distance of between 150 and 200 m, and the accident could have been avoided without problems.

Table 1: Dynamic parameters

Vehicle	Initial speed v0 [km/h]	Speed for maximum brake efficiency vb [km/h]	Impact speed v1 [km/h]	Braking deceleration ab [m/s²]
	90	81.5	40	-6.87
	Time to impact t [s]	Reaction time tr [s]	Time for braking system activation tl [s]	Time elapsed from maximum braking to impact tb [s]
	3.56	0.80	0.20	1.96
	Total space s[m]	Distance covered during reaction time sr[m]	Distance covered from the start of braking until maximum braking efficiency sl[m]	Distance covered to impact with maximum braking sb[m]
	72.10	20	19.06	33.5
	Avoidance deceleration aa [m/s²]	Avoidance reaction time atr [s]	Avoidance speed av [km/h]	Avoidance space as [m]
	7.32	0.38	82.85	82.58

3. CONCLUSION

In real traffic situations, special circumstances most often arise that contribute to road accidents with unpleasant consequences. Among the causes of accidents that occur at night, the most common is the lack of visibility correlated with an improper equipping of the traffic partners.

One with particularly serious consequences is the vehicle-pedestrian accident type, which can be produced from various causes.

This paper aimed to describe the dynamics of the vehicle pedestrian impact by using the simulation software PCCrash, accident generated by the lack of visibility of pedestrians in traffic at night on a road outside the city. Lack of sufficient visibility is a major contributor to increased risk for driving at night. This is even more evident in the case of accidents involving pedestrians. Human visual performance is limited in adapting to the sudden darkness or from darkness to light.

It may be noted that in these circumstances of the accident occurrence, the speed difference from 90 km/h to 82.85 km/h of the vehicle involved in the accident may determine the avoidance of the accident. We can say that road events that happen in special circumstances, as the lack of visibility at night can be avoided by compliance with road safety regulations, by the use of active safety devices designed to compensate physiological deficiencies of the driver. Under these conditions the improvement of the traffic safety at night, depends heavily on the quality of vehicle lighting systems, whose evolution is growing.

REFERENCES

- [1] Datentechik S., PC-CRASH A Simulation Program for Vehicle Accidents, Operating Manual, Version 9.1, Linz, Austria, 2011.
- [2] Wood D. P., Simms C. K., Walsh D. G., Vehicle-Pedestrian Collisions: Validated Models for Pedestrian Impact and Projection
- [3] Gaiginschi R., Reconstrucția și Expertiza Accidentelor Rutiere, Editura Tehnică, București, 2009.
- [4] Trusca D., s.a., Influence of Various Anthropometric Constitution of Pedestrian in case of Vehicle Pedestrian Impact, The 11th International Congress on Automotive and Transport Engineering CONAT 2010, Volume IV-Advanced Transport Systems and Road Traffic, ISSN 2069-0401, Brasov, 2010.

Editors: Nouras Barbu Lupulescu, Snejana Yordanova, Valeri Mladenov



Recent Researches in Neural Networks, Fuzzy Systems, Evolutionary Computing & Automation

- ▷ 12th WSEAS International Conference on Neural Networks (NN '11)
- ▷ 12th WSEAS International Conference on Fuzzy Systems (FS '11)
- ▷ 12th WSEAS International Conference on Evolutionary Computing (EC '11)
- ▷ 12th WSEAS International Conference on Automation & Information (ICAI '11)

Sponsor and Organizer



Transilvania University of Brasov, Romania, April 11-13, 2011

ISBN: 978-960-474-292-9

Recent Researches in Neural Networks, Fuzzy Systems, Evolutionary Computing & Automation



RECENT RESEARCHES in NEURAL NETWORKS, FUZZY SYSTEMS, EVOLUTIONARY COMPUTING and AUTOMATION

**12th WSEAS International Conference on NEURAL NETWORKS (NN '11)
12th WSEAS International Conference on FUZZY SYSTEMS (FS '11)
12th WSEAS International Conference on EVOLUTIONARY COMPUTING
(EC '11)
12th WSEAS International Conference on AUTOMATION &
INFORMATION (ICAI '11)**

**Transilvania University of Brasov, Romania
April 11-13, 2011**

RECENT RESEARCHES in NEURAL NETWORKS, FUZZY SYSTEMS, EVOLUTIONARY COMPUTING and AUTOMATION

12th WSEAS International Conference on NEURAL NETWORKS (NN '11)
12th WSEAS International Conference on FUZZY SYSTEMS (FS '11)
12th WSEAS International Conference on EVOLUTIONARY COMPUTING (EC '11)
12th WSEAS International Conference on AUTOMATION & INFORMATION (ICAI '11)

Transilvania University of Brasov, Romania
April 11-13, 2011

Published by WSEAS Press

www.wseas.org

Copyright © 2011, by WSEAS Press

All the copyright of the present book belongs to the World Scientific and Engineering Academy and Society Press. All rights reserved. No part of this publication may be reproduced, stored in a retrieval system, or transmitted in any form or by any means, electronic, mechanical, photocopying, recording, or otherwise, without the prior written permission of the Editor of World Scientific and Engineering Academy and Society Press.

All papers of the present volume were peer reviewed by two independent reviewers. Acceptance was granted when both reviewers' recommendations were positive.
See also: <http://www.worldses.org/review/index.html>

ISBN: 978-960-474-292-9



World Scientific and Engineering Academy and Society

RECENT RESEARCHES in NEURAL NETWORKS, FUZZY SYSTEMS, EVOLUTIONARY COMPUTING and AUTOMATION

12th WSEAS International Conference on NEURAL NETWORKS (NN '11)
12th WSEAS International Conference on FUZZY SYSTEMS (FS '11)
**12th WSEAS International Conference on EVOLUTIONARY COMPUTING
(EC '11)**
**12th WSEAS International Conference on AUTOMATION &
INFORMATION (ICAI '11)**

Transilvania University of Brasov, Romania
April 11-13, 2011

Editors:

Prof. Nouras Barbu Lupulescu, Dean of Faculty of Technological Engineering and Industrial Management, Romania

Prof. Snejana Yordanova, Technical University of Sofia, Bulgaria

Prof. Valeri Mladenov, Technical University of Sofia, Bulgaria

International Program Committee Members:

Karol Velisek, SLOVAKIA

Peter Kostal, SLOVAKIA

A.M. Goncalves Coelho, PORTUGAL

Slobodan NAVALUSIC, SERBIA

Schlegel Daniel, FRANCE

Roman Adriana, FRANCE

Ciobanu Valentina, ROMANIA

Razvan Udroi, ROMANIA

Lubomir Dimitrov, BULGARIA

Tasho Tashev, BULGARIA

Gerardo Acosta, SPAIN

Ping An, CHINA

Kiyoshi Akama, JAPAN

Mehrdad Ardebilipour, IRAN

Carlos Aviles-Cruz, MEXICO

Yun Bai AUSTRALIA

Ana Madureira, PORTUGAL

Petr Ekel, BRAZIL

Yue-shan Chang, TAIWAN

Chip Hong Chang, SINGAPORE

Sheng-Gwo Chen, TAIWAN

George Antoniou, USA

Tanglong Chen, CHINA

Lotfi Zadeh, USA

Michael Wasfy, USA

Myeonggil Choi, KOREA

Yuk Ying Chung, AUSTRALIA

Metin Demiralp, TURKEY

Angelos Zachariadis, GREECE

Costas Polychronopoulos, GREECE

Toshio Eisaka, JAPAN

Alessandra Flammini, ITALY

Donata Francescato, ITALY

Tapio Frantti, FINLAND

Georges Fried, FRANCE

Rocco Furferi, ITALY

James Gao, UNITED KINGDOM

Gilson Giraldi, BRAZIL

Sungho Ha, KOREA

Nualsawat Hiransakolwong, THAILAND

A. Manikas, UK

Dil Hussain, DENMARK

Philippe Dondon, FRANCE,

Muhammad Ibrahimy, MALAYSIA

Michael Katchabaw, CANADA

Seong Baeg Kim, KOREA

Jin-tae Kim, KOREA

Mallikarjun Kodabagi, INDIA

M. I. Garcia-Planas, SPAIN

Xiaoyu Li, CHINA

Jie Li, CHINA

Jiang Liu, UNITED STATES

Afif Mghawish, JORDAN

Tetsushi Miki, JAPAN

Zhong Ming, CHINA

Hasnaoui Othman, TUNISIA

Zeljko Panian, CROATIA (HRVATSKA)

PooGyeon Park, KOREA

Vidyasagar Potdar, AUSTRALIA

Sangmun Shin, KOREA

Li Shuhong, CHINA

Yu Shunkun, CHINA

Andrzej Sluzek, SINGAPORE

Hokeun Song, KOREA

Paulo Sousa, PORTUGAL

Sarawut Sujitjorn, THAILAND

Yi Sun, CHINA

Guangzhong Sun, CHINA

Yoshihiro Tanada, JAPAN

Lixin Tao, USA

Nam Tran, AUSTRALIA

Argyrios Varonides, USA

Peter Trkman, SLOVENIA

Lamberto Tronchin, ITALY

Amritasu Sinha, INDIA

Ming-Jer Tsai, TAIWAN

Woei-Jiunn Tsaur, TAIWAN

Kuo-Hung Tseng, TAIWAN

Hiroshi Umeo, JAPAN

Ronald Yager, USA

Pragya Varshney, INDIA

Lusheng Wang, HONG KONG S.A.R.

Lei Wang, CHINA

Zhongfei Wang, CHINA

Hironori Washizaki, JAPAN

Wang Wen, CHINA

Kin Yeung Wong, MACAU S.A.R.

Jyh-Yang Wu, TAIWAN

Hsiaokuang Wu, TAIWAN

Yinshui Xia, CHINA

Yi Xie, CHINA

Xinli Xu, CHINA

Yong Xu, CHINA

Yinlong Xu, CHINA

Xinli Xu, CHINA

Bin Xu, CHINA

Hongwen Yan, CHINA

Hung-Jen Yang, TAIWAN

Thomas Yang, USA

Hung-Jen Yang, TAIWAN

Houjun Yang, CHINA

Hsieh-Hua Yang, CHINA

Wenrong Yang, CHINA
Hung-Jen Yang, TAIWAN
Sumanth Yenduri, USA
Alimujiang Yiming, JAPAN
Jianfei Yin, CHINA
Liuguo Yin, CHINA
Ren Yong Feng, CHINA
Tetsuya Yoshida, JAPAN
Hsiang-fu Yu, TAIWAN
S.Y.Chen, GERMANY
Adela-Eliza Dumitrascu, ROMANIA
Adriana Fota, ROMANIA
Dragoi Viorel Mircea, ROMANIA
Oancea Gheorghe, ROMANIA
Laurentiu Mihail, ROMANIA
Camil Lancea, ROMANIA
Lucia Chicos, ROMANIA
Ionescu Mihai, ROMANIA
Ditu Valentin, ROMANIA
Popa Luminita, ROMANIA

Table of Contents

Keynote Lecture: Fluctuation Free Matrix Representation in Expectation Value Dynamical Issues and their Applications	12
<i>Metin Demiralp</i>	
Plenary Lecture 1: Fault Detection and Isolation using Neuro-Fuzzy Systems	14
<i>Francklin Rivas-Echeverria</i>	
Plenary Lecture 2: Monitoring Distributed Parameter Systems Based on Expert Systems and Sensor Networks	15
<i>Constantin Volosencu</i>	
Prediction of Material Removal Rate for Ti-5Al-2.5Sn in EDM using Multi-Layered Perceptron Neural Network Technique	17
<i>M. M. Rahman, Ashikur Rahman Khan, K. Kadirgama, Rosli A. Bakar</i>	
Consumer Behaviour Fuzziness in the New Market Environments	24
<i>Rawshan Basha, Jamal Ameen</i>	
People, Automation, and Complexity Concerns Affecting Manufacturing Enterprise Information Integration	29
<i>Ionel Botef</i>	
On Fuzzy-Logic-Based Ontology Decision Support System for Government Sector	34
<i>Sameera Al Shayji, Nahla El Zant El Kadhi, Zidong Wong</i>	
Accessible Web-Based Educational System	42
<i>Fatima AlDhaen, Nahla El Zant El Kadhi, Hadeel Al-Obaidy</i>	
Modeling of Fuzzy-Neural Systems Using the Coevolutionary Algorithm	49
<i>Samir Omanovic, Zikrija Avdagic</i>	
The Development of Virtual Organizations in Romania	54
<i>Larion Valentin, Tofan Dan Constantin, Dinca Lavinia Mihaela</i>	
Detection of Objects in Moving Images and Implementation of the Purification Algorithm on Analog CNN and DSP Processors	60
<i>Emel Arslan, Zeynep Orman, Sabri Arik</i>	
Model of Biological ANN Based on Homeostatic Neurons	66
<i>Martin Ruzek, Tomas Brandejsky</i>	
Innovative Strategy of SOMA Control Parameter Setting	70
<i>Pavel Varacha</i>	
The Informatic System Architecture for Monitoring Anti-Hail Network	76
<i>Constantin Sulea, Gheorghe Manolea, Laurentiu Alboteanu</i>	

Information Technology Standards – A Viable Solution to Reach the Performance <i>Manole Velicanu, Iulia Surugiu, Daniela Litan, Ovidiu Raduta, Aura-Mihaela Mocanu (Virgolici)</i>	82
About L-Infinity Space for Fuzzy Measures <i>Alina Gavrilut, Anca Croitoru</i>	88
Neural Network Synthesis via Asynchronous Analytic Programming <i>Pavel Varacha</i>	92
Existence of Fuzzy Equilibria for Fuzzy Abstract Economies with Q'-Majorized Correspondences <i>Monica Patriche</i>	98
Pattern Recognition in Wireless Sensor Networks in Presence of Sensor Failures <i>Janos Csirik, Peter Bertholet, Horst Bunke</i>	104
About Fuzzy Integrals for Vector Valued Multifunctions <i>Cristina Stamate</i>	110
Monitoring Distributed Parameter Systems Based on Expert Systems and Sensor Networks <i>Constantin Volosencu</i>	114
A Design and Simulation of Fuzzy PID Controller for the Optimization of Temperature and Humidity in the Thermodynamic System <i>Stefan Koprda, Zoltan Balogh, Milan Turcani</i>	119
Experimental Researches of Fuelling Systems and Alcohol Blends on Combustion and Emissions in a Two Stroke Si Engine <i>Mihai Aleonte, Corneliu Cofaru, Radu Cosgarea, Maria Luminita Scutaru, Liviu Jelenschi, Gabriel Sandu</i>	126
An Approach for Modeling the Valve Train System to Control the Homogeneous Combustion in a Compression Ignition Engine <i>Radu Cosgarea, Corneliu Cofaru, Mihai Aleonte, Maria Luminita Scutaru, Liviu Jelenschi, Gabriel Sandu</i>	131
The Braking Process at the Stroke end of Linear Hydraulic Motors <i>Ioan Cristian</i>	136
The Absorbent's Solution Flow Process, Non-Parametric Identification into an Absorption Chiller for Air Conditioning <i>Adrian Danila</i>	140
Aspects Regarding the Monte-Carlo Simulation of Products Reliability <i>Dumitrascu Adela-Eliza, Duicu Simona</i>	145
On Some Multi-Attribute Decision Models Based on Fuzzy Techniques <i>Dorin Lixandroi</i>	150
Fuzzy Control Design for a Gas Absorber System <i>Mohamed Mas Mahmoud</i>	155
A New Approach to Fuzzy-Control Large Scale Systems <i>Mohamed Mas Mahmoud</i>	161

The Calculation of the Testing Period of the Reliability of Products by Using the Model of Exponential Distribution	169
<i>Morariu Cristin-Olimpiu, Zaharia Sebastian Marian</i>	
Single Cylinder Diesel Engine Performances Estimation Using AVL Boost software	173
<i>Dumitrascu Dorin Ion, Nedelcu Anisor</i>	
Mathematical Modeling of a Stochastic Branching Process	177
<i>Stoian Nadia Mirela, Orman V. Gabriel, Crismaru Nicolae</i>	
A New Concept of Intensifier for Double Acting Hydraulic Power Workholding Systems	181
<i>Tudor Paunescu</i>	
Kinematic Analysis of Three Bar Mechanism Linked with Rotation Joints	185
<i>Ioana Petre, Tudor Deaconescu, Andrea Deaconescu, Dan Petre</i>	
Automated Material Handling Systems (AMHS) in Libraries and Archives. Automated Storage/Retrieval and Return/Sorting Systems	189
<i>Corina Pop, Gabriela Mailat</i>	
Fuzzy Logic Based Approach to Optimal Hydraulic Cylinders Assembly	195
<i>Snejana Yordanova, Lubomir Dimitrov</i>	
Brownian Motion and Stochastic Models	201
<i>Dana Damian, Sorina Stoian, Oana Rachieru, Alina Stoica</i>	
Optimizing Protein Importance Assessment Through a Dijkstra-Based Sequential Optimization Technique	207
<i>Razvan Bocu, Dorin Bocu</i>	
Scene Text Extraction Using Modified Cylindrical Distance	213
<i>Hrvoje Dujmic, Matko Saric, Josko Radic</i>	
ISPRS: Intelligent Services for Poverty Reduction Schemes	219
<i>Petar Solic, Matko Saric, Darko Stipanicev</i>	
Authors Index	225

Single Cylinder Diesel Engine Performances Estimation Using AVL Boost software

DUMITRASCU DORIN ION¹, NEDELICU ANISOR²
 Automotive Engineering Department¹, Manufacturing Engineering Department²
 “Transilvania” University of Brasov
 Eroilor Street, No. 29, 500036, Brasov
 ROMANIA
 d.dumitrascu@unitbv.ro; a.nedelcu@unitbv.ro;

Abstract: - The objective of this paper is to present the results and advantages of the engine cycle simulation of a single cylinder direct injection diesel engine using AVL Boost software. The simulation results highlighted the energetically and economical performances of the engine and the evolution and the control of engine cycle parameters.

Key-Words: - simulation, model, engine cycle, performances, estimation, parameter

1 Introduction

AVL BOOST represents an advanced and fully integrated “Virtual Engine Simulation Tool” with advanced models for accurately predicting engine performance. The code can simulate the entire engine cycle including combustion [1]. Some typical applications include [1]:

- Torque curve prediction;
- Fuel consumption
- Manifold design and tuning
- Valve timing optimization
- Turbocharger matching, waste gate, VTG
- Acoustic analysis (intake/exhaust orifice noise)
- Combustion and emission analysis
- EGR with Boost-Fire Link
- Turbocharger response.

2 Engine Cycle Simulation

2.1 The simulation main steps

- Design the model (the model can be designed by placing the elements in the working area first and then connecting them with the pipes)
- General input data (e.g. engine speed, mixture preparation, fuel, reference conditions, cycle, etc.);
- Element input data (e.g. engine constructive characteristics, combustion model, heat transfer, valve port specifications, etc.);
- Run simulation;

- Post-processing (e.g. engine overall performances);

2.2 The model

In figure 1 is presented the single cylinder diesel engine model used for the analysis. The model consists of the following elements:

- SB - system boundaries;
- MP - measuring points;
- C - cylinder;

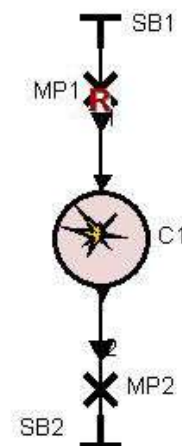


Fig.1

2.3 Engine characteristics

The characteristics of the engine are:

- bore: 76 mm
- stroke: 65 mm
- displacement: 295 cm³

- power: 4 kW
- speed: 3000 rpm
- compression ratio: 17:1

The Diesel engines by small power have a wide range of application for the mechanization of the most activities in industry and agriculture. This type of engines, with power up to 10kW, is using, in most of the cases, the air-cooling.

3 Simulation Results

The general performances of engine torque, power, specific and per hour consumption against engine speed are shown in figure 2.

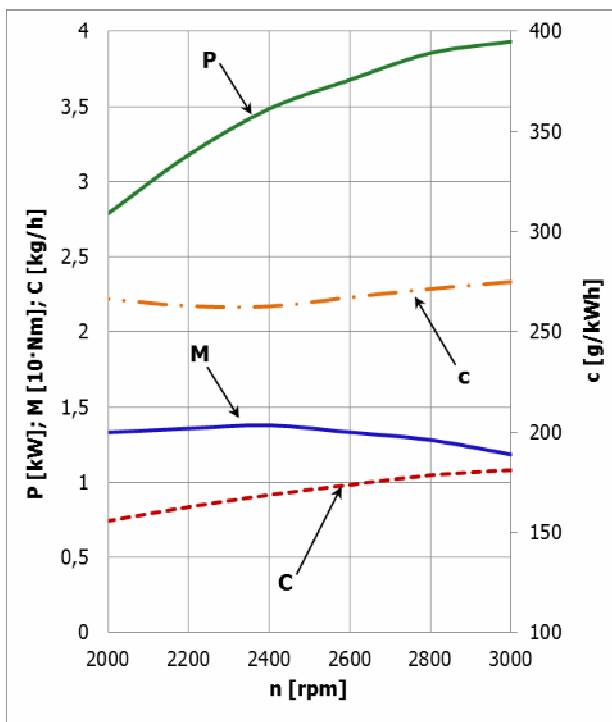


Fig.2

Table 1

Parameter	Unit	Results
Power	kW	3,93
Maximum torque	Nm	13,79
Specific consumption at nominal power	g/kWh	275
Specific consumption at maximum torque/speed	g/kWh	262,8
	rpm	2400

Effective mean pressure variation is illustrated in figure 3. The range of it is between 0.54 to 0.58 MPa, the values are close to the real case of engines in this class. Figure 4 shows the variation of excess air ratio and the volumetric efficiency relative to speed. By increasing the speed, the volumetric

efficiency will decrease, it reduces the intake valve opening time and the filling worsens. The volumetric efficiency values are in the range from 0.91 to 0.93. The coefficient of excess air is in the range from 1.54 to 1.55, values characteristic of diesel engines.

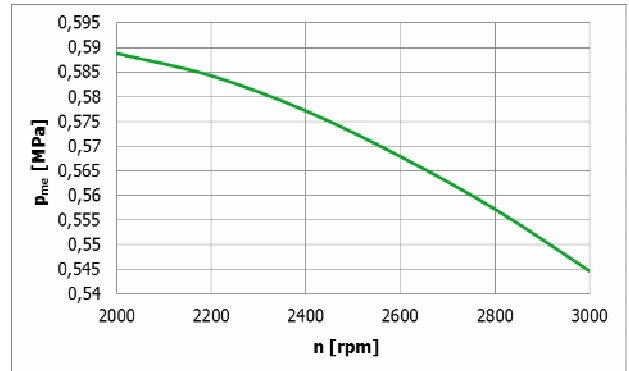


Fig.3

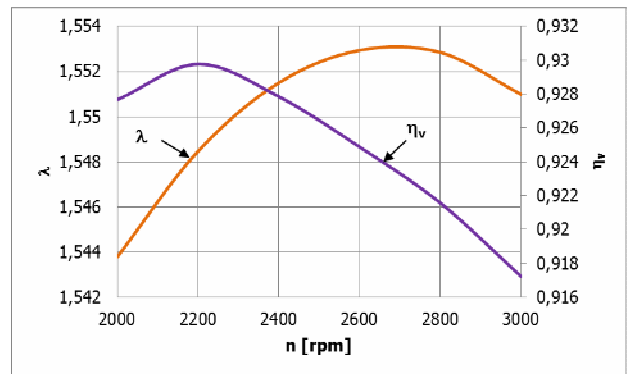


Fig.4

Figure 5 presents the influence of speed on residual gas coefficient. Specific range of diesel engines is between 0.03 and 0.06. The values obtained indicate a proper discharge of the cylinder.

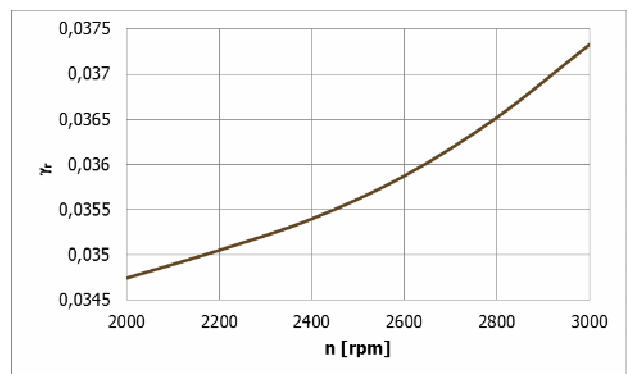


Fig.5

The main results of the simulation, from the two

measuring points MP1, MP2 located in inlet and exhaust manifolds, are represented in the following figures.

Figure 6 illustrates the air mass flow, figure 7 the air rate and figure 8 mean air pressure in inlet manifold.



Fig.6

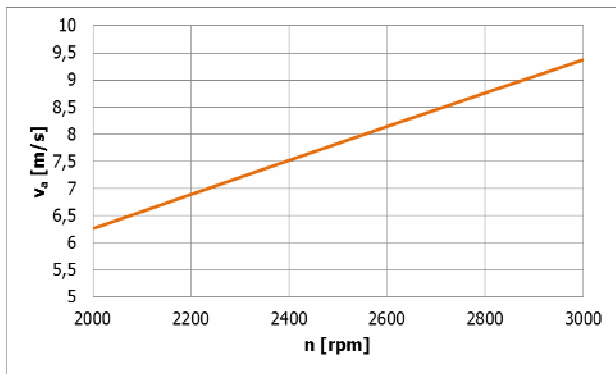


Fig.7

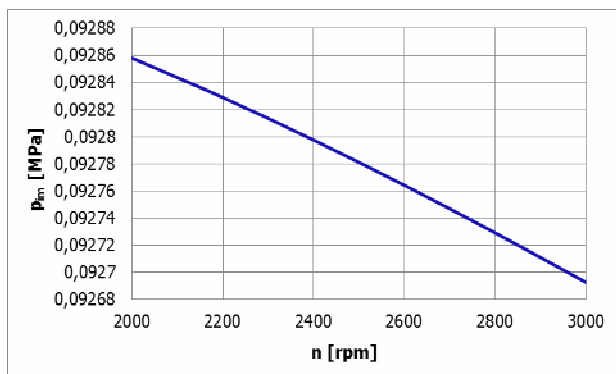


Fig.8

Once engine speed increases, both, mass flow of fresh air that enters the cylinder and inlet pressure decrease because of the increased admission rate that diminishes the volumetric efficiency. In the same time an increase of exhaust gas rate occurs, that accelerate the gas column (figure 9). In figure 10 is presented the mean pressure of exhaust gas.

Figure 11 illustrates exhaust gas flow.

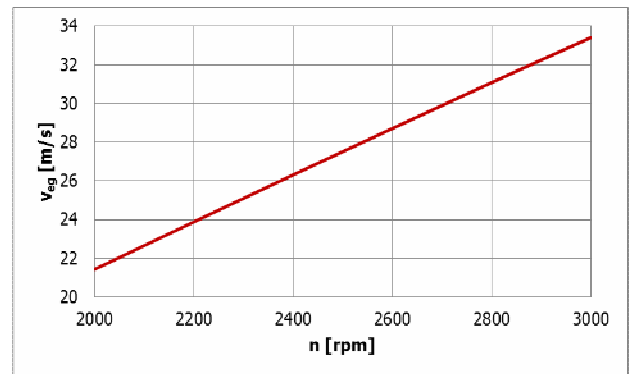


Fig.9

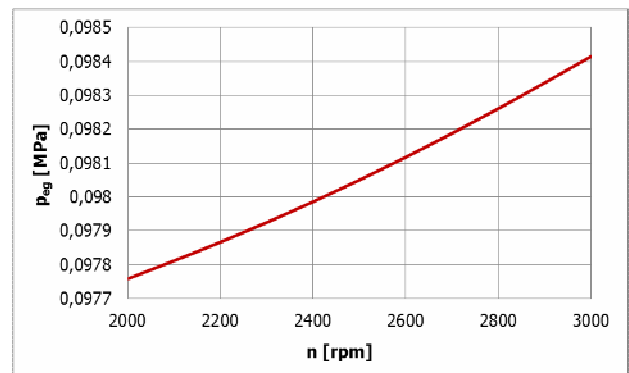


Fig.10

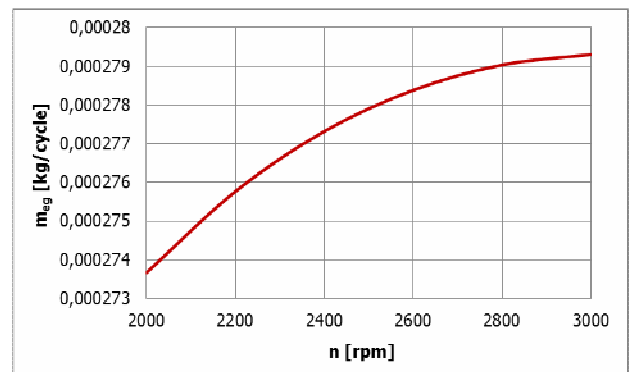


Fig.11

In figure 12 are presented the evolution of the cylinder pressure and temperature for the 3000 rpm engine speed. Maximum cycle pressure is 5.9 MPa and temperature of 2065.97 K. The maximum duration of the ignition delay is ~ 5.5 °CA, at this stage are visible the processes resulting with heat absorption (latent heat vaporization of diesel fuel, the first reaction of oxidation) and causes a reduction in air pressure and temperature increase. Growth rate of the pressure is within normal limits, causing a quiet running engine (figure 13). Heat

release rate (figure 14) captures the typical phases of the combustion process: the ignition delay, premixed (chemistry-controlled), heat release rate reaching the maximum at about 6 °CA after TDC and then the diffusive burning (mixing-controlled). The premixed combustion lasts ~ 10 °CA and total combustion duration is about 30 °CA.

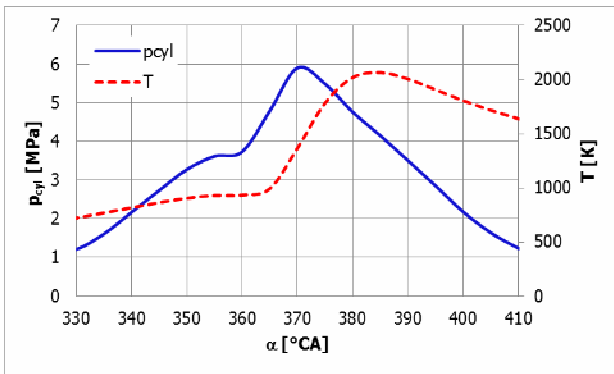


Fig.12

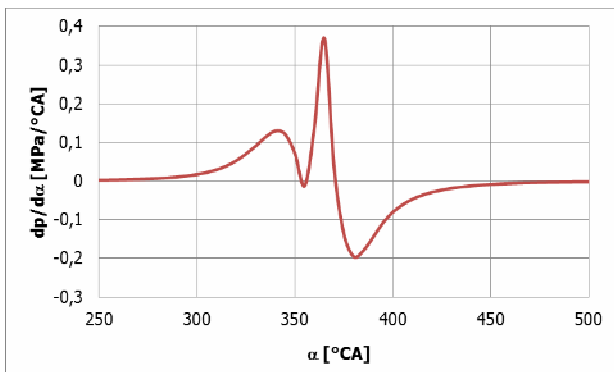


Fig.13

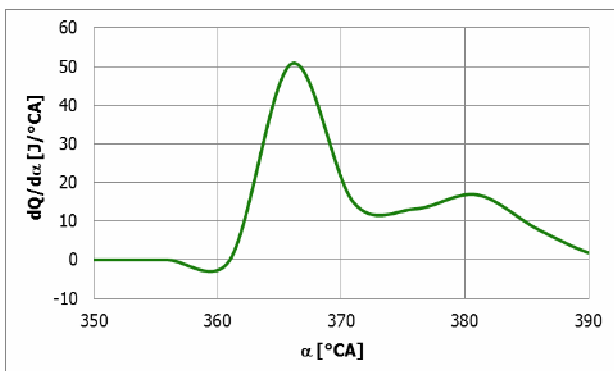


Fig.14

In figure 15 is represented the total heat flow through walls.

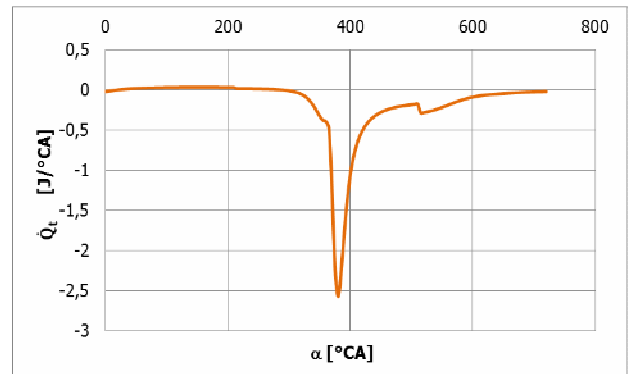


Fig.15

Largest amount of heat lost through the walls is concentrated around the combustion process, a lower proportion belonging to expansion stroke, this indicating an optimum combustion process.

4 Conclusion

The simulation of the engine cycle processes highlighted the evolution of the main specific parameters. Analyzing the values of the energetically and economical parameters obtained, it finds that they correspond to the real range of variation for this type of engines.

The results obtained by simulation shows that this method offers an accurate picture of the progress of real processes from a diesel engine.

Concluding it can be mentioned that AVL Boost software represents a powerful tool for engine cycle simulation of internal combustion engines.

References:

- [1] www.avl.com
- [2] *AVL Boost*, Version 5.0 examples, October 2006
- [3] J.B. Heywood, *Internal Combustion Engine Fundamentals*, McGraw - Hill Book Company, 1988



**Transilvania
University
of Brasov**

**FACULTY OF
MECHANICAL ENGINEERING**

IN ASSOCIATION WITH:



ACADEMY OF
TECHNICAL
SCIENCES OF
ROMANIA



ROMANIAN
SOCIETY OF
THEORETICAL
AND APPLIED
MECHANICS



THE ROMANIAN
ACOUSTIC
SOCIETY



RESEARCH INSTITUTE
FOR CONSTRUCTION
EQUIPMENT AND
TECHNOLOGY –
ICECON S.A.

**The 8th International Conference on
Computational Mechanics and Virtual Engineering
COMEC 2019**

**The 43rd International Conference on “Mechanics of
Solids” – ICMS 2019– “P.P. Teodorescu”**

FINAL PROGRAMME

Braşov, ROMANIA, 21-22 November 2019

15. **Dorin Dumitrascu**
ASSESSMENT OF POTENTIAL RISKS THAT INFLUENCE THE TRAFFIC ACCIDENTS
16. **Daniela Sova, Mariana Domnica Stanciu, Elena Belea, Sergiu V. Georgescu**
THERMAL CONDUCTIVITY EXPERIMENTS ON INSULATING PANELS
17. **G.L. Mitu, AL. Bejinaru Mihoc**
OVERVIEW OF POLYIMIDE PROPERTIES AND APPLICATIONS
18. **Ioan Trif, Ioan Szava, Costel Bejan**
DEFINING AND GEOMETRICAL MODELING OF A NEW FUNCTIONAL CHARACTERISTICS FOR EXCAVATORS WITH BUCKET
19. **Virgil Barbu Ungureanu, Liviu Costiuc**
SIMULATION OF BOILING FLOW IN A HEAT PIPE
20. **Cristina Chilibaru-Oprîtescu, Amalia Țîrdea**
THE ANALYZING OF THE MECHANICAL BEHAVIOR OF WOOD BY NUMERICAL SIMULATION
21. **Amalia Țîrdea, Cristina Chilibaru-Oprîtescu**
BEHAVIOUR OF THE SANDWICH PANELLIS WITH DIFFERENT CORE BY NUMERICAL SIMULATION
22. **Ana Gheorghe, Carmen Alexandru, Gabriela Mindu**
EVALUAREA CONFORMITĂȚII MATERIALELOR FONOABSORBANTE ȘI ANTIVIBRATILE PENTRU CONSTRUCȚII
23. **Nicușor Drăgan, Ov. Vasile, Anca Tiuc, Adrian Țabrea, Oleg Chilari**
PANOURI MODULARE DIN MATERIAL COMPOSITE CU CARACTERISTICI FONOABSORBANTE ȘI FONOIZOLATOARE
24. **A. Tiuc, A. Țabrea, Ovidiu Vasile, Oleg Chilari, C. Oprîtescu, A. Țîrdea**
ANALIZA VARIETĂȚILOR DEȘEURILOR NEMETALICE ÎN SCOPUL REALIZĂRII MATERIALELOR COMPOSITE FONOABSORBANTE
25. **Ovidiu Vasile**
EVALUAREA CAPACITĂȚII DE IZOLARE ACUSTICĂ PRIN ÎNCERCĂRI INSTRUMENTALE
26. **S. Popa**
EVALUAREA COMPARATIVĂ A PARTICULARITĂȚILOR SPECIFICE APARATELOR DE REAZEM ȘI DISPOZITIVELOR ANTISEISMICE ELASTOMERICE ÎN RAPORT CU DOCUMENTAȚIA DE REFERINȚĂ ÎN DOMENIUL REGLEMENTAT
27. **M. Lazăr, C. Dima**
BARIERE ACUSTICE DESTINATE TRAFICULUI RUTIER PE BAZA MATERIALELOR COMPOZITE DIN DEȘEURI DE CAUCIUC
28. **A. Țabrea, G. Mindu, O. Vasile**
PROTECȚIA LA ZGOMOT ȘI VIBRAȚII PE BAZA UTILIZĂRII MATERIALELOR ȘI PRODUSELOR INTELIGENTE



ASSESSMENT OF POTENTIAL RISKS THAT INFLUENCE THE TRAFFIC ACCIDENTS

Dorin Dumitrascu¹

¹ Transilvania University, Brasov, ROMANIA, d.dumitrascu@unitbv.ro

Abstract: In this paper are presented some general aspects regarding bicycle crash types, cyclist injury and the assessment of the main potential risks that influences the traffic accidents between cars and two wheeled vehicle and single bicycle – crashes. Traffic accidents are events out of the ordinary, generally characterized by more or less information on the crash causes, on some parameter measurement and observation tools. The statistical analyses of the potential risks and their influences on traffic accidents between cars and two wheeled vehicles it was performed using cumulative density function based on 87th percentile.

Keywords: accidents, bicycle, risks assessment, injury, cumulative density function.

1. INTRODUCTION

The traffic accident is an event produced on public roads, consisting of the collision of two or more vehicles, or of a vehicle with another obstacle, hitting pedestrians, cyclists or other participants to the traffic and resulting in injury to corporal integrity of some persons, material damage, as well as disturbing circulation. The traffic accidents are classified by: severity of injury to persons, type of collision, impact configuration, determined factors.

In road accidents are involved three components of the traffic system: vehicles, people and the road together with the environment.

The bicyclists are included in the category of the most vulnerable road users and the bicycle riding becomes a popular means of transportation. Thereby the bicycles are used for travel to work, shopping and for leisure purposes. In the same time the increasing intensity of bicycles usage was generated by: the growth of urban traffic intensity, some economic facts, a healthy lifestyle, the increasing environmental pollution.

Considering the aspects previously presented it becomes obvious that cycling injuries and fatalities are on an increasing tendency, being necessary that the causes and effects of the road accidents involving this category of traffic participants need to be taken into account.

Analyzing the potential risks that influence the accidents between vehicles and two wheeled vehicles, in particular bicycles can be developed techniques, methods and systems in order to increase the safety of this category of traffic participants.

The events in which is involved the tandem bicycle – cyclist can be split into two categories: bicycle-car crashes and single bicycle – cyclist crashes, including here for example obstacle collision, falls due to road surface condition or quality. Bicycle defects represent a reduced cause in crashes.

Another important factor in accidents incidence is represented by the light condition: night, twilight and daylight. Other determinant factors are: age and sex, speed, bicycle type, knowing the location, alcohol use, physical problems, etc.

Obviously, bicyclists become one of the most exposed participants in traffic, who suffer injuries in case of an accident. Compared to cars, the bicycles have a reduced visibility (preponderantly frontal), are less stable and offer a much less protection to the cyclist. Taking into account the unprotected or partially protected body in comparison to the cars, the bicyclist usually falls from his bicycle and hits some hard elements, non-deformable structures of other vehicles or infrastructures, suffering the most severe injuries: to head and extremities fractures.

2. PROCEDURES AND ANALIZING METHODS

The methodology of assessment of potential risks consist of the following elements, performed, more or less, in the following order: identify, assess the vulnerability of critical assets to specific threats, the quantification of risk (the expected likelihood and consequences), identify ways to reduce those risks and prioritize risk reduction measures based on a strategy [2],[3].

In figure 1, by using a realistic evaluation of security control effectiveness, a more accurate prioritization can be made. The most extreme risks will obviously take precedence over the low, moderate, and high-risk areas.

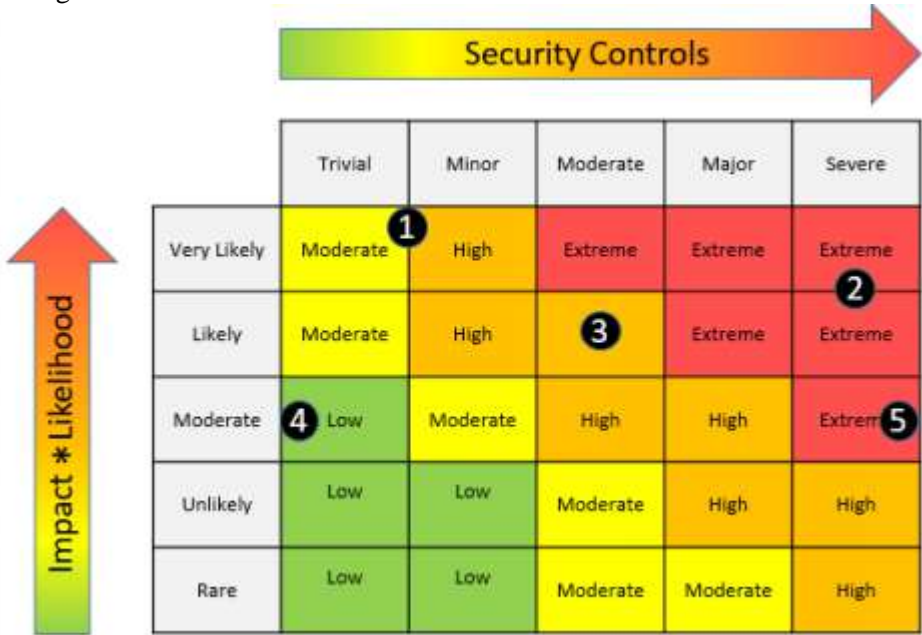


Figure 1: Overlaying control effectiveness enables differentiation between risks and illustrates residual risk [1]

The present study refers to the estimation of the potential risks that can be manifested in the case of cyclists traveling on public roads. 29 potential risks were identified, being quantified both qualitatively and quantitatively.

The assessment of risk impact is graphically detailed in figure 2. It can be observed that a number of 17 potential risks can have a significant impact.

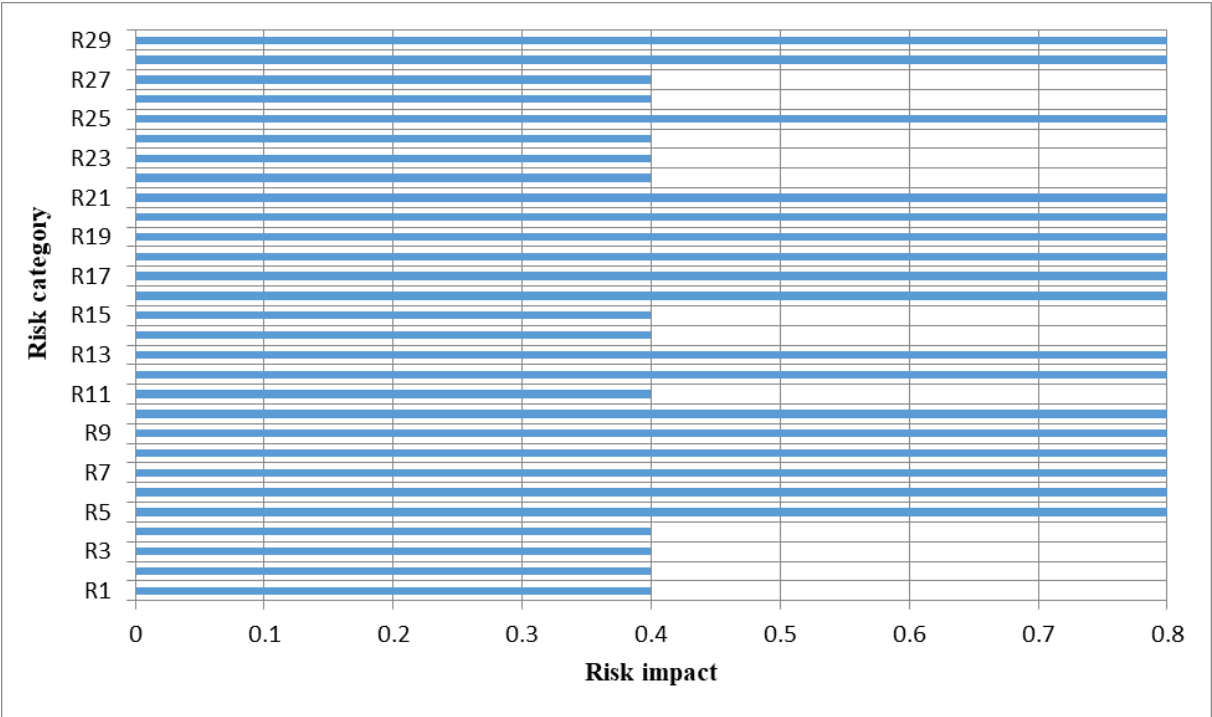


Figure 2: The distribution of risks impact

Analyzing figure 3, it can be pointed out that the vast majority of the estimated risks have a high probability of occurrence.

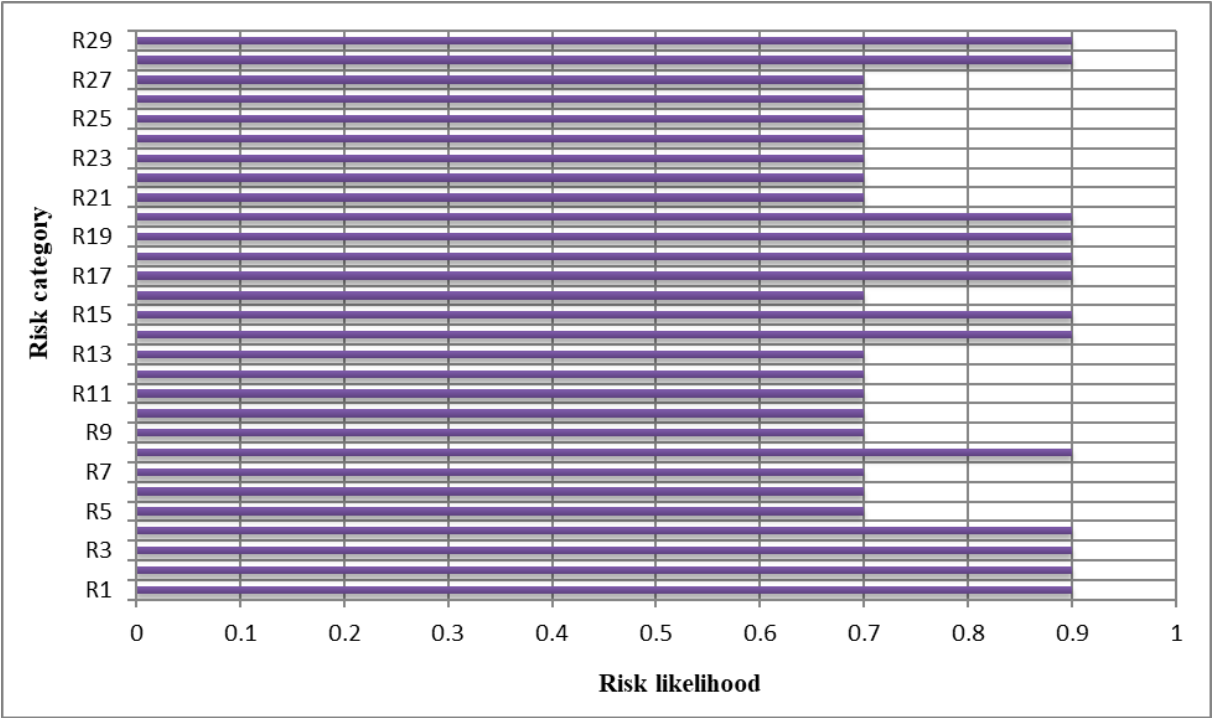


Figure 3: The distribution of risks likelihood

The priority score of the potential risks is established according to the probability of occurrence and the impact score of the risk.

The quantification of the risk score indicates that the risks fall into the high-risk area (figure 4).

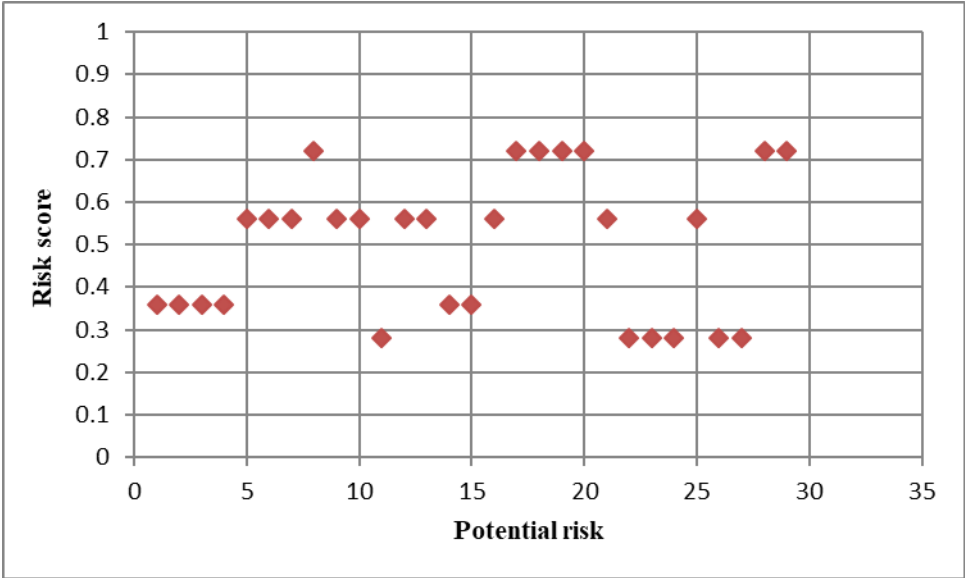


Figure 4: The distribution of risk based on risk score

By using the specific cumulative density functions applied to each identified risk, the influence of cumulative risks was analyzed (figure 5). The results expressed by the cumulative density functions show that for a probability of 87th, the risks have a score of 0.6876. Thus, these risks can be classified in the category of high risks with negative influences.

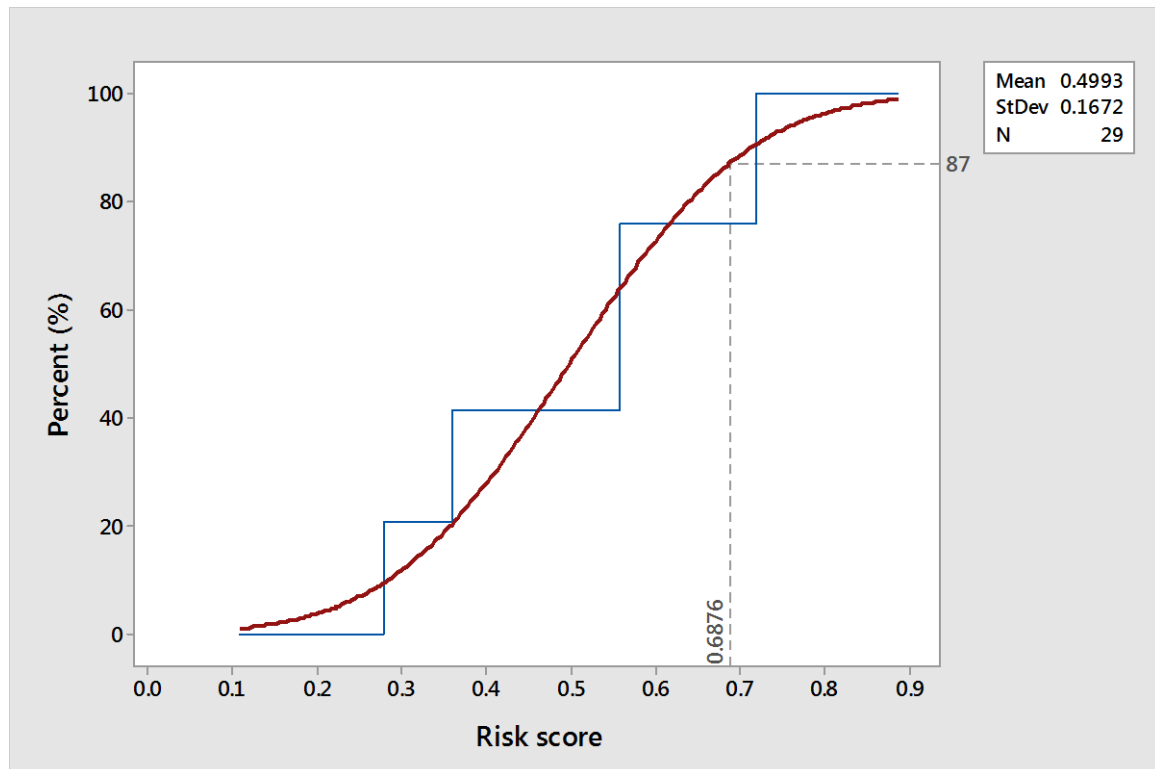


Figure 4: The cumulative density functions of potential risk

3. CONCLUSION

Analyzing the results of the risk score evaluation, the significant risks are the following:

- Frontal accident with a vehicle;
- Rear accident with a vehicle;
- Overtaking on the left side;
- The intersection on the right side;
- Door open in front of the bicyclist;
- Transit on the red color of the traffic light;
- Driving under the influence of alcohol;
- Failure to observe the limit distance that is needed to be maintained both, for moving vehicles and for parked cars;
- The cyclist driving at night time;
- The condition, quality of the road and the presence of different obstacles on it.

REFERENCES

- [1] . Baze A., Realistic Risk Management Using the CIS 20 Security Controls, 2016.
- [2] Duijm, N. J., Recommendations on the use and design of risk matrices, Safety Science, 2015.
- [3] Hanna Landell, The Risk Matrix as a tool for risk analysis, Student thesis, 2016.
- [4] Schepers P., Single-Bicycle Crash Types and Characteristics, Cycling Research International, Vol. 2 2012, 119 – 135 ISSN 2200-5366.
- [5] Elvik, R., Vaa, T., The Handbook of Road Safety Measures. Oxford: Elsevier, 2009.
- [6] Orsi, C., Marchetti, P., Marinoni, A., Morandi, A., Risk factors for road traffic accidents severity in the province of Milan, Italy. Biomedical Statistics and Clinical Epidemiology 3 (3), 143-154, 2009.
- [7] Chiara O., Dietmar O., Accident configurations and injuries for bicyclists based on German In-Depth-Accident Study, ISBN: 978-3-95606-021-2, 2013.
- [8] Orsi, C., Road accidents involving bicycles: configurations and injuries, 2017.
- [9] European Commission, Traffic Safety Basic Facts 2018 – Cyclists.